

Climate4you update July 2021



1

Summary of observations until July 2021:

- 1: Observed average global air temperature change last 30 years is about $+0.17^{\circ}\text{C}$ per decade. If unchanged, additional average global air temperature increase by year 2100 will be about $+1.3^{\circ}\text{C}$.
- 2: Tide gauges along coasts indicate a typical global sea level increase of about 1-2 mm/yr. Coastal sea level change rate last 100 year has essentially been stable, without recent acceleration. If unchanged, global sea level at coasts will typically increase 8-16 cm by year 2100, although many locations in regions affected by glaciation 20,000 years ago, will experience a relative sea level drop.
- 3: Since 2004 the global oceans above 1900 m depth on average have warmed about 0.07°C . The maximum warming (about 0.2°C , 0-100 m depth) mainly affects oceans near Equator, where the incoming solar radiation is at maximum.
- 4: Changes in atmospheric CO_2 follow changes in global air temperature. Changes in global air temperature follow changes in ocean surface temperature.
- 5: There is no perceptible effect on atmospheric CO_2 due to the COVID-related drop in GHG emissions. Natural sinks and sources for atmospheric CO_2 far outweigh human contributions.

Contents:

Page 3:	July 2021 global surface air temperature overview
Page 4:	July 2021 global surface air temperature overview versus July last 10 years
Page 5:	July 2021 global surface air temperature compared to July 2020
Page 6:	Temperature quality class 1: Lower troposphere temperature from satellites
Page 7:	Temperature quality class 2: HadCRUT global surface air temperature
Page 8:	Temperature quality class 3: GISS and NCDC global surface air temperature
Page 11:	Comparing global surface air temperature and satellite-based temperatures
Page 12:	Global air temperature linear trends
Page 13:	Global temperatures: All in one, Quality Class 1, 2 and 3
Page 15:	Global sea surface temperature
Page 18:	Ocean temperature in uppermost 100 m
Page 20:	North Atlantic heat content uppermost 700 m
Page 21:	North Atlantic temperatures 0-800 m depth along 59N, 30-0W
Page 22:	Global ocean temperature 0-1900 m depth summary
Page 23:	Global ocean net temperature change since 2004 at different depths
Page 24:	La Niña and El Niño episodes, Oceanic Niño Index
Page 25:	Zonal lower troposphere temperatures from satellites
Page 26:	Arctic and Antarctic lower troposphere temperatures from satellites
Page 27:	Arctic and Antarctic surface air temperatures
Page 30:	Temperature over land versus over oceans
Page 31:	Troposphere and stratosphere temperatures from satellites
Page 32:	Sea ice; Arctic and Antarctic
Page 36:	Sea level in general
Page 36:	Global sea level from satellite altimetry
Page 38:	Global sea level from tide gauges
Page 39:	Snow cover; Northern Hemisphere weekly and seasonal
Page 41:	Atmospheric specific humidity
Page 42:	Atmospheric CO ₂
Page 43:	Relation between annual change of atm. CO ₂ and La Niña and El Niño episodes
Page 44:	Phase relation between atmospheric CO ₂ and global temperature
Page 45:	Global air temperature and atmospheric CO ₂
Page 49:	Latest 20-year QC1 global monthly air temperature change
Page 50:	Sunspot activity and QC1 average satellite global air temperature
Page 51:	Sunspot activity and average neutron counts
Page 52:	Sunspot activity, ONI, and change rates of atmospheric CO ₂ and specific humidity
Page 53:	Monthly lower troposphere temperature and global cloud cover
Page 54:	Climate and history: <i>9 AD: Battle of the Teutoburg Forest</i>

July 2021 global surface air temperature overview

General: This newsletter contains graphs and diagrams showing a selection of key meteorological variables, if possible updated to the most recent past month. All temperatures are given in degrees Celsius.

In the maps on pages 4-5, showing the geographical pattern of surface air temperature anomalies, the last previous 10 years are used as reference period.

The rationale for comparing with this recent period instead of various 'normal' periods defined for parts of the past century, is that such reference periods often will be affected by past cold periods, like, e.g., 1945-1980. Most modern comparisons with such reference periods will inevitably appear as warm, and it will be difficult to decide if modern temperatures are increasing or decreasing. Comparing instead with the last previous 10 years overcomes this problem and clearer displays the modern dynamics of ongoing change. This decadal approach also corresponds well to the typical memory horizon for many people and is now also adopted as reference period by other institutions, e.g., the Danish Meteorological Institute (DMI).

3

In addition, most temperature databases display temporal instability for past data (see, e.g., p. 9). Any comparison with such reference periods will therefore be influenced by ongoing monthly changes of mainly administrative nature. A fluctuating value is clearly not suited as reference value. Simply comparing with the last previous 10 years is more useful as reference for modern changes. Please see also additional reflections on page 47-48.

The different air temperature records have been divided into three quality classes, QC1, QC2 and QC3, respectively, as described on page 9.

In many diagrams shown in the present newsletter the thin line represents the monthly global average value, and the thick line indicate a simple running average, in most cases a simple moving 37-month average, nearly corresponding to a three-year average. The 37-month average is calculated from values covering a range from 18 months before to 18 months after, with equal weight given to all individual months.

The year 1979 has been chosen as starting point in many diagrams, as this roughly corresponds to both the beginning of satellite observations and the onset of the late 20th century warming period. However, several of the data series have a much longer record length, which may be inspected in greater detail on www.climate4you.com.

July 2021 surface air temperature

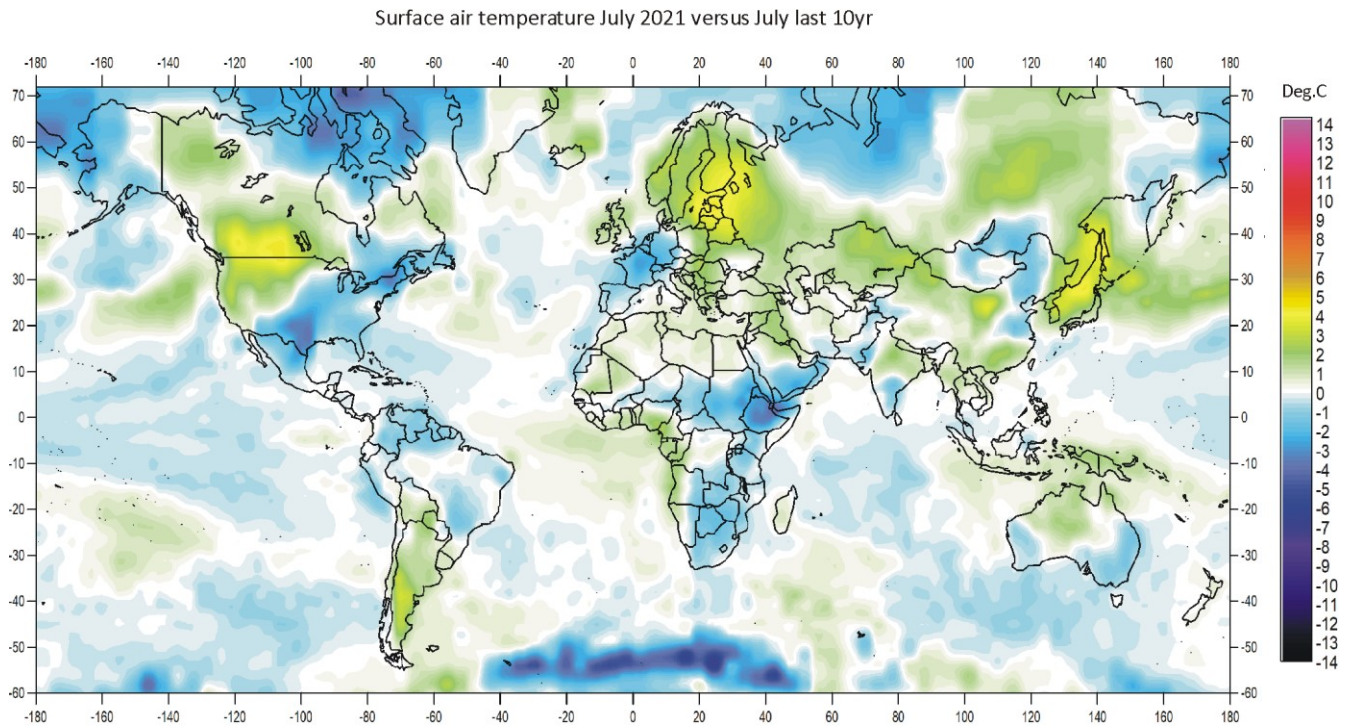
General: For July 2021, the GISS portal supplied 16200 AIRS interpolated surface air data points, based on satellite observations, and visualised here on pages 4-5. According to most global surface temperature databases, the July 2021 global average air temperature anomaly was somewhat higher than in the previous month (June). According to AIRS July 2021 was a little cooler than July 2020.

The Northern Hemisphere 10-yr surface temperature anomaly pattern (p.4) was as usual characterised by regional contrasts, mainly controlled by the dominant jet stream configuration, leading to a heat wave in western USA and Canada from late June into July. Other jet stream generated positive anomalies existed over northern Europe. In contrast, in between these positive anomalies regions with negative (cold) anomalies existed, especially over northern Russia and -Canada, and in the Bering Strait region, also mainly caused by the jet stream configuration. Ocean wise, most of the North Atlantic was near average conditions, while regions in the North Pacific was below average surface conditions. In the Arctic, relatively cold conditions characterised almost the entire region.

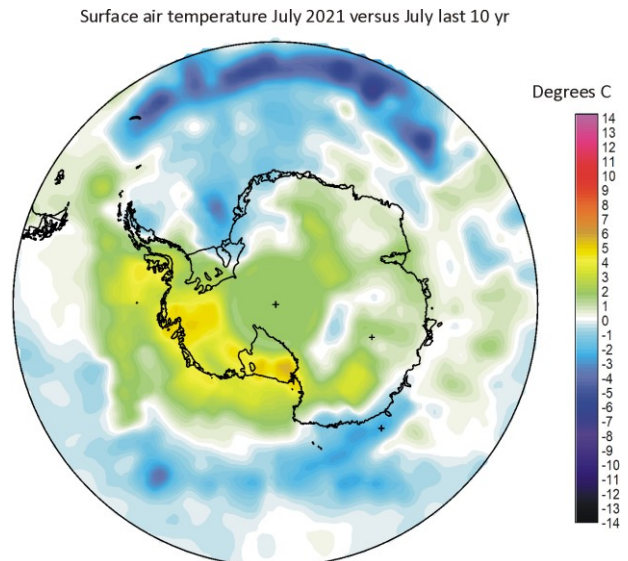
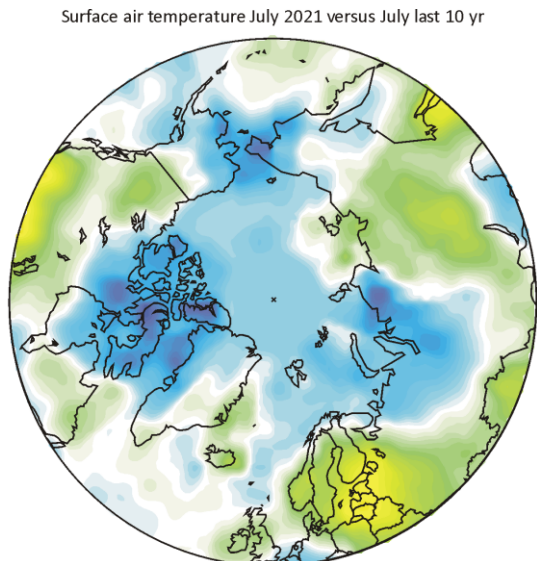
Near the Equator temperatures were mostly below (especially in the Pacific Ocean) the 10-year average.

The Southern Hemisphere temperatures were largely below or near the average for the previous 10 years. Argentina, however, was relatively warm, as was northern Australia, while New Zealand was near average conditions. Large regions in southern Africa were relatively cold. Ocean wise, surface temperatures conditions were near average or below. Parts of the South Atlantic were very cold. In the Antarctic, with few exceptions, conditions were relatively warm.

July 2021 global surface air temperature overview versus average July last 10 years

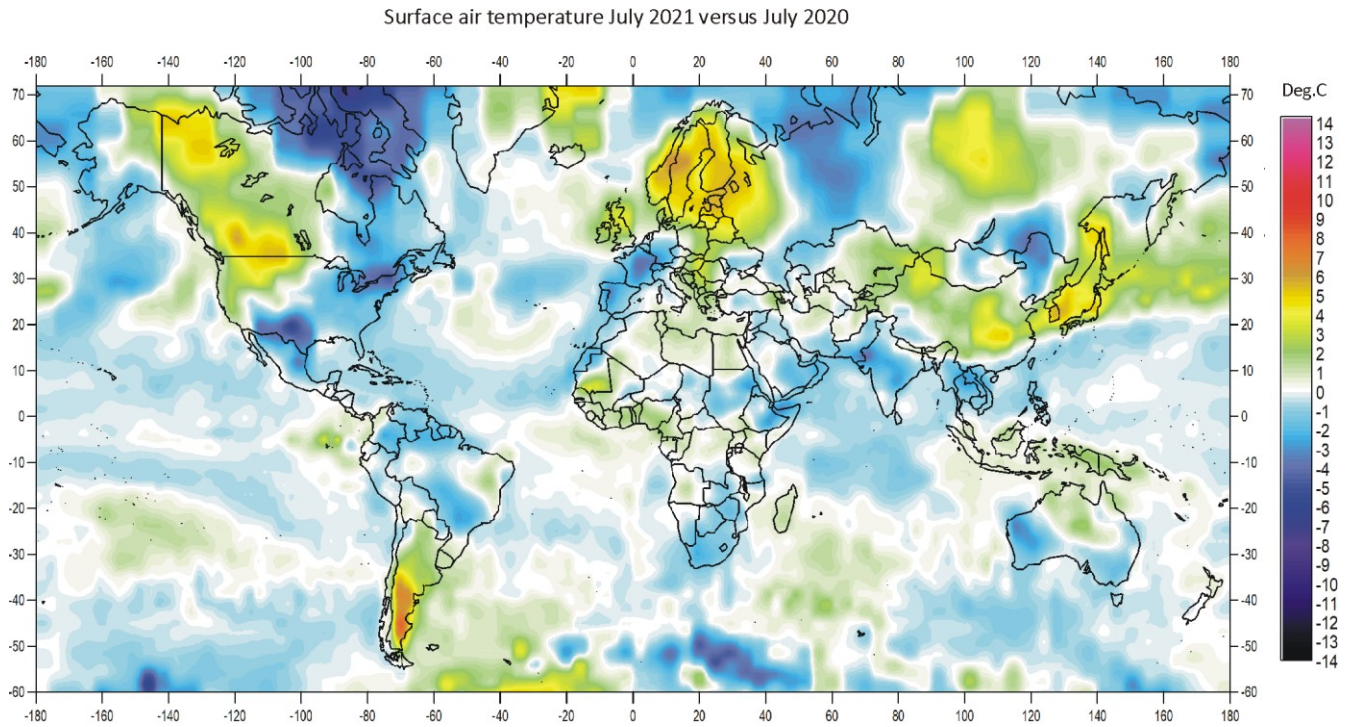


4



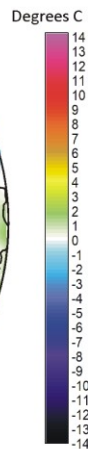
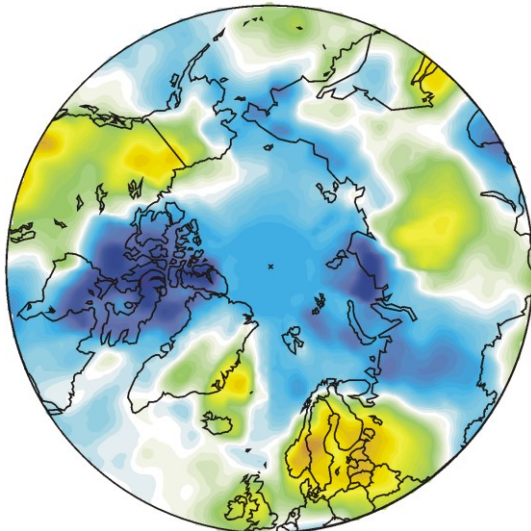
July 2021 surface air temperature compared to the average of July over the last 10 years. Green-yellow-red colours indicate areas with higher temperature than the 10-year average, while blue colours indicate lower than average temperatures. Data source: Remote Sensed Surface Temperature Anomaly, AIRS/Aqua L3 Monthly Standard Physical Retrieval 1-degree x 1-degree V007 (<https://airs.jpl.nasa.gov/>), obtained from the GISS data portal (https://data.giss.nasa.gov/gistemp/maps/index_v4.html).

July 2021 global surface air temperature compared to July 2020

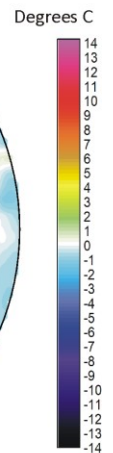
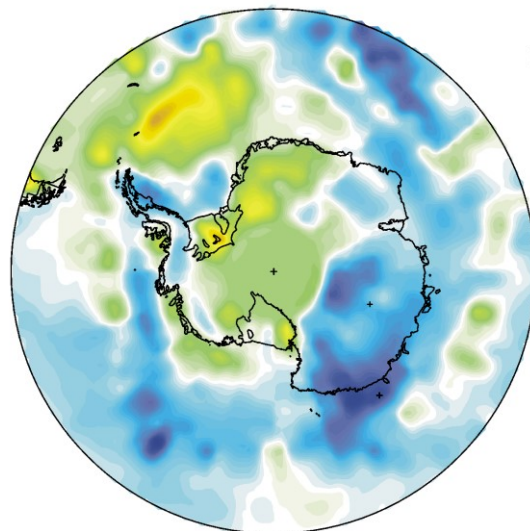


5

Surface air temperature July 2021 versus July 2020



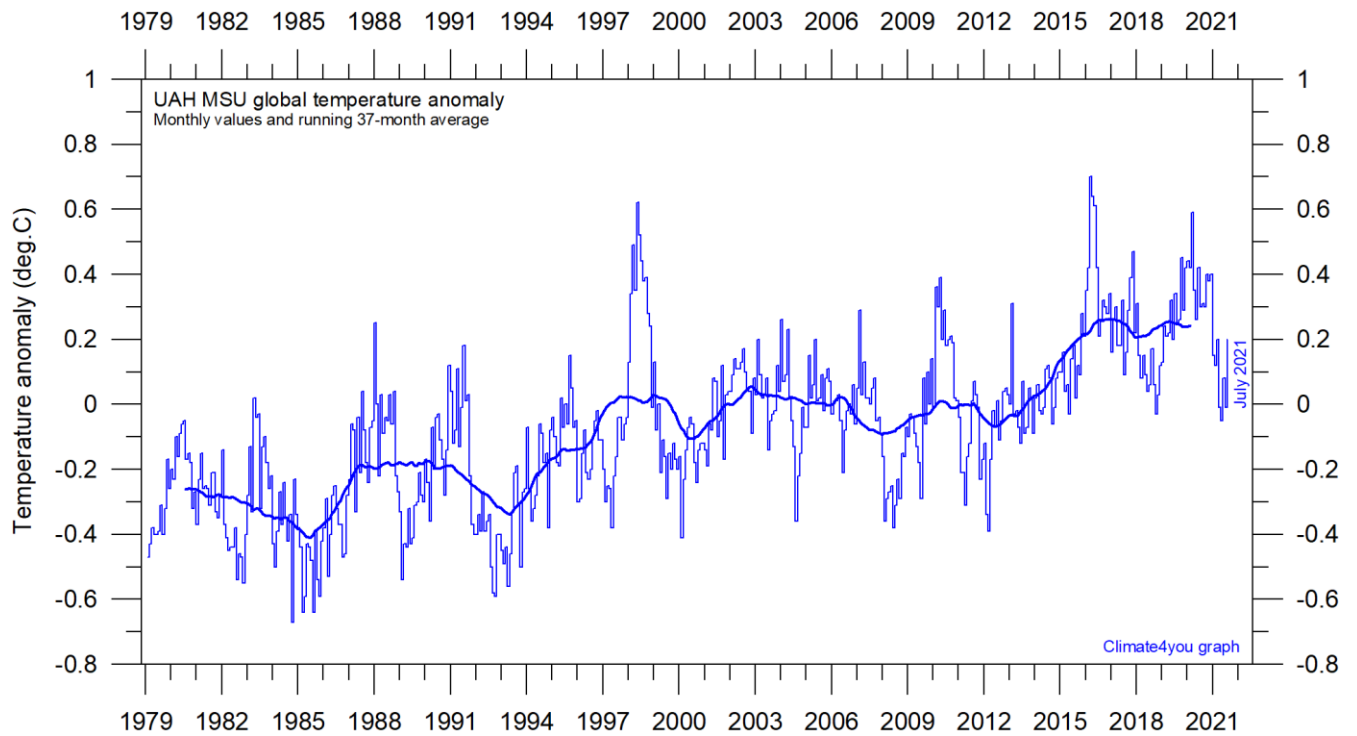
Surface air temperature July 2021 versus July 2020



July 2021 surface air temperature compared to July 2020. Green-yellow-red colours indicate regions where the present month was warmer than last year, while blue colours indicate regions where the present month was cooler than last year. Variations in monthly temperature from one year to the next has no tangible climatic importance but may nevertheless be interesting to study. Data source: Remote Sensed Surface Temperature Anomaly, AIRS/Aqua L3 Monthly Standard Physical Retrieval 1-degree x 1-degree V007 (<https://airs.jpl.nasa.gov/>), obtained from the GISS data portal (https://data.giss.nasa.gov/gistemp/maps/index_v4.html).

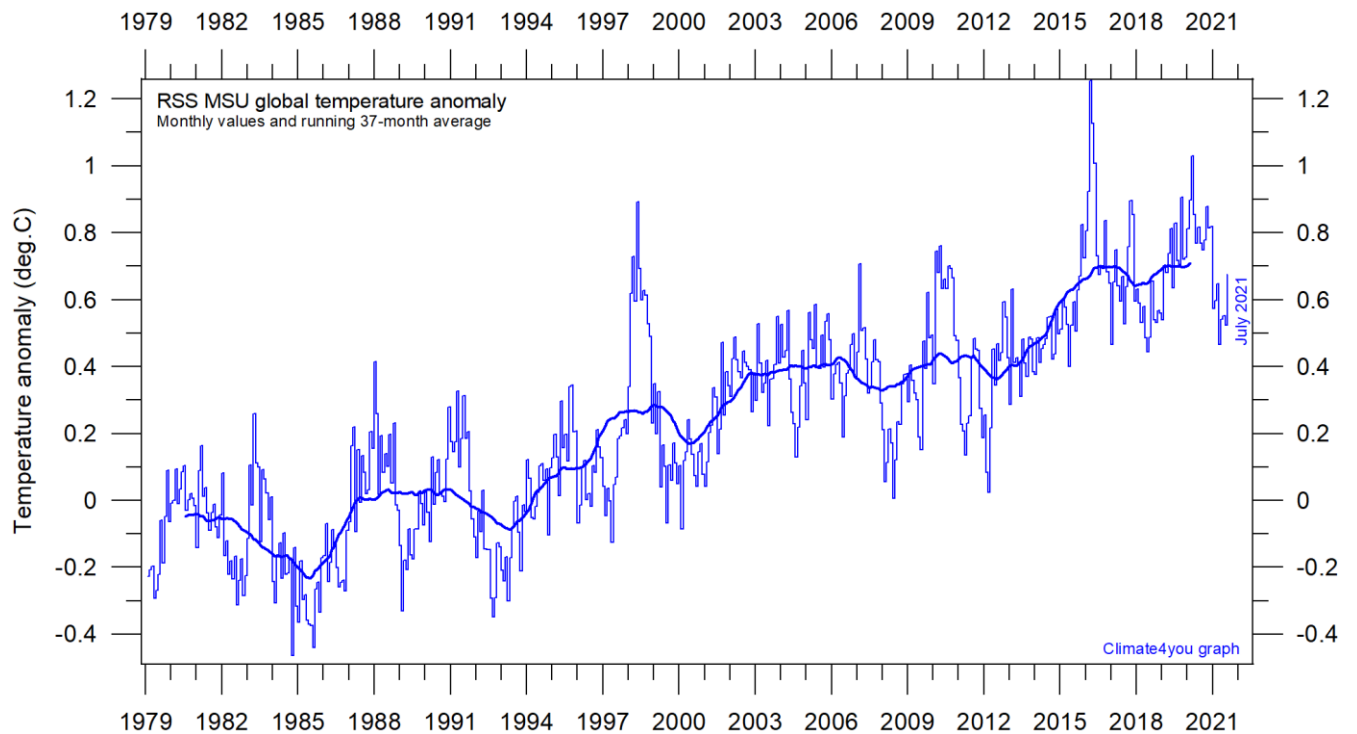
Temperature quality class 1: Lower troposphere temperature from satellites, updated to July 2021

(see page 9 for definition of classes)



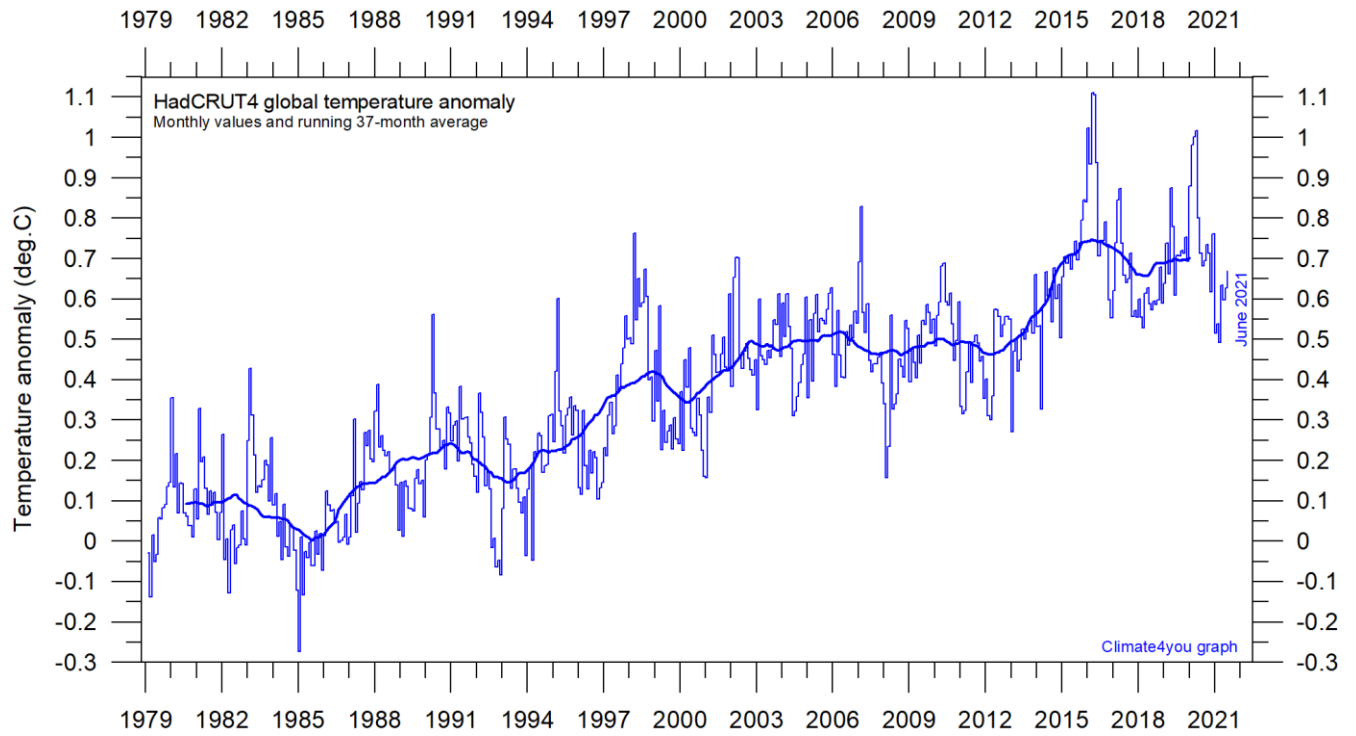
Global monthly average lower troposphere temperature (thin line) since 1979 according to [University of Alabama](#) at Huntsville, USA. The thick line is the simple running 37-month average. Reference period 1991-2020.

6



Global monthly average lower troposphere temperature (thin line) since 1979 according to [Remote Sensing Systems](#) (RSS), USA. The thick line is the simple running 37-month average.

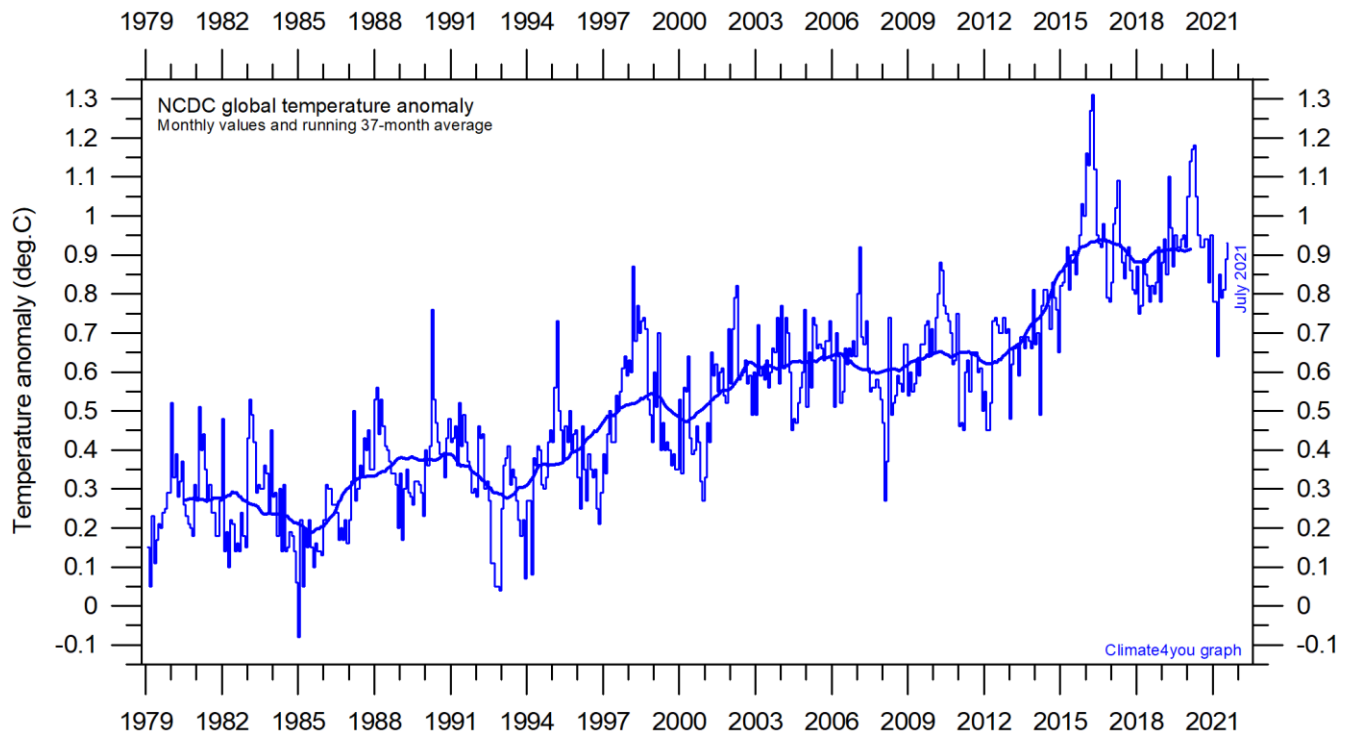
Temperature quality class 2: HadCRUT global surface air temperature, updated to June 2021



7

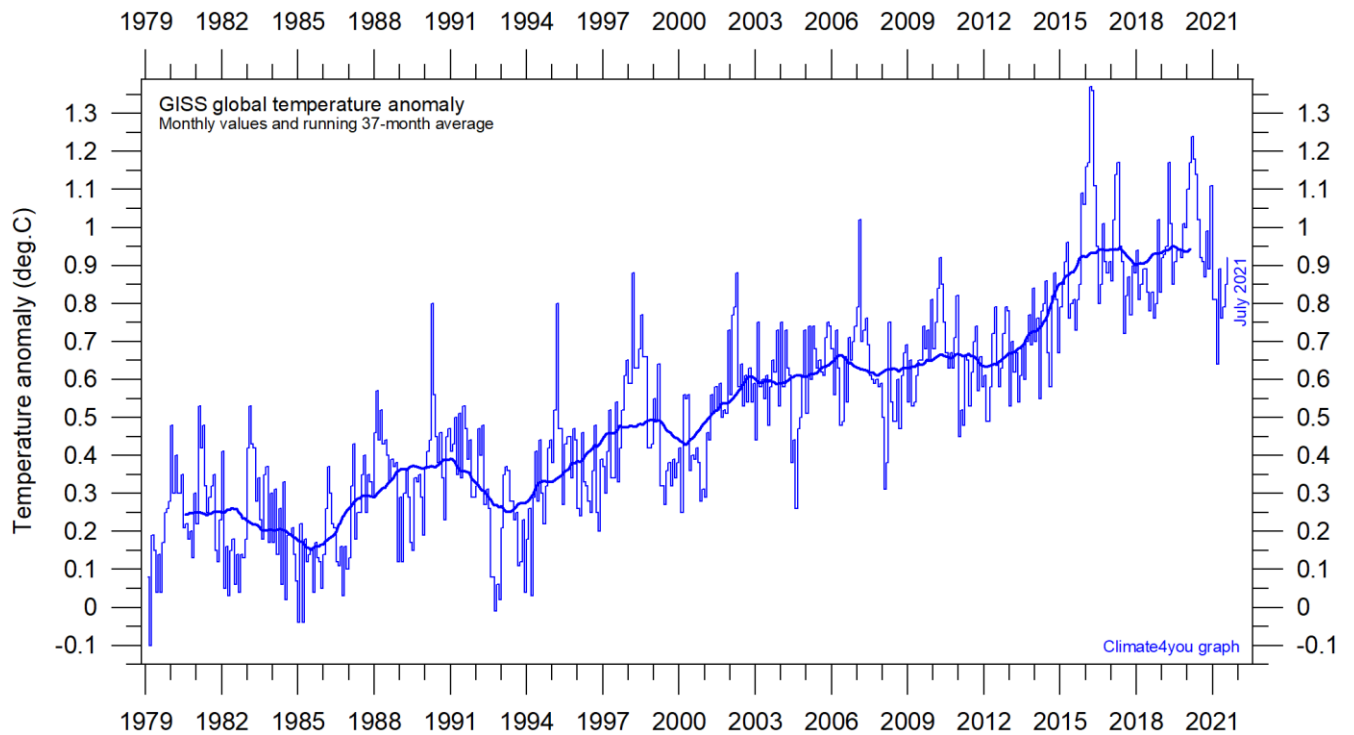
Global monthly average surface air temperature (thin line) since 1979 according to according to the Hadley Centre for Climate Prediction and Research and the University of East Anglia's [Climatic Research Unit \(CRU\)](#), UK. The thick line is the simple running 37-month average. Please note that HadCRUT4 is not yet updated beyond January 2021.

Temperature quality class 3: GISS and NCDC global surface air temperature, updated to July 2021



Global monthly average surface air temperature since 1979 according to according to the [National Climatic Data Center \(NCDC\)](#), USA. The thick line is the simple running 37-month average.

8



Global monthly average surface air temperature (thin line) since 1979 according to according to the [Goddard Institute for Space Studies \(GISS\)](#), at Columbia University, New York City, USA, using ERSST_v4 ocean surface temperatures. The thick line is the simple running 37-month average.

A note on data record stability and -quality:

The temperature diagrams shown above all have 1979 as starting year. This roughly marks the beginning of the recent episode of global warming, after termination of the previous episode of global cooling from about 1940. In addition, the year 1979 also represents the starting date for the satellite-based global temperature estimates (UAH and RSS). For the three surface air temperature records (HadCRUT, NCDC and GISS), they begin much earlier (in 1850 and 1880, respectively), as can be inspected on www.climate4you.com.

For all three surface air temperature records, but especially NCDC and GISS, administrative changes to anomaly values are quite often introduced, even affecting observations many years back in time. Some changes from the recent past may be due to the delayed addition of new station data or change of station location, while others probably have their origin in changes of the technique implemented to calculate average values from the raw data. It is clearly impossible to evaluate the validity of such administrative changes for the outside user of these records; it is only possible to note that such changes quite often are introduced (see example diagram next page).

In addition, the three surface records represent a blend of sea surface data collected by moving ships or by other means, plus data from land stations of partly unknown quality and unknown degree of representativeness for their region. Many of the land stations also has been moved geographically during their period of operation, instrumentation have been changed, and they are influenced by changes in their near surroundings (vegetation, buildings, etc.).

The satellite temperature records also have their problems, but these are generally of a more technical nature and probably therefore better correctable. In addition, the temperature sampling by satellites is more regular and complete on a global basis than that represented by the surface records. It is also important that the sensors on

satellites measure temperature directly by emitted radiation, while most modern surface temperature measurements are indirect, using electronic resistance.

Everybody interested in climate science should gratefully acknowledge the big efforts put into maintaining the different temperature databases referred to in the present newsletter. At the same time, however, it is also important to realise that all temperature records cannot be of equal scientific quality. The simple fact that they to some degree differ shows that they cannot all be correct.

On this background, and for practical reasons, Climate4you therefore operates with three quality classes (1-3) for global temperature records, with 1 representing the highest quality level:

Quality class 1: The satellite records (UAH and RSS).

Quality class 2: The HadCRUT surface record.

Quality class 3: The NCDC and GISS surface records.

The main reason for discriminating between the three surface records is the following:

While both NCDC and GISS often experience quite large administrative changes (see example on p.10), and therefore essentially must be considered as unstable records, the changes introduced to HadCRUT are fewer and smaller. For obvious reasons, as the past does not change, any record undergoing continuing changes cannot describe the past correctly all the time. Frequent and large corrections in a database inevitably signal a fundamental uncertainty about what is likely to represent the correct values.

You can find more on the issue of lack of temporal stability on www.climate4you.com (go to: *Global Temperature*, and then proceed to *Temporal Stability*).

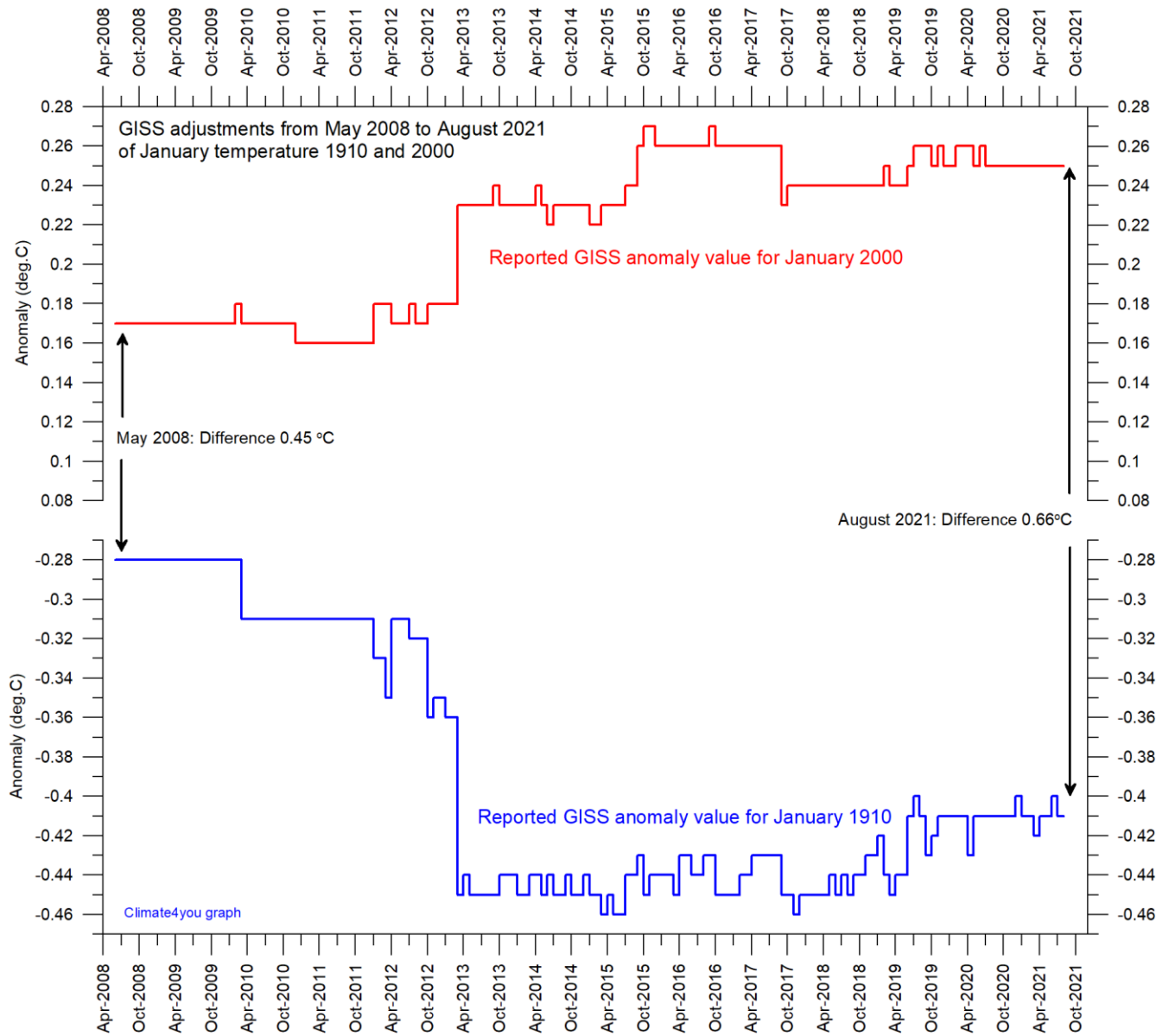
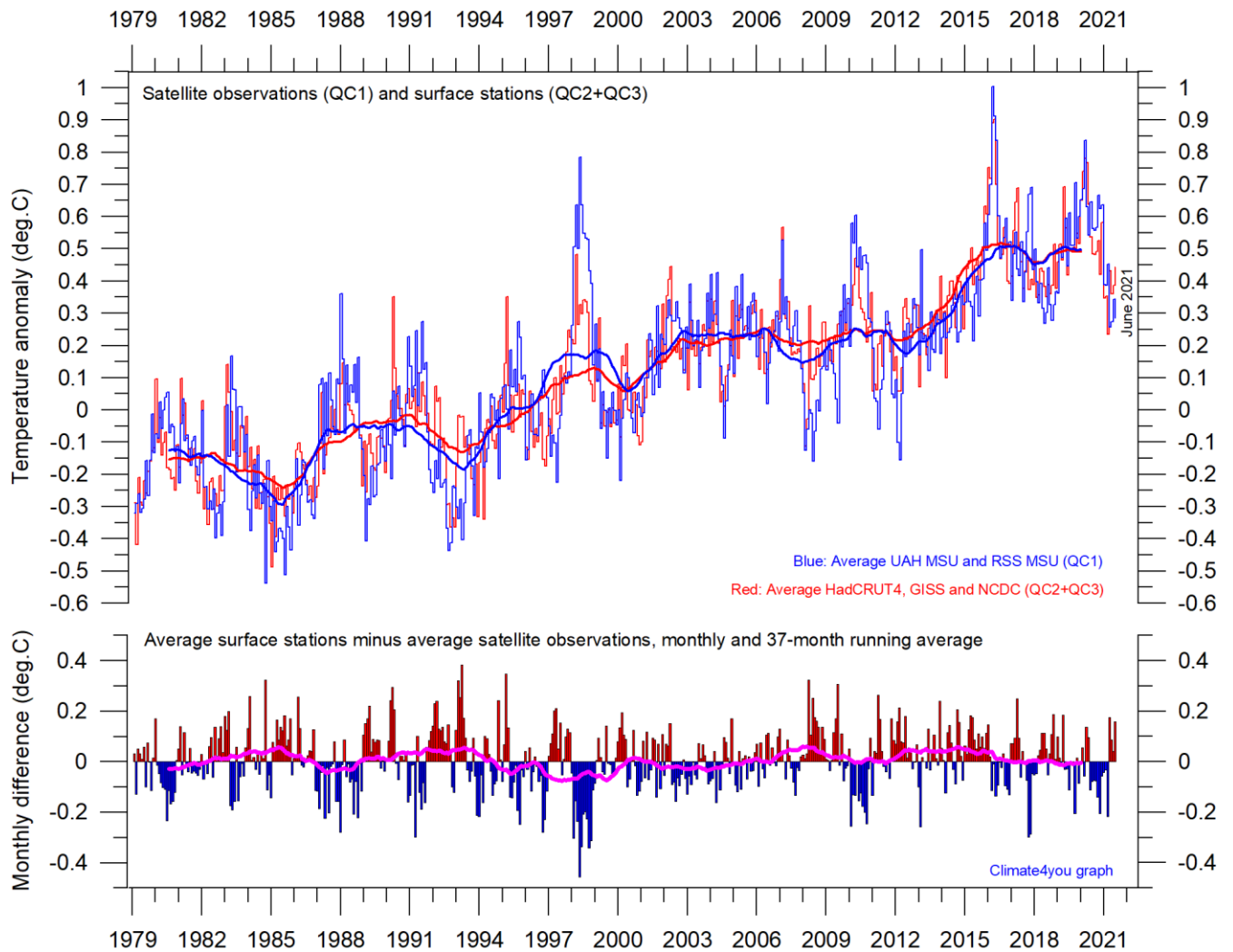


Diagram showing the monthly adjustments made since May 2008 by the [Goddard Institute for Space Studies \(GISS\)](#), USA, as recorded by published anomaly values for the two months January 1910 and January 2000.

The administrative upsurge of the temperature increase from January 1915 to January 2000 has grown from 0.45 (reported May 2008) to 0.66°C (reported August 2021). This represents an about 47% administrative temperature increase over this period, meaning that nearly half of the apparent global temperature increases from January 1910 to January 2000 (as reported by GISS) is due to administrative changes of the original data since May 2008.

Comparing global surface air temperature and lower troposphere satellite temperatures; updated to June 2021



Plot showing the average of monthly global surface air temperature estimates (HadCRUT4, GISS and NCDC) and satellite-based temperature estimates (RSS MSU and UAH MSU). The thin lines indicate the monthly value, while the thick lines represent the simple running 37-month average, nearly corresponding to a running 3-yr average. The lower panel shows the monthly difference between average surface air temperature and satellite temperatures. As the base period differs for the different temperature estimates, they have all been normalised by comparing to the average value of 30 years from January 1979 to December 2008.

Global air temperature linear trends updated to June 2021

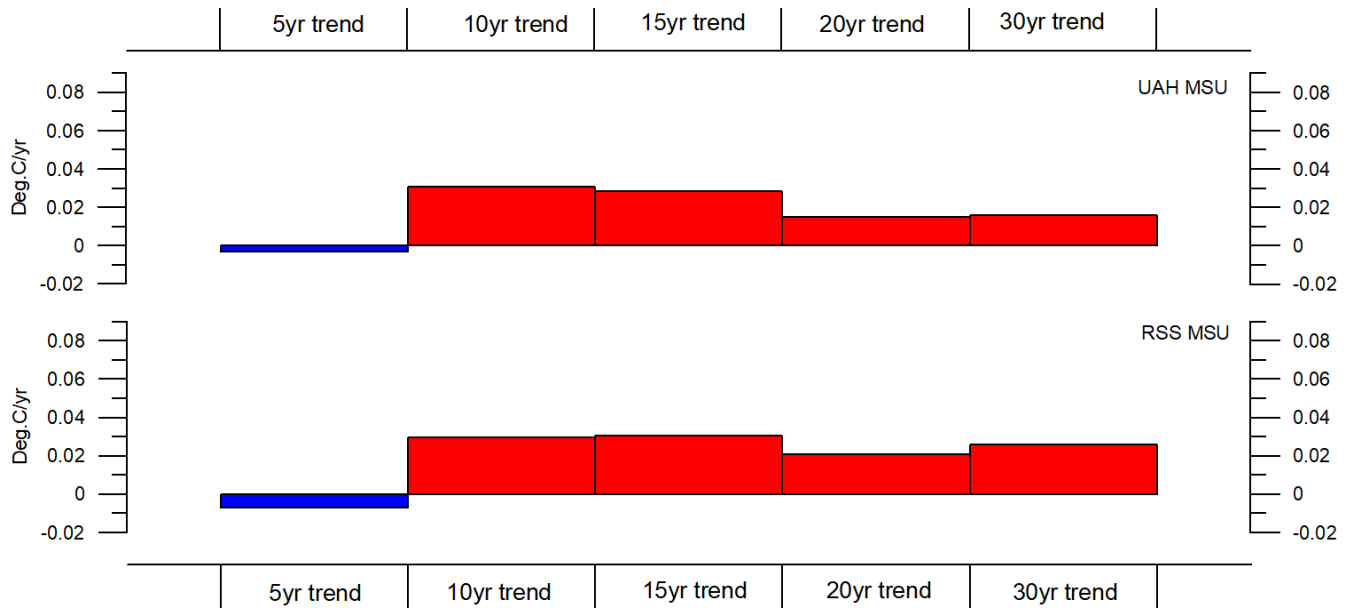


Diagram showing the latest 5, 10, 20 and 30-yr linear annual global temperature trend, calculated as the slope of the linear regression line through the data points, for two satellite-based temperature estimates (UAH MSU and RSS MSU).

12

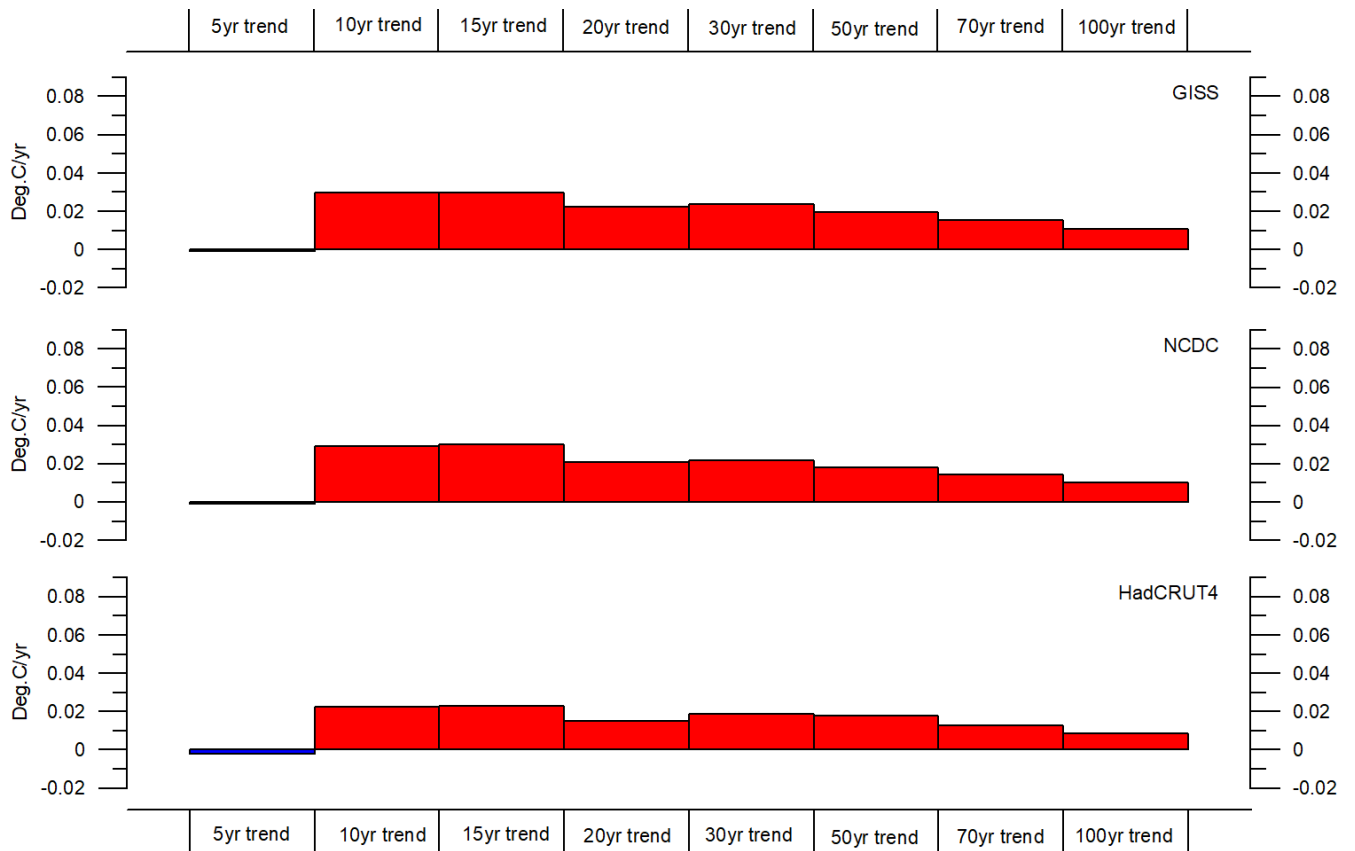
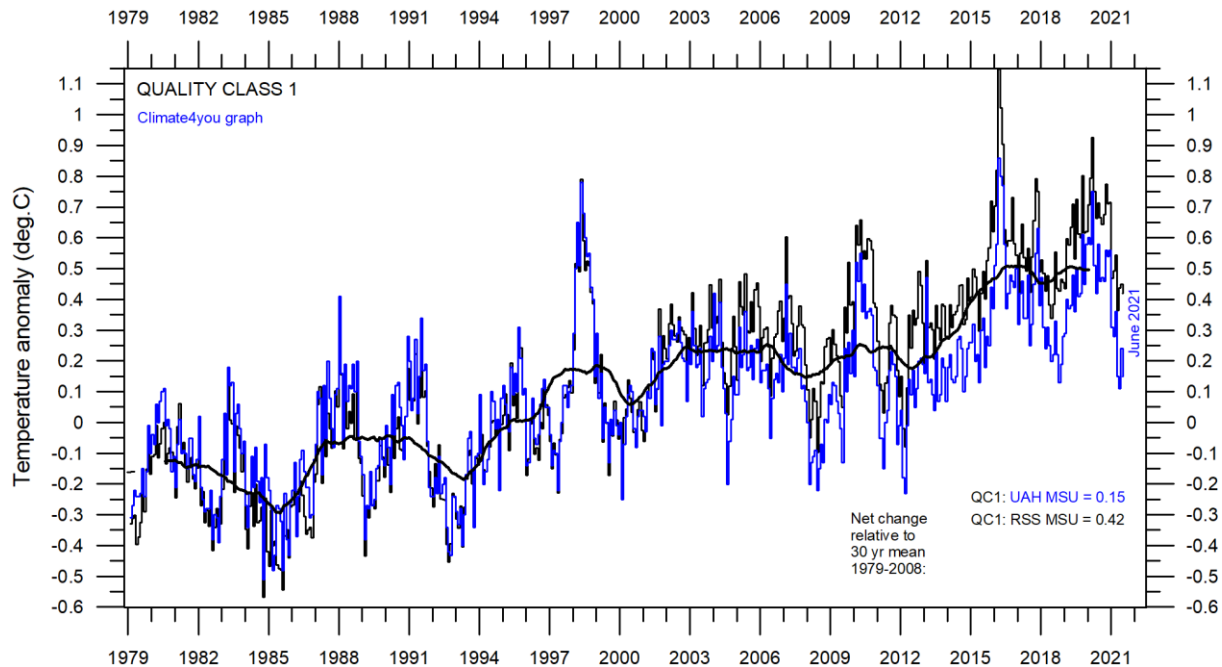


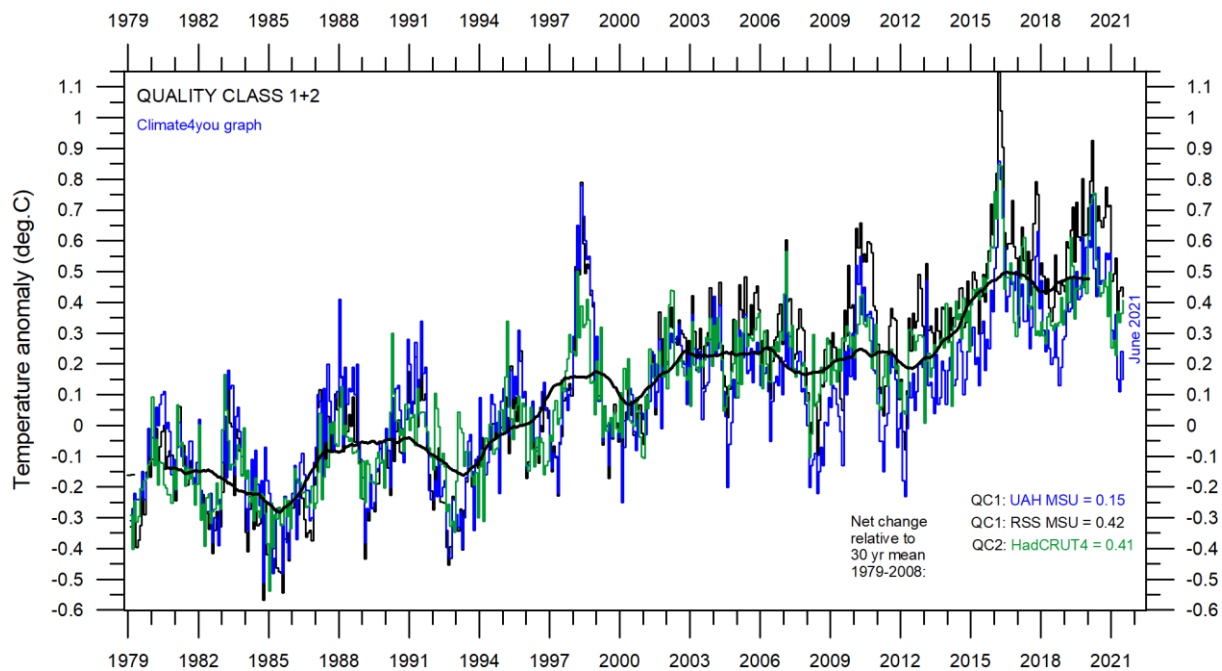
Diagram showing the latest 5, 10, 20, 30, 50, 70 and 100-year linear annual global temperature trend, calculated as the slope of the linear regression line through the data points, for three surface-based temperature estimates (GISS, NCDC and HadCRUT4).

All in one, Quality Class 1, 2 and 3; updated to June 2021

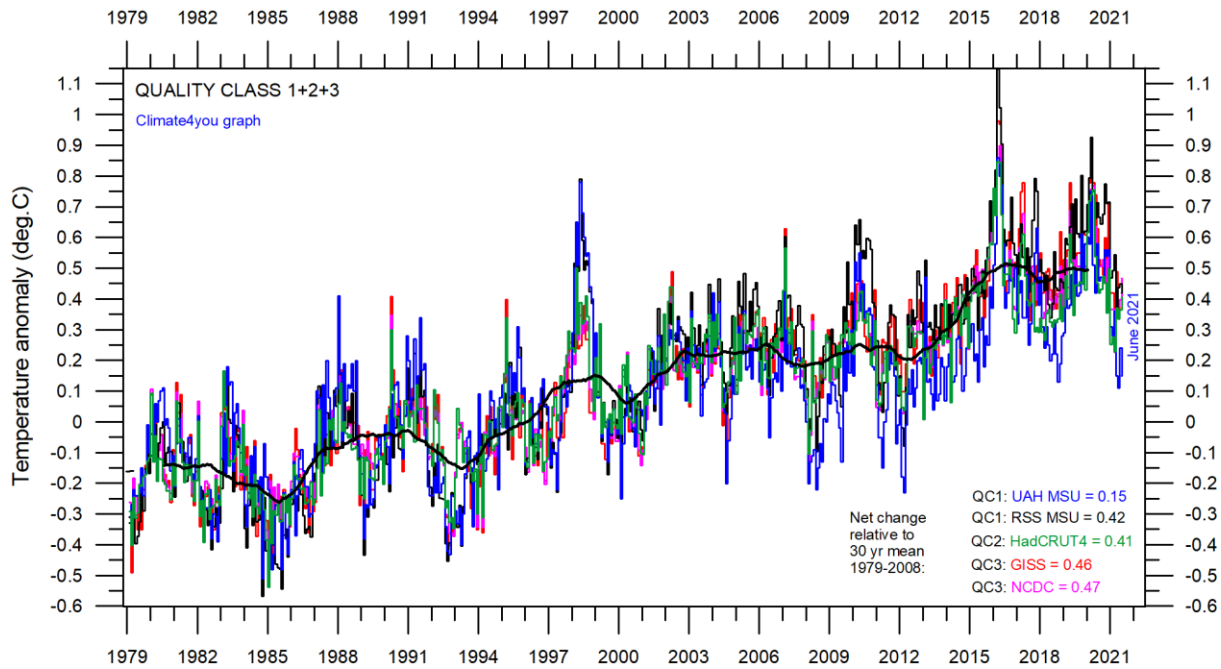


Superimposed plot of Quality Class 1 (UAH and RSS) global monthly temperature estimates. As the base period differs for the individual temperature estimates, they have all been normalised by comparing with the average value of the initial 120 months (30 years) from January 1979 to December 2008. The heavy black line represents the simple running 37 month (c. 3 year) mean of the average of both temperature records. The numbers shown in the lower right corner represent the temperature anomaly relative to the individual 1979-2008 averages.

13



Superimposed plot of Quality Class 1 and 2 (UAH, RSS and HadCRUT4) global monthly temperature estimates. As the base period differs for the individual temperature estimates, they have all been normalised by comparing with the average value of the initial 120 months (30 years) from January 1979 to December 2008. The heavy black line represents the simple running 37 month (c. 3 year) mean of the average of all three temperature records. The numbers shown in the lower right corner represent the temperature anomaly relative to the individual 1979-2008 averages.



Superimposed plot of Quality Class 1, 2 and 3 global monthly temperature estimates (UAH, RSS, HadCRUT4, GISS and NCDC). As the base period differs for the individual temperature estimates, they have all been normalised by comparing with the average value of the initial 120 months (30 years) from January 1979 to December 2008. The heavy black line represents the simple running 37 month (c. 3 year) mean of the average of all five temperature records. The numbers shown in the lower right corner represent the temperature anomaly relative to the individual 1979-2008 averages.

Please see reflections on page 9 relating to the above three quality classes.

Satellite- and surface-based temperature estimates are derived from different types of measurements and comparing them directly as in the above diagrams therefore may be somewhat ambiguous.

However, as both types of estimates often are discussed together in various news media, the above composite diagrams may nevertheless be of some interest.

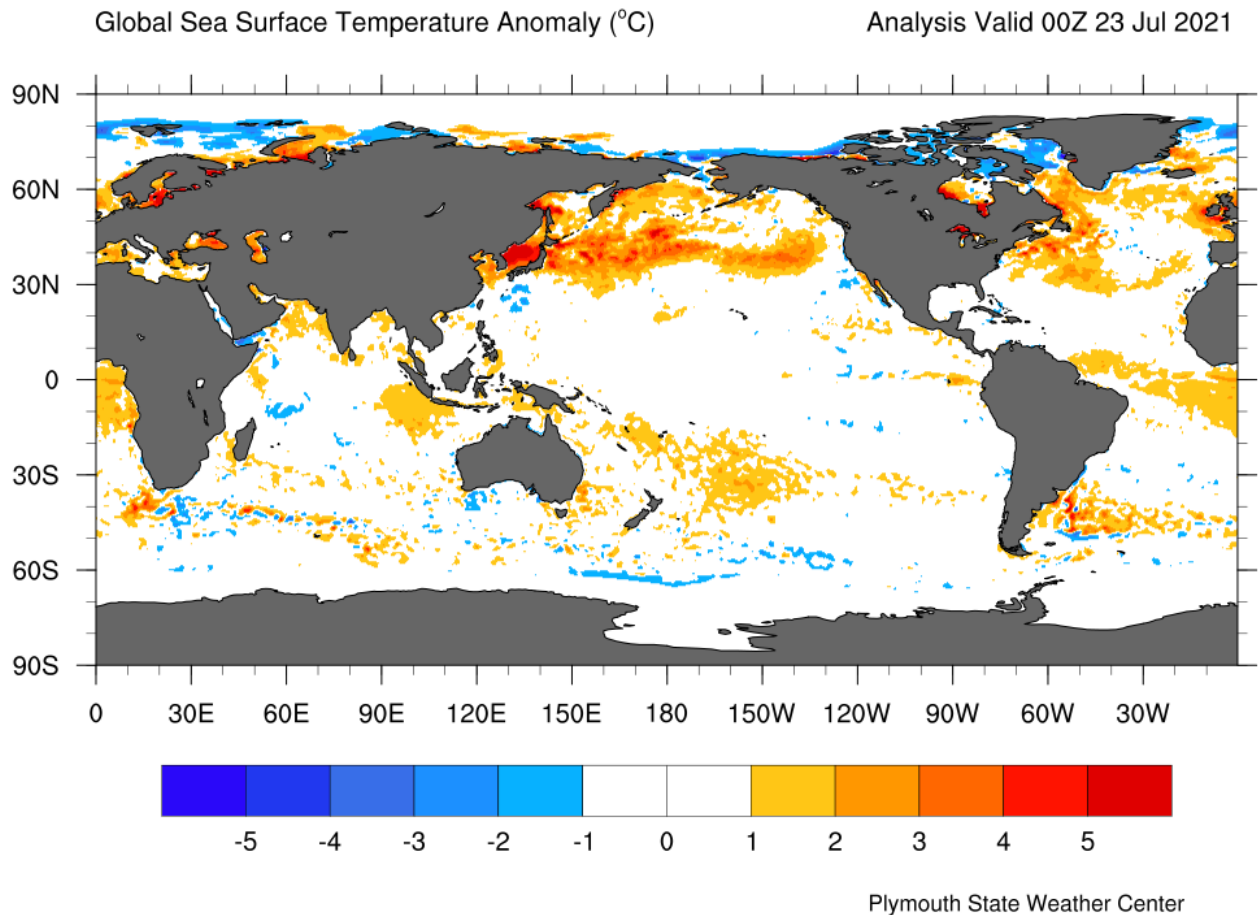
In fact, the different types of temperature estimates appear to agree as to the overall temperature variations on a 2-3-year scale, although on a shorter time scale there are often considerable differences between the individual records. However, since about 2003 the surface records used to be drifting towards higher temperatures than the combined satellite record, but this overall tendency was much removed by the major adjustment of the RSS satellite series in 2015 (see lower diagram on page 6).

The combined records (diagram above) suggest a modest global air temperature increase over the last 30 years, about 0.15°C per decade. It should be noted that the apparent temperature increases since about 2003 at least partly is the result of ongoing administrative adjustments (page 9-10). At the same time, the temperature records considered here do not indicate any general temperature decrease during the last 20 years.

The present temperature development does not exclude the possibility that global temperatures may begin to increase significantly later. On the other hand, it also remains a possibility that Earth just now is passing an overall temperature peak, and that global temperatures may begin to decrease during the coming years.

As always, time will show which of these possibilities is correct.

Global sea surface temperature, updated to July 2021



15

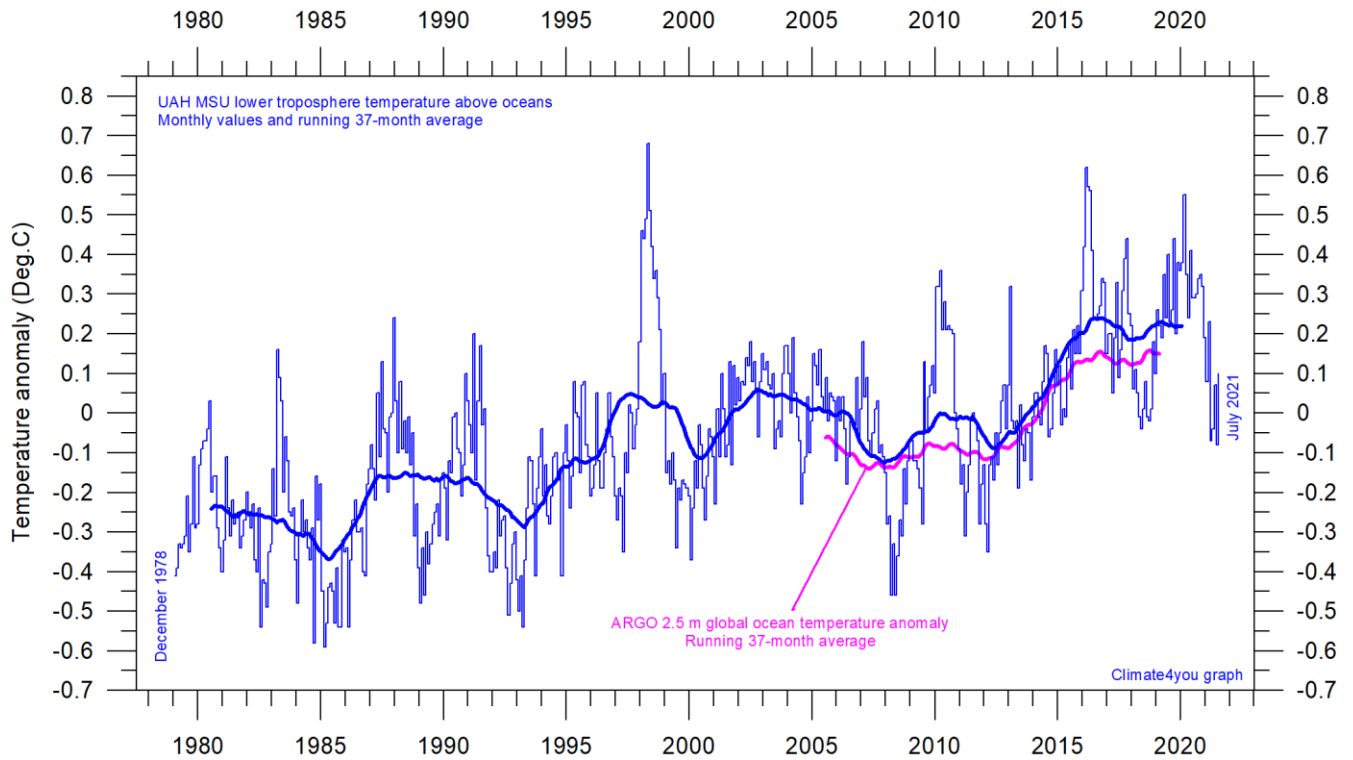
Sea surface temperature anomaly on 23 July 2021. Map source: Plymouth State Weather Center. Reference period: 1977-1991.

Because of the large surface areas near Equator, the temperature of the surface water in these regions is especially important for the global atmospheric temperature (p. 6-8). In fact, no less than 50% of planet Earth's surface area is located within 30°N and 30°S.

A mixture of relatively warm and cold water dominates much of the ocean surface, but with notable differences from month to month. All such ocean surface temperature changes will be influencing global air temperatures in the months to come. Now a cold new La Niña episode is ending in the Pacific Ocean (see p. 24). Relatively warm surface water is found a band in the northern hemisphere, between 30°N and 60°N.

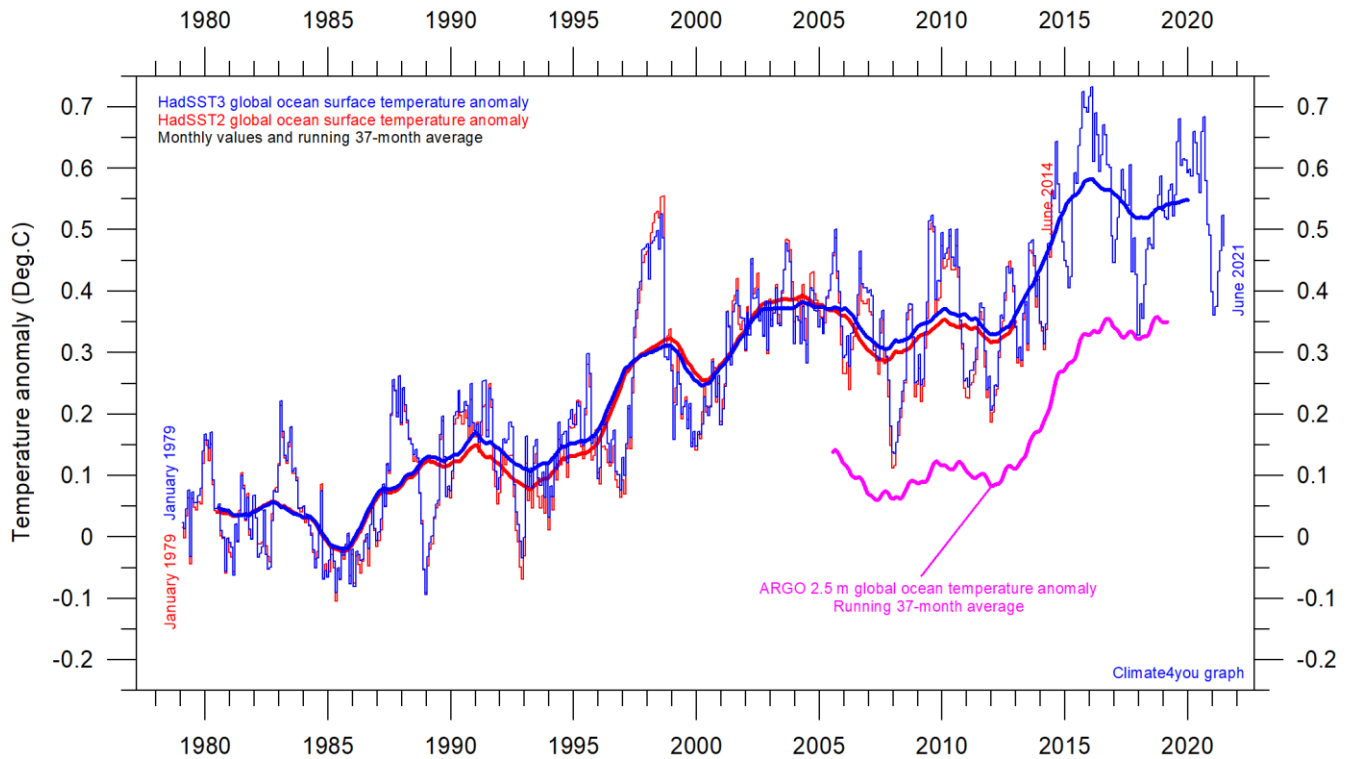
The significance of any short-term cooling or warming reflected in air temperatures should not be overstated. Whenever Earth experiences cold La Niña or warm El Niño episodes major heat exchanges take place between the Pacific Ocean and the atmosphere above, sooner or later showing up in estimates of the global air temperature.

However, this does not necessarily reflect similar changes in the total heat content of the atmosphere-ocean system. In fact, global net changes can be small and such heat exchanges may mainly reflect redistribution of energy between ocean and atmosphere. What matters is the overall temperature development when seen over several years.

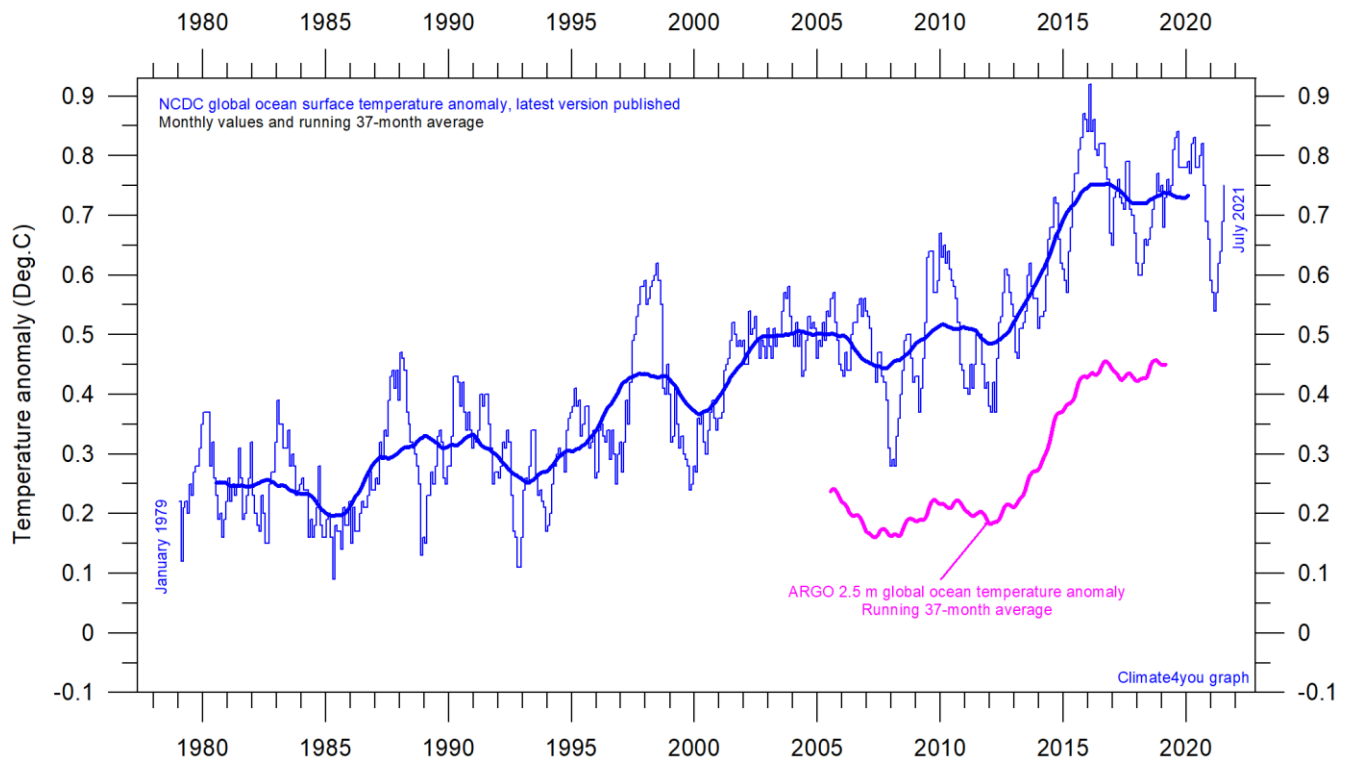


Global monthly average lower troposphere temperature over oceans (thin line) since 1979 according to [University of Alabama](#) at Huntsville, USA. The thick line is the simple running 37-month average. Insert: Argo global ocean temperature anomaly from floats, displaced vertically to make visual comparison easier. UAH reference period: 1991-2020.

16

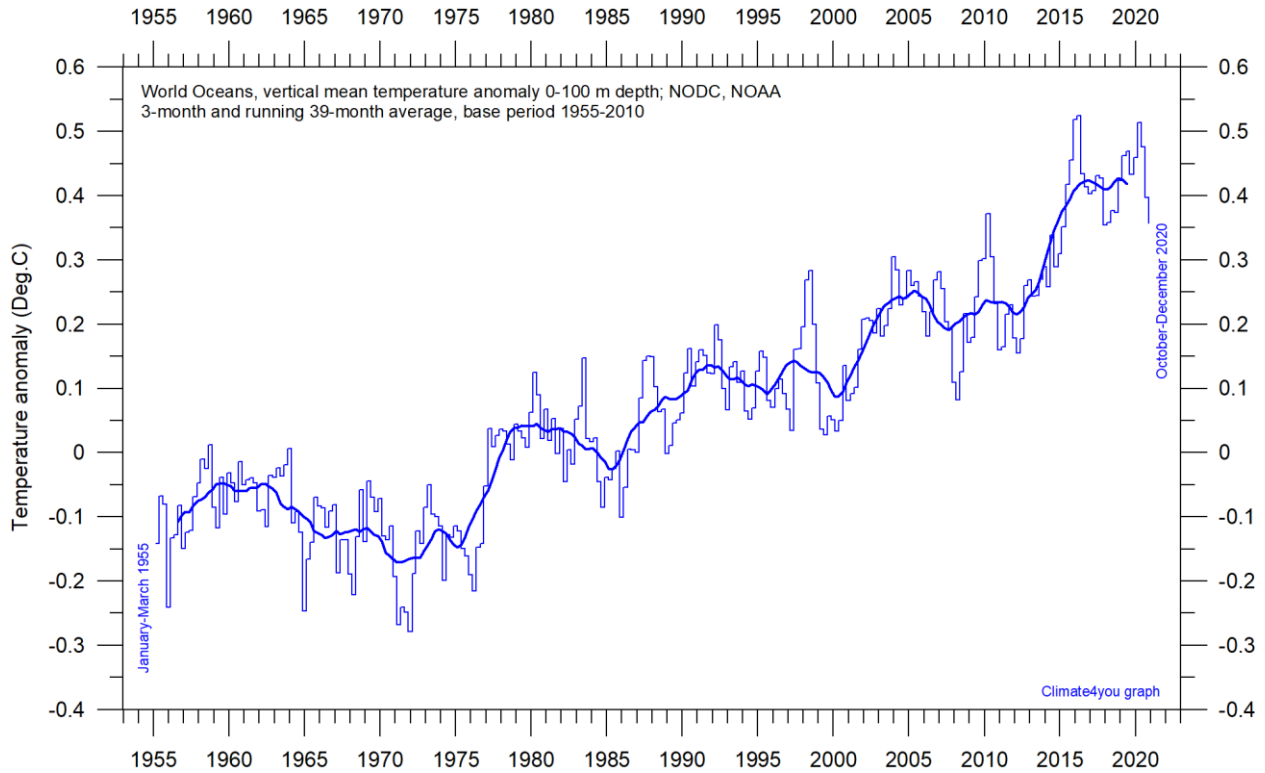


Global monthly average sea surface temperature since 1979 according to University of East Anglia's [Climatic Research Unit \(CRU\)](#), UK. Base period: 1961-1990. The thick line is the simple running 37-month average. Insert: Argo global ocean temperature anomaly from floats, displaced vertically to make visual comparison easier.



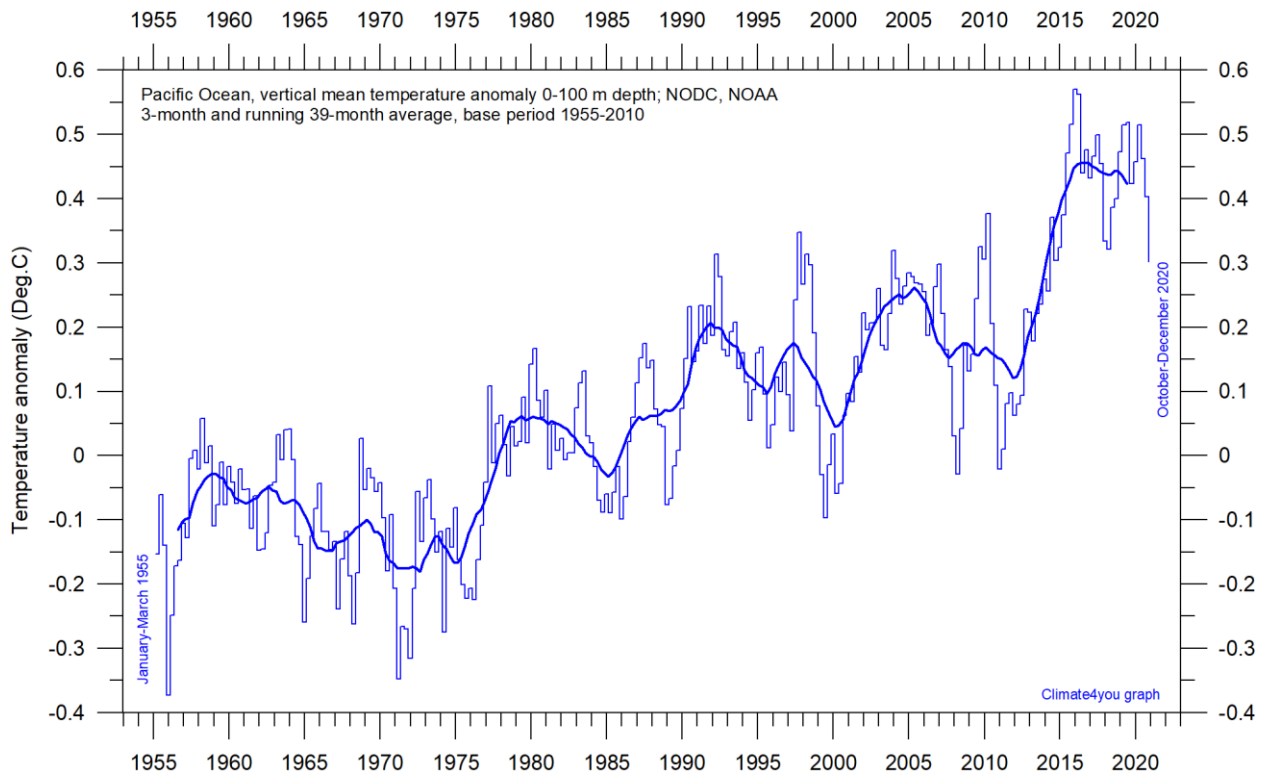
Global monthly average sea surface temperature since 1979 according to the [National Climatic Data Center \(NCDC\)](#), USA. Base period: 1901-2000. The thick line is the simple running 37-month average. Insert: Argo global ocean temperature anomaly from floats, displaced vertically to make visual comparison easier.

Ocean temperature in uppermost 100 m, updated to December 2020

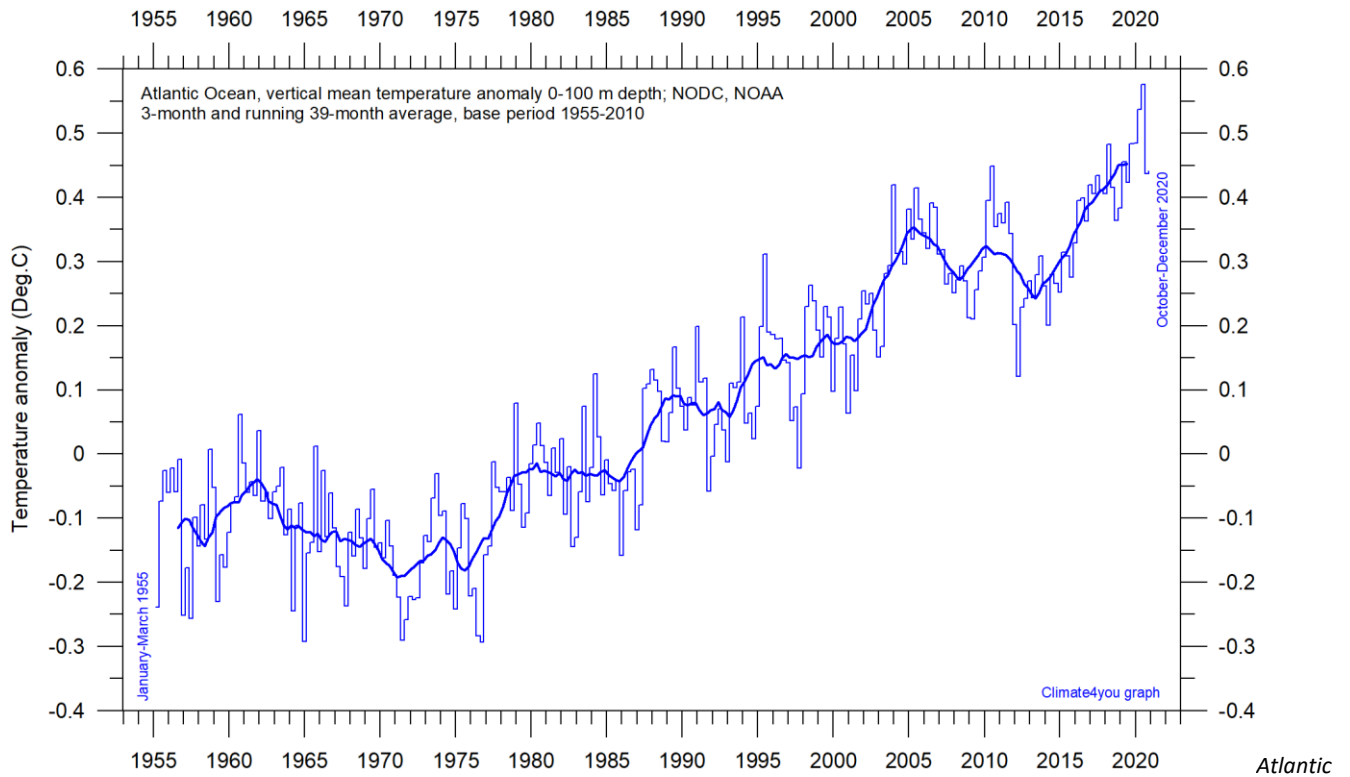


World Oceans vertical average temperature 0-100 m depth since 1955. The thin line indicates 3-month values, and the thick line represents the simple running 39-month (c. 3 year) average. Data source: [NOAA National Oceanographic Data Center \(NODC\)](#). Base period 1955-2010.

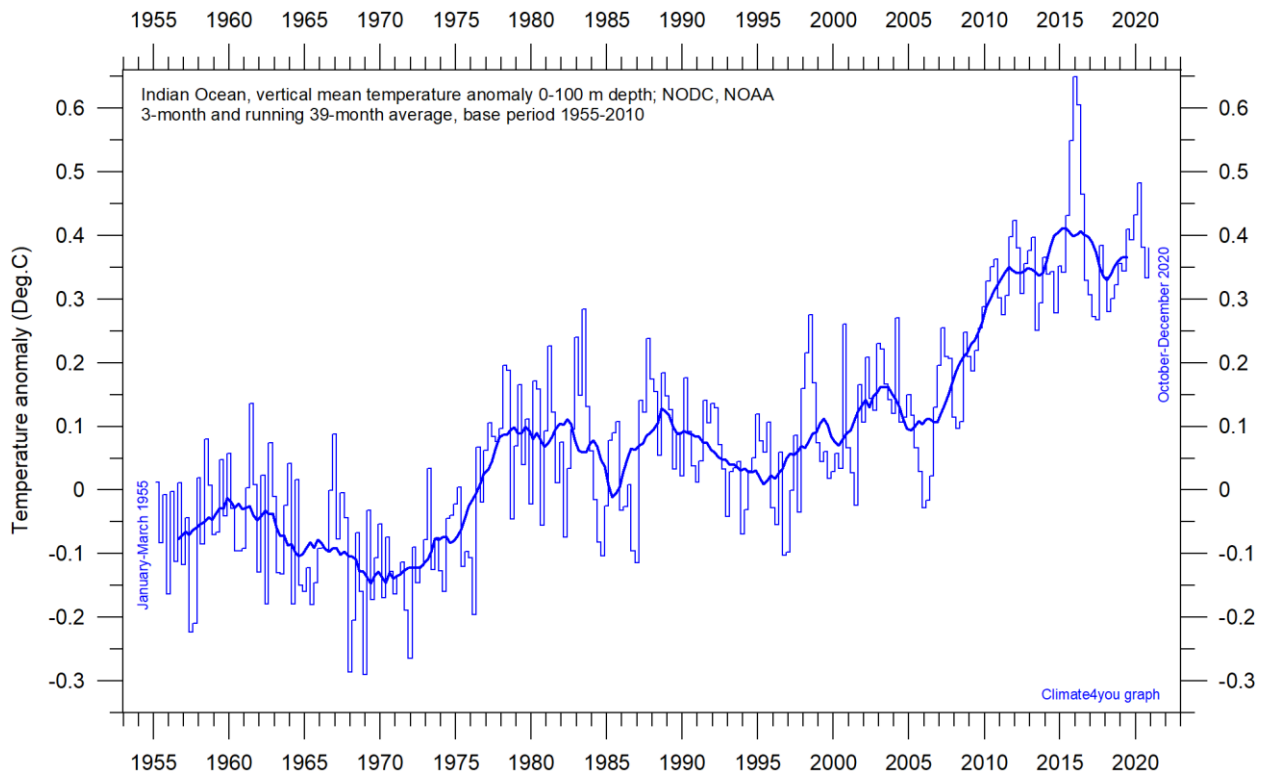
18



Pacific Ocean vertical average temperature 0-100 m depth since 1955. The thin line indicates 3-month values, and the thick line represents the simple running 39-month (c. 3 year) average. Data source: [NOAA National Oceanographic Data Center \(NODC\)](#). Base period 1955-2010.

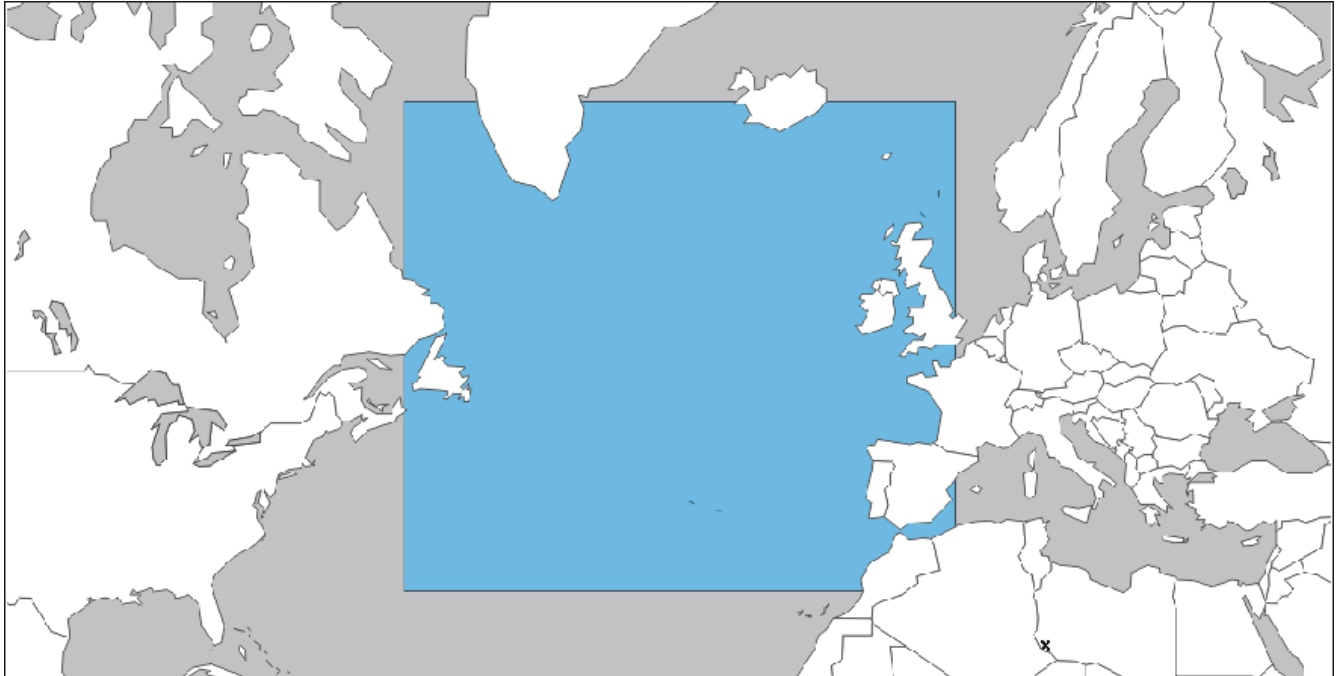


Atlantic Ocean vertical average temperature 0-100 m depth since 1955. The thin line indicates 3-month values, and the thick line represents the simple running 39-month (c. 3 year) average. Data source: [NOAA National Oceanographic Data Center \(NODC\)](https://www.noaa.gov/data/atlantic-ocean-temperature). Base period 1955-2010.

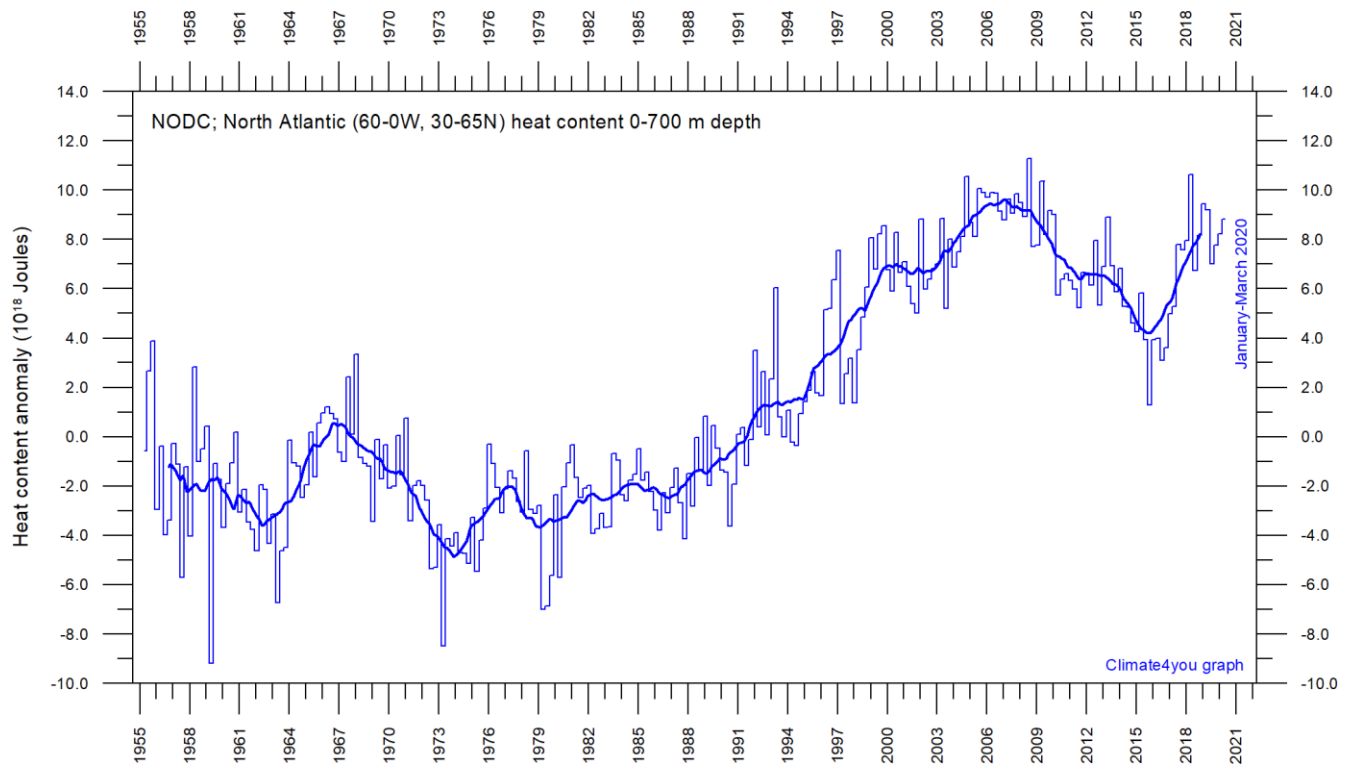


Indian Ocean vertical average temperature 0-100 m depth since 1955. The thin line indicates 3-month values, and the thick line represents the simple running 39-month (c. 3 year) average. Data source: [NOAA National Oceanographic Data Center \(NODC\)](https://www.noaa.gov/data/indian-ocean-temperature). Base period 1955-2010.

North Atlantic heat content uppermost 700 m, updated to March 2020

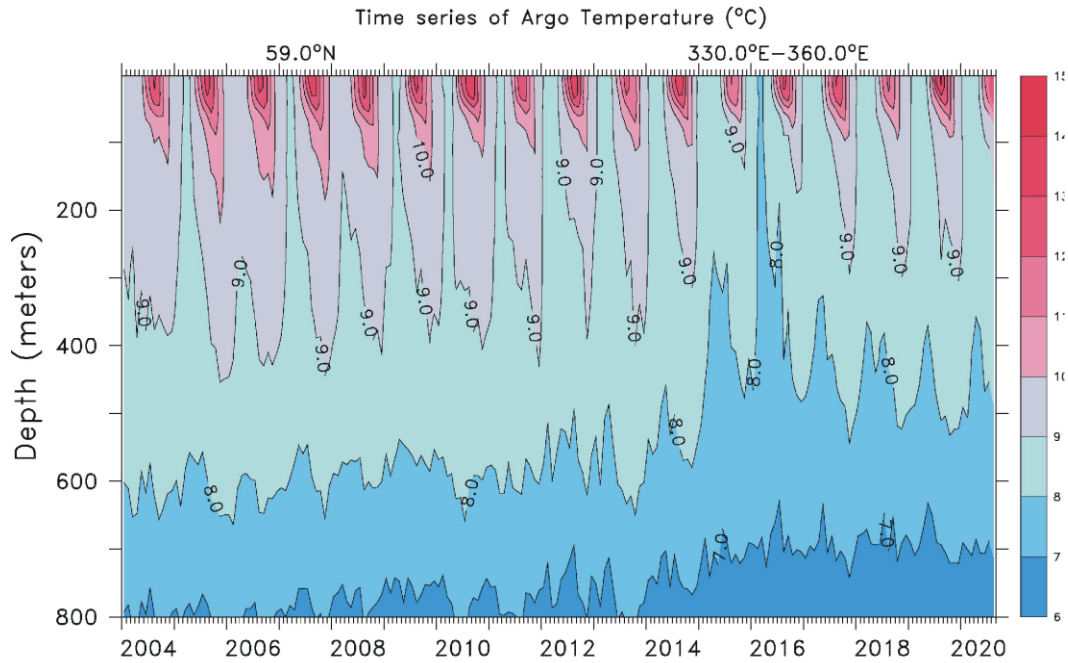


20



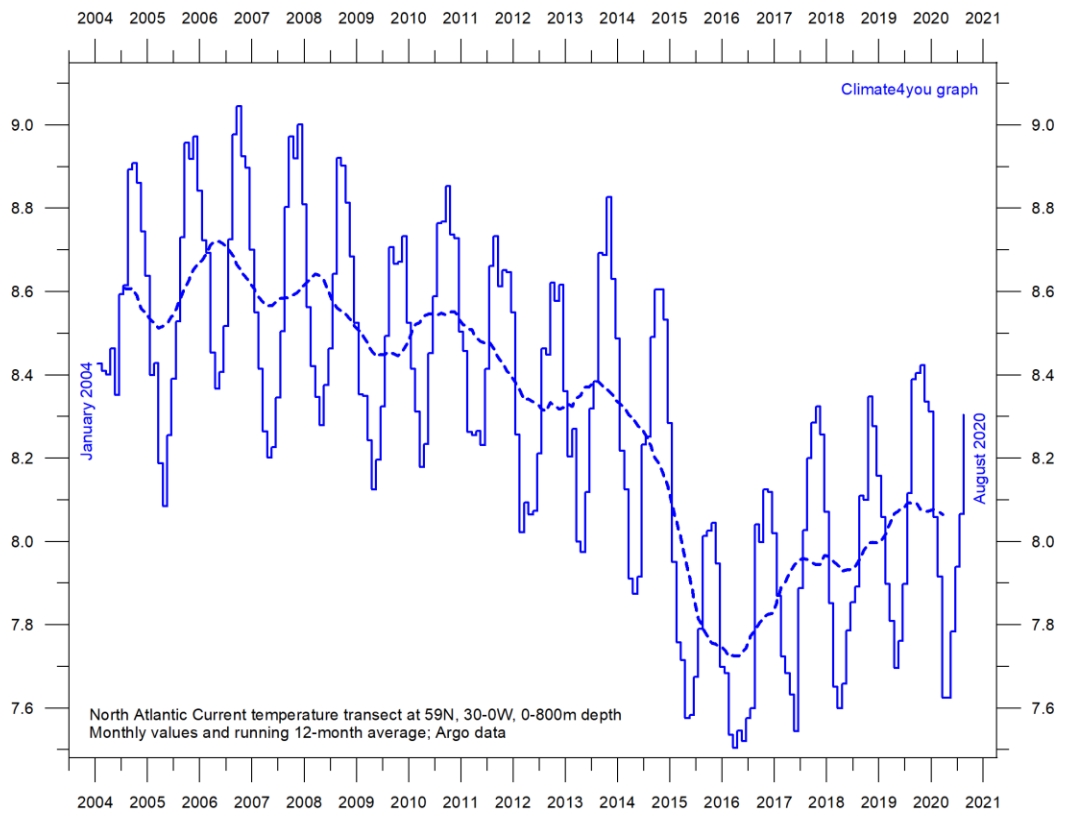
Global monthly heat content anomaly (10^{18} Joules) in the uppermost 700 m of the North Atlantic (60-0W, 30-65N; see map above) ocean since January 1955. The thin line indicates monthly values, and the thick line represents the simple running 37-month (c. 3 year) average. Data source: [National Oceanographic Data Center](#) (NODC).

North Atlantic temperatures 0-800 m depth along 59°N, 30-0W, updated to August 2020



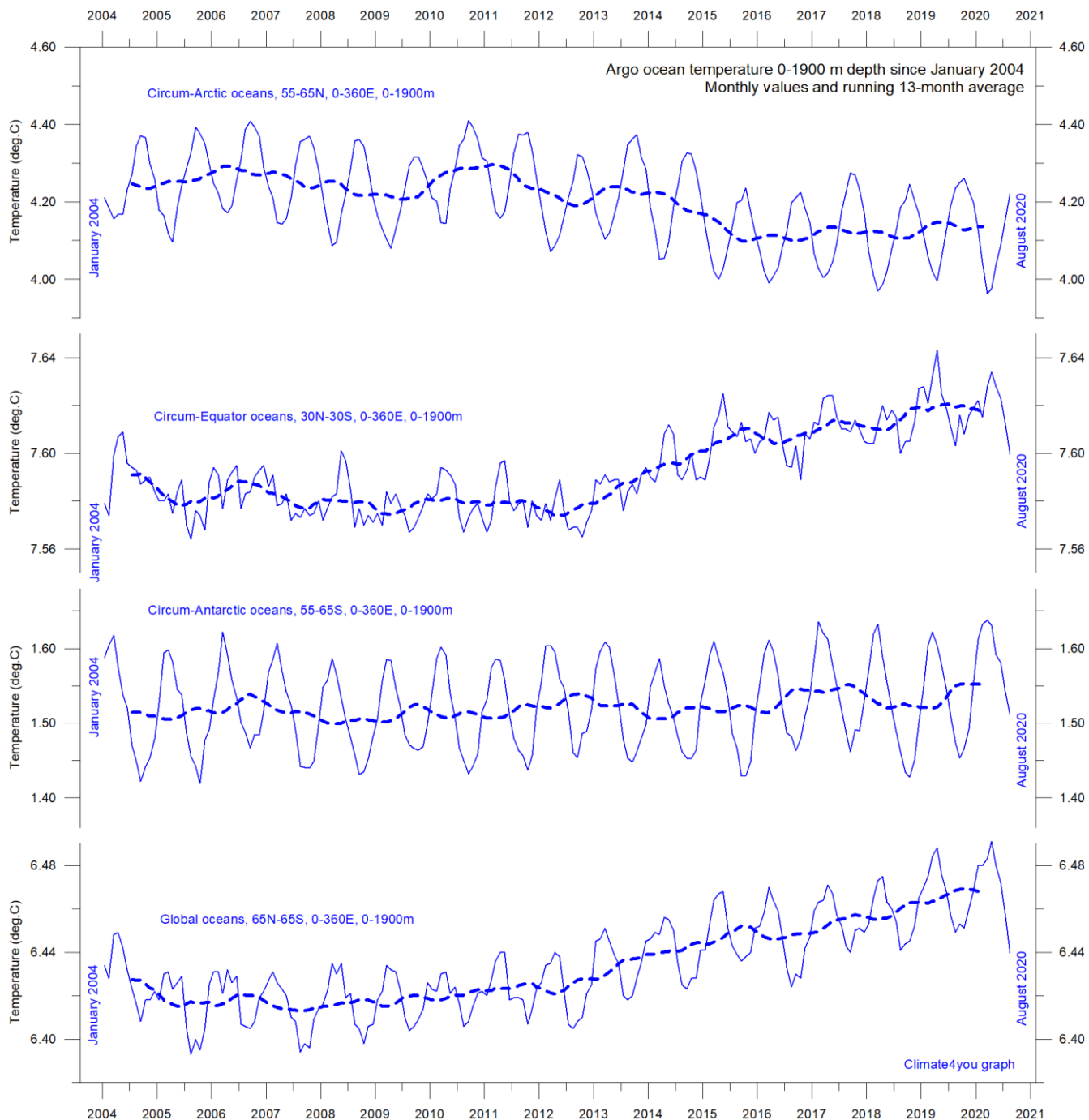
Time series depth-temperature diagram along 59 N across the North Atlantic Current from 30°W to 0°W, from surface to 800 m depth. Source: [Global Marine Argo Atlas](#). See also the diagram below.

21



Average temperature along 59 N, 30-0W, 0-800m depth, corresponding to the main part of the North Atlantic Current, using [Argo-data](#). Source: [Global Marine Argo Atlas](#). Additional information can be found in: Roemmich, D. and J. Gilson, 2009. The 2004-2008 mean and annual cycle of temperature, salinity, and steric height in the global ocean from the Argo Program. [Progress in Oceanography](#), 82, 81-100.

Global ocean temperature 0-1900 m depth summary, updated to August 2020

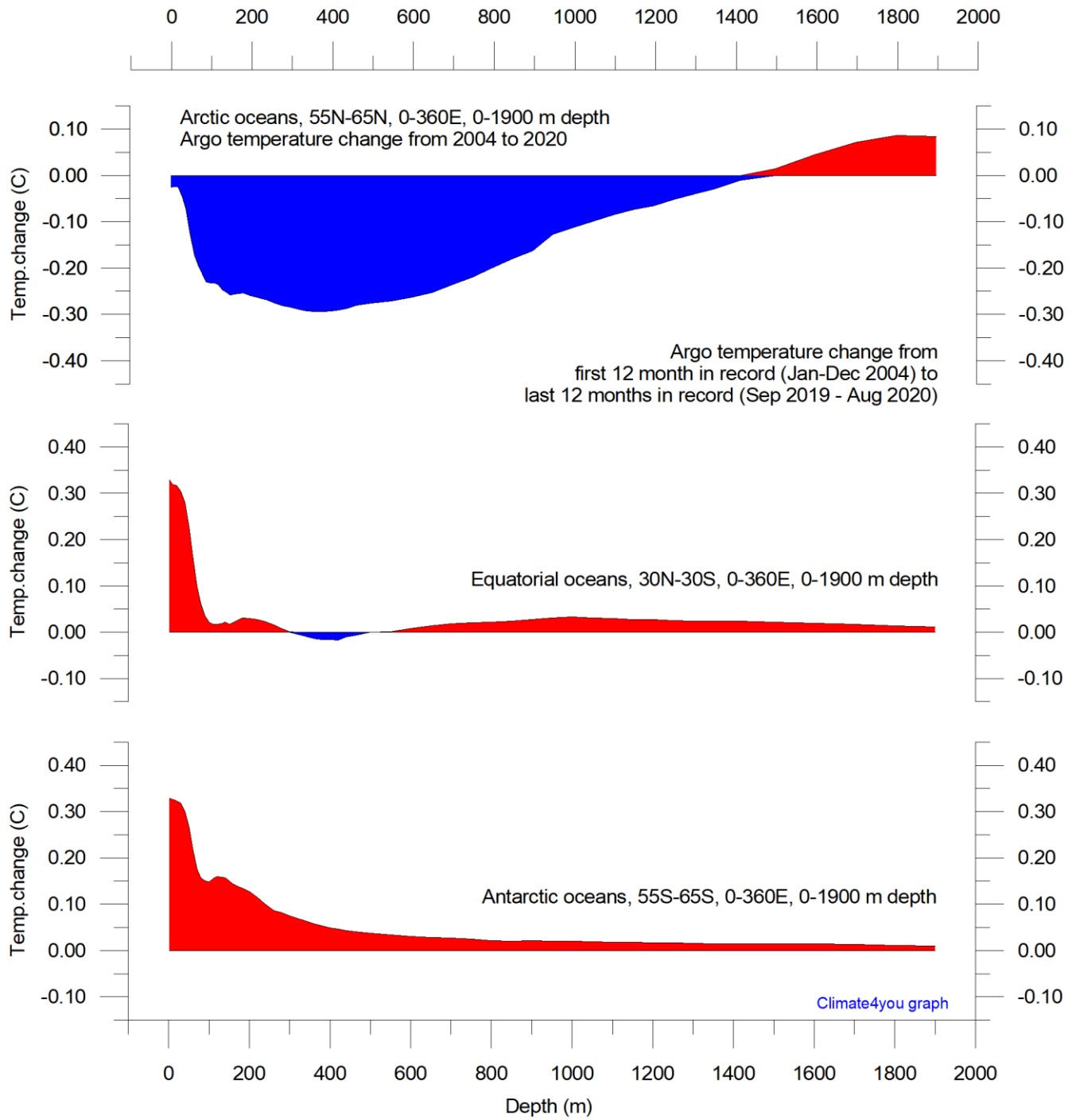


Summary of average temperature in uppermost 1900 m in different parts of the global oceans, using [Argo](#)-data. Source: [Global Marine Argo Atlas](#). Additional information can be found in: Roemmich, D. and J. Gilson, 2009. The 2004-2008 mean and annual cycle of temperature, salinity, and steric height in the global ocean from the Argo Program. [Progress in Oceanography](#), 82, 81-100.

The global summary diagram above shows that, on average, the temperature of the global oceans down to 1900 m depth has been increasing since about 2011. It is also seen that this increase since 2013 dominantly is due to oceanic changes occurring near the Equator, between

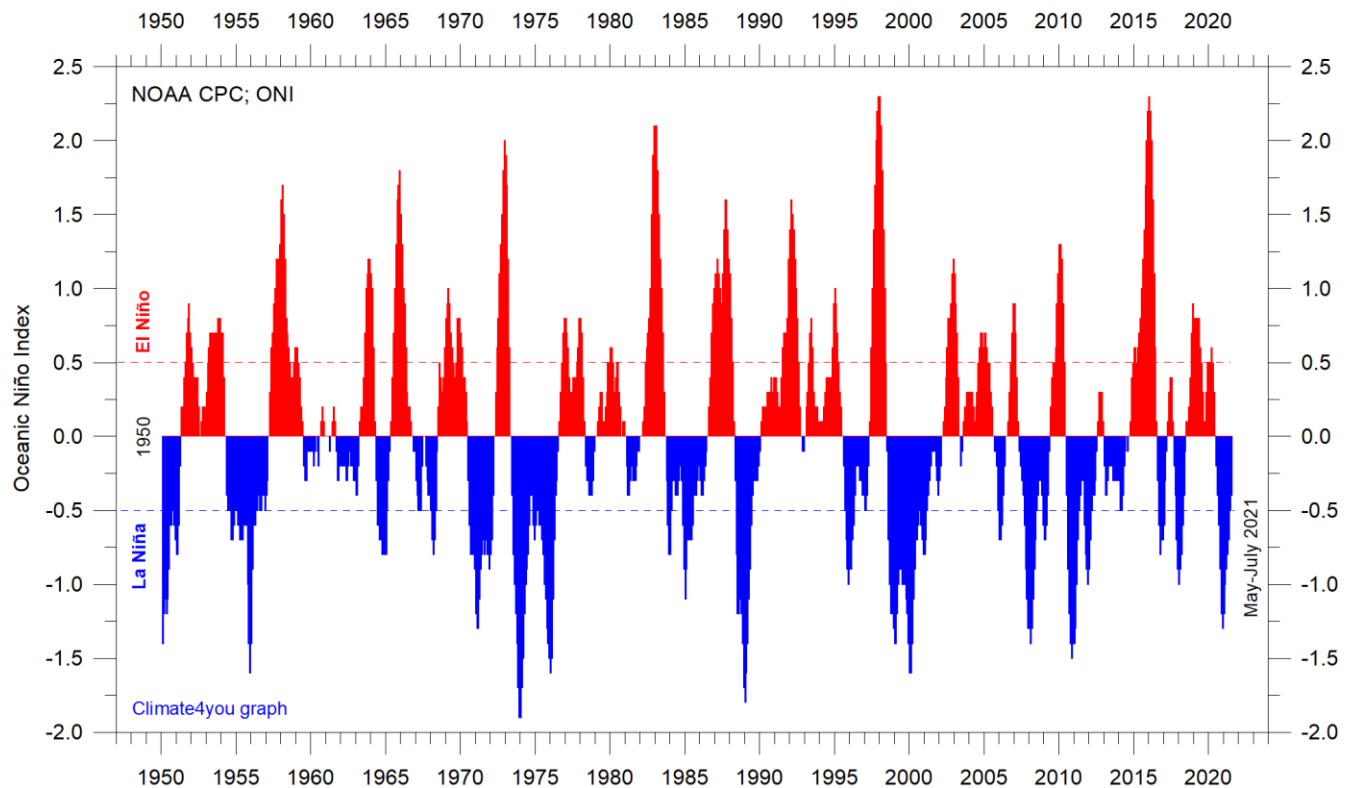
30°N and 30°S. In contrast, for the circum-Arctic oceans north of 55°N, depth-integrated ocean temperatures have been decreasing since 2011. Near the Antarctic, south of 55°S, temperatures have essentially been stable. At most latitudes, a clear annual rhythm is seen.

Global ocean net temperature change since 2004 at different depths, updated to August 2020



Net temperature change since 2004 from surface to 1900 m depth in different parts of the global oceans, using [Argo](#)-data. Source: [Global Marine Argo Atlas](#). Additional information can be found in: Roemmich, D. and J. Gilson, 2009. The 2004-2008 mean and annual cycle of temperature, salinity, and steric height in the global ocean from the Argo Program. [Progress in Oceanography](#), 82, 81-100. Please note that due to the spherical form of Earth, northern and southern latitudes represent only small ocean volumes, compared to latitudes near the Equator.

La Niña and El Niño episodes, Oceanic Niño Index (ONI), updated to July 2021



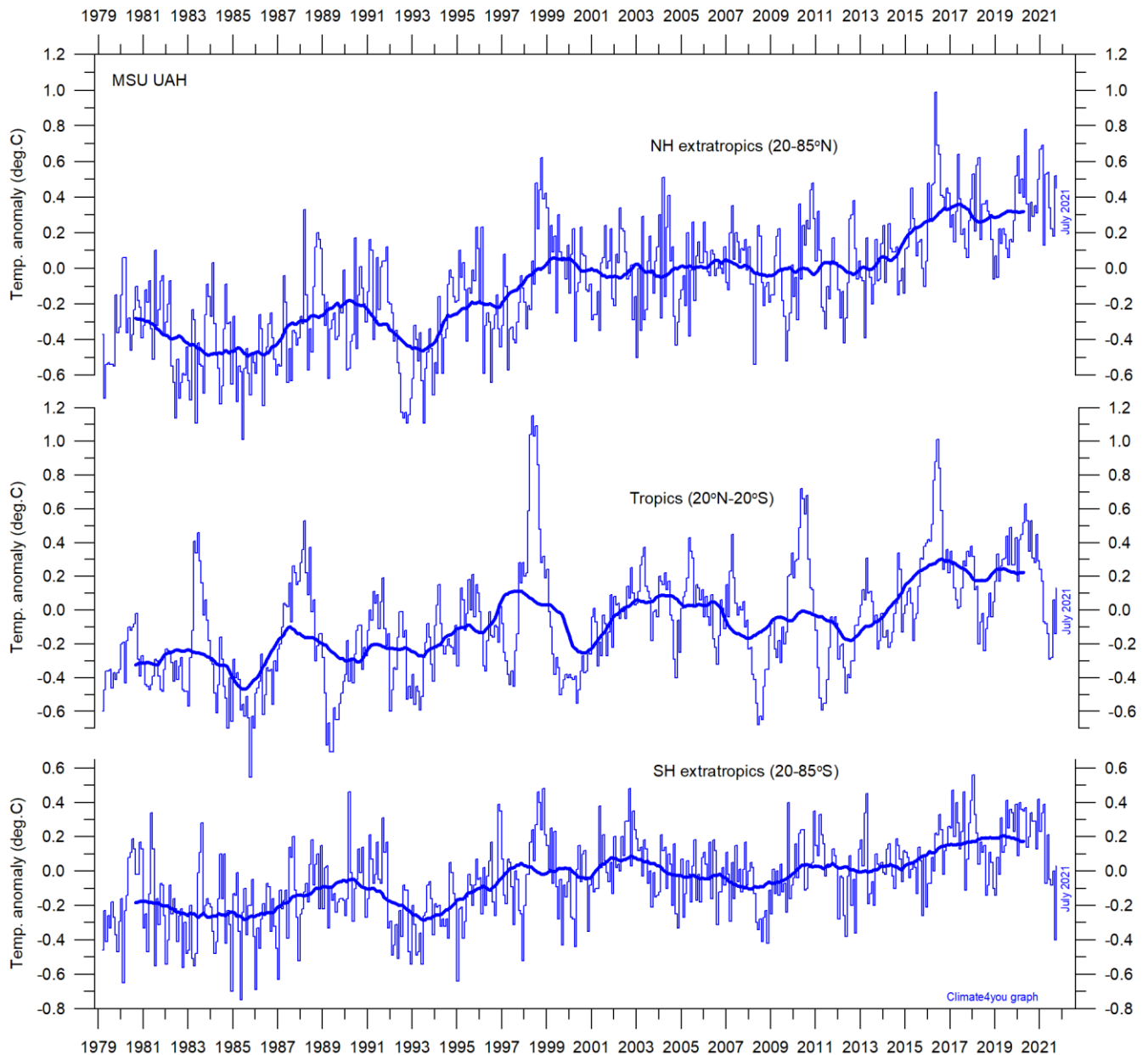
24

Warm ($>+0.5^{\circ}\text{C}$) and cold ($<-0.5^{\circ}\text{C}$) episodes for the [Oceanic Niño Index \(ONI\)](#), defined as 3 month running mean of ERSSTv4 SST anomalies in the Niño 3.4 region (5°N - 5°S , 120° - 170°W). For historical purposes cold and warm episodes are defined when the threshold is met for a minimum of 5 consecutive over-lapping seasons. Anomalies are centred on 30-yr base periods updated every 5 years.

The subrecent 2015-16 El Niño episode is among the strongest since the beginning of the record in 1950. Considering the entire record, however, recent

variations between El Niño and La Niña episodes do not appear abnormal in any way. See also diagrams on pages 43 and 52.

Zonal lower troposphere temperatures from satellites, updated to July 2021



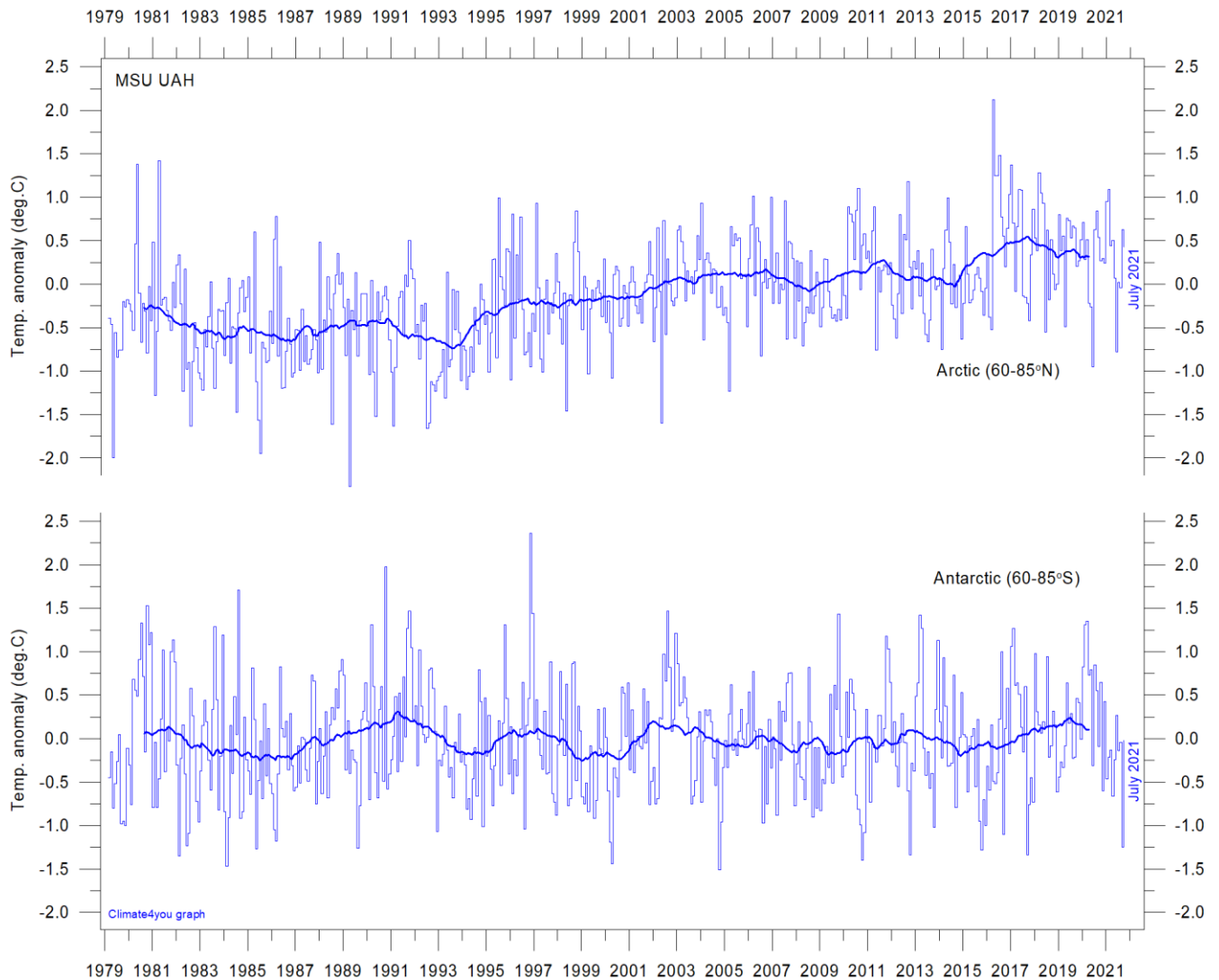
25

Global monthly average lower troposphere temperature since 1979 for the tropics and the northern and southern extratropics, according to University of Alabama at Huntsville, USA. Thin lines show the monthly temperature. Thick lines represent the simple running 37-month average, nearly corresponding to a running 3-year average. Reference period 1981-2010.

The overall warming since 1980 has dominantly been a northern hemisphere phenomenon, and mainly played out as a marked step change between 1994 and 1999. However, this rather rapid temperature change is influenced by the Mt. Pinatubo eruption 1992-93 and the

subsequent 1997 El Niño episode. The diagram also shows the temperature effects of the strong Equatorial El Niño's in 1997 and 2015-16, as well as the moderate El Niño in 2019. Apparently, these effects were spreading to higher latitudes in both hemispheres with some delay.

Arctic and Antarctic lower troposphere temperature, updated to July 2021



Global monthly average lower troposphere temperature since 1979 for the North Pole and South Pole regions, based on satellite observations ([University of Alabama](#) at Huntsville, USA). Thin lines show the monthly temperature. The thick line is the simple running 37-month average, nearly corresponding to a running 3-year average. Reference period 1991-2020.

In the Arctic region, warming mainly took place 1994-96, and less so subsequently. In 2016, however, temperatures peaked for several months, presumably because of oceanic heat given off to the atmosphere during the 2015-15 El Niño (see also figure on page 24) and subsequently advected to higher latitudes.

This underscores how Arctic air temperatures may be affected not only by variations in local conditions but also by variations playing out in geographically remote

regions. A small overall temperature decrease has characterised the Arctic since the 2016 peak (see also diagrams on page 29-31).

In the Antarctic region, temperatures have basically remained stable since the onset of the satellite record in 1979. In 2016-17 a small temperature peak visible in the monthly record may be interpreted as the subdued effect of the recent El Niño episode.

Arctic and Antarctic surface air temperature, updated to June 2021

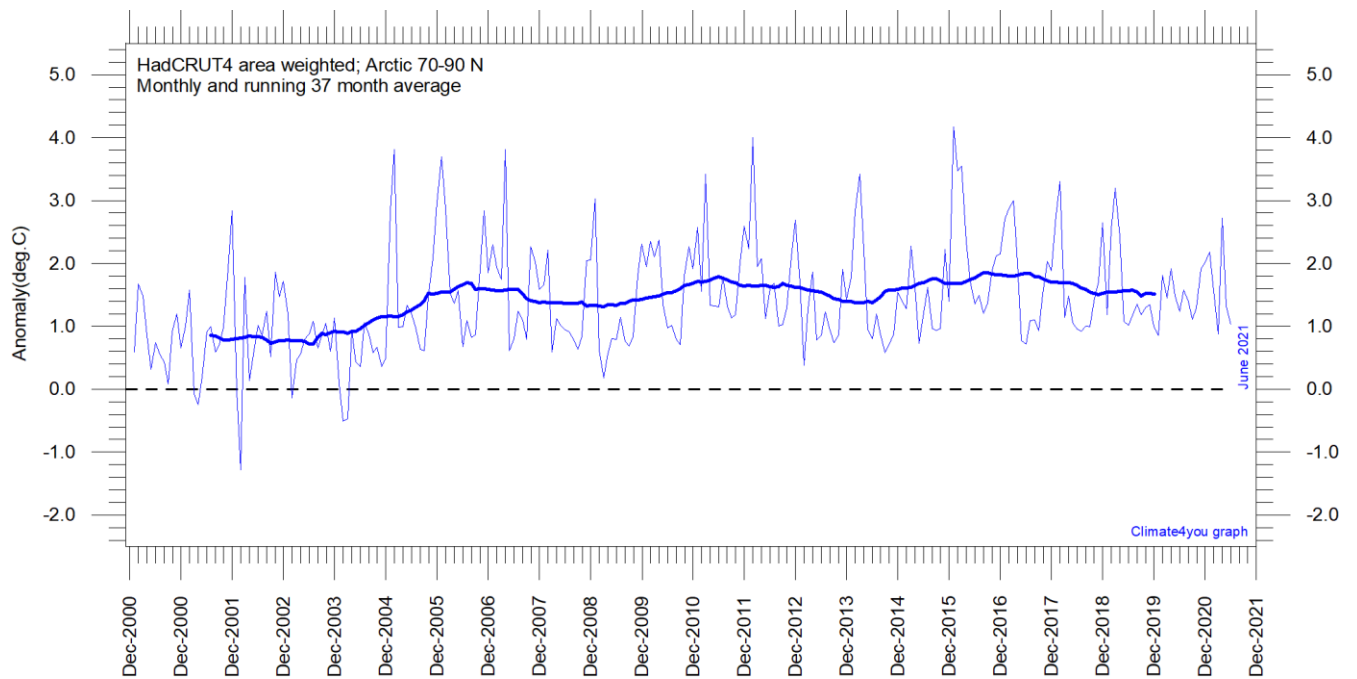


Diagram showing area weighted Arctic (70-90°N) monthly surface air temperature anomalies ([HadCRUT4](#)) since January 2000, in relation to the WMO [normal period](#) 1961-1990. The thin line shows the monthly temperature anomaly, while the thicker line shows the running 37-month (c. 3 year) average.

27

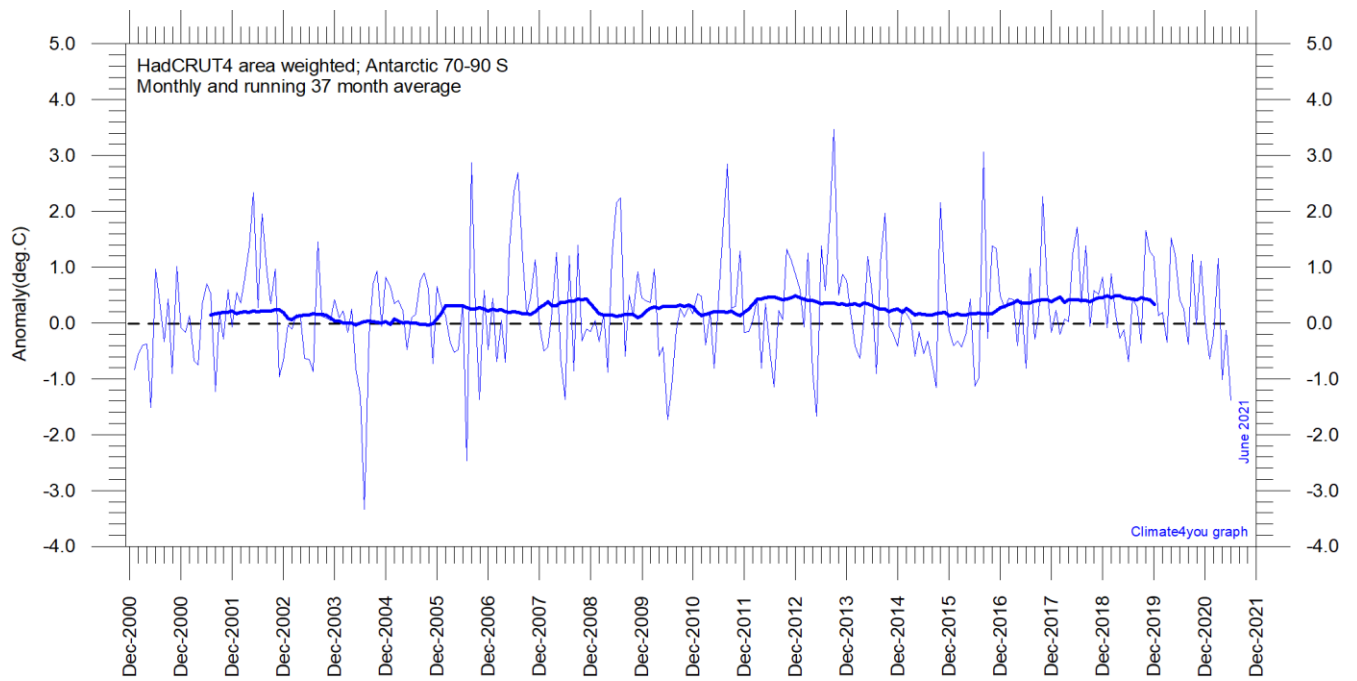


Diagram showing area weighted Antarctic (70-90°S) monthly surface air temperature anomalies ([HadCRUT4](#)) since January 2000, in relation to the WMO [normal period](#) 1961-1990. The thin line shows the monthly temperature anomaly, while the thicker line shows the running 37-month (c. 3 year) average.

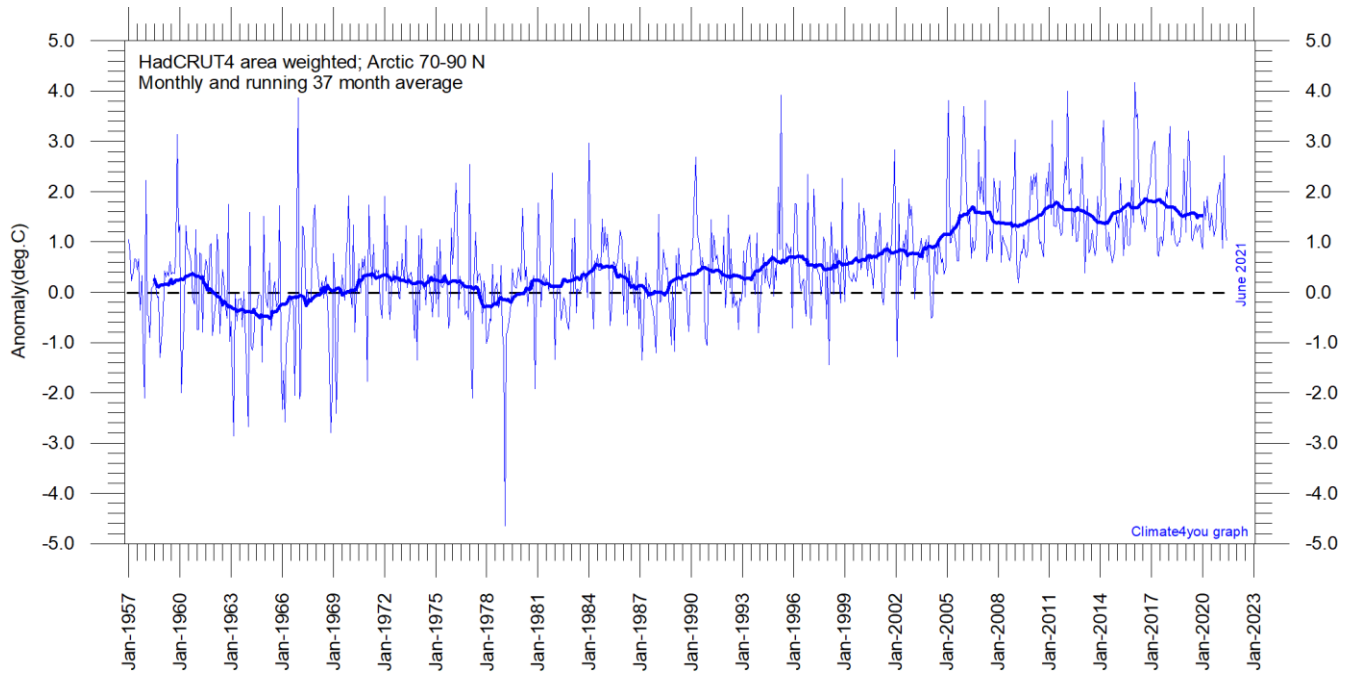


Diagram showing area weighted Arctic (70-90°N) monthly surface air temperature anomalies ([HadCRUT4](#)) since January 1957, in relation to the WMO [normal period](#) 1961-1990. The thin line shows the monthly temperature anomaly, while the thicker line shows the running 37-month (c. 3 year) average.

28

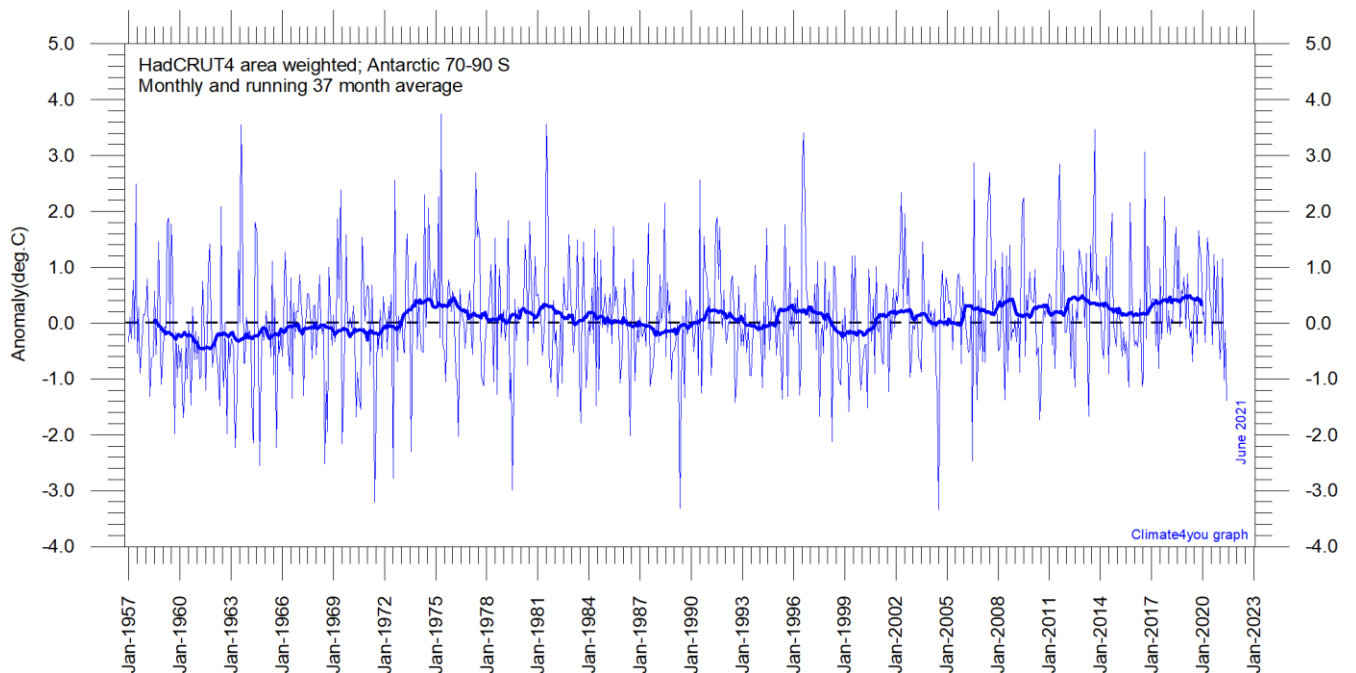


Diagram showing area weighted Antarctic (70-90°S) monthly surface air temperature anomalies ([HadCRUT4](#)) since January 1957, in relation to the WMO [normal period](#) 1961-1990. The thin line shows the monthly temperature anomaly, while the thicker line shows the running 37-month (c. 3 year) average.

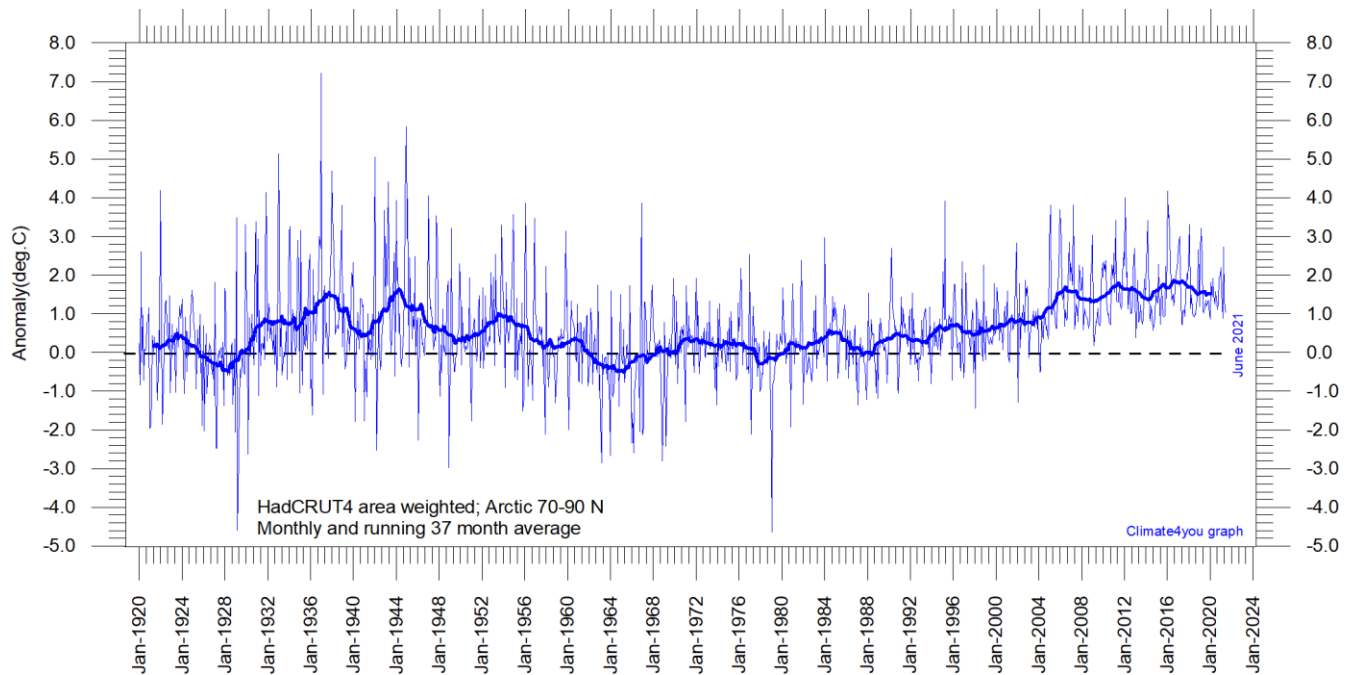


Diagram showing area-weighted Arctic (70-90°N) monthly surface air temperature anomalies ([HadCRUT4](#)) since January 1920, in relation to the WMO [normal period](#) 1961-1990. The thin line shows the monthly temperature anomaly, while the thicker line shows the running 37-month (c. 3 year) average.

Because of the relatively small number of Arctic stations before 1930, month-to-month variations in the early part of the Arctic temperature record 1920-2018 are bigger than later (diagram above).

The period from about 1930 saw the establishment of many new Arctic meteorological stations, first in Russia and Siberia, and following the 2nd World War, also in North America, explaining the above difference.

The period since 2005 is warm, about as warm as the period 1930-1940.

As the HadCRUT4 data series has improved high latitude coverage data coverage (compared to the HadCRUT3 series), the individual 5°x5° grid cells have been weighted according to their surface area. This area correction is especially important for polar regions, where longitudes

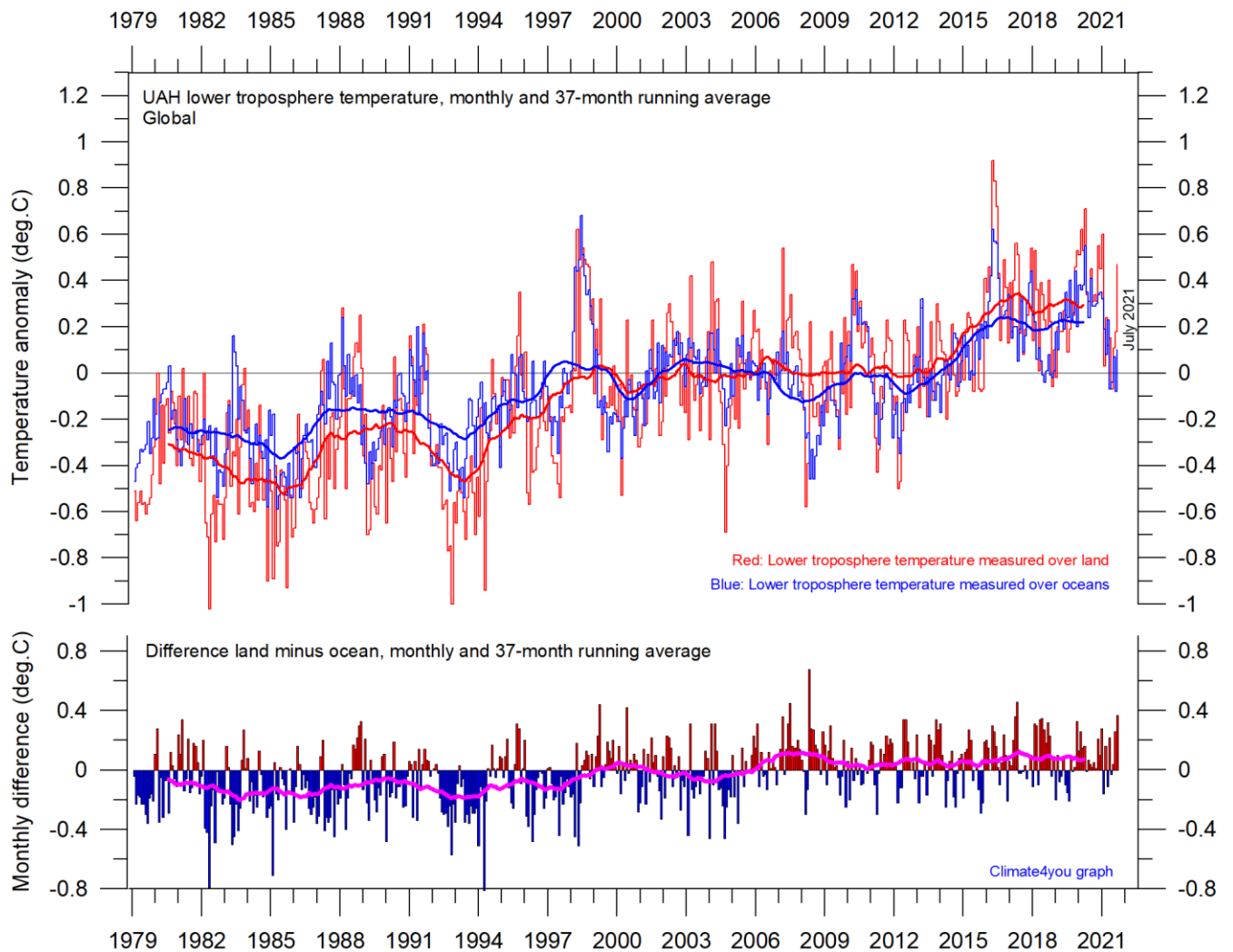
converge rapidly. This approach differs from the approach used by Gillett et al. 2008, which calculated a simple average, with no correction for the substantial latitudinal surface area effect in polar regions.

The area weighted HadCRUT4 surface air temperature records (p.29-31) correspond rather well to the lower troposphere temperature records recorded by satellites (p.27).

Literature:

Gillett, N.P., Stone, D.A., Stott, P.A., Nozawa, T., Karpechko, A.Y.U., Hegerl, G.C., Wehner, M.F. and Jones, P.D. 2008. Attribution of polar warming to human influence. *Nature Geoscience* 1, 750-754.

Temperature over land versus over oceans, updated to July 2021

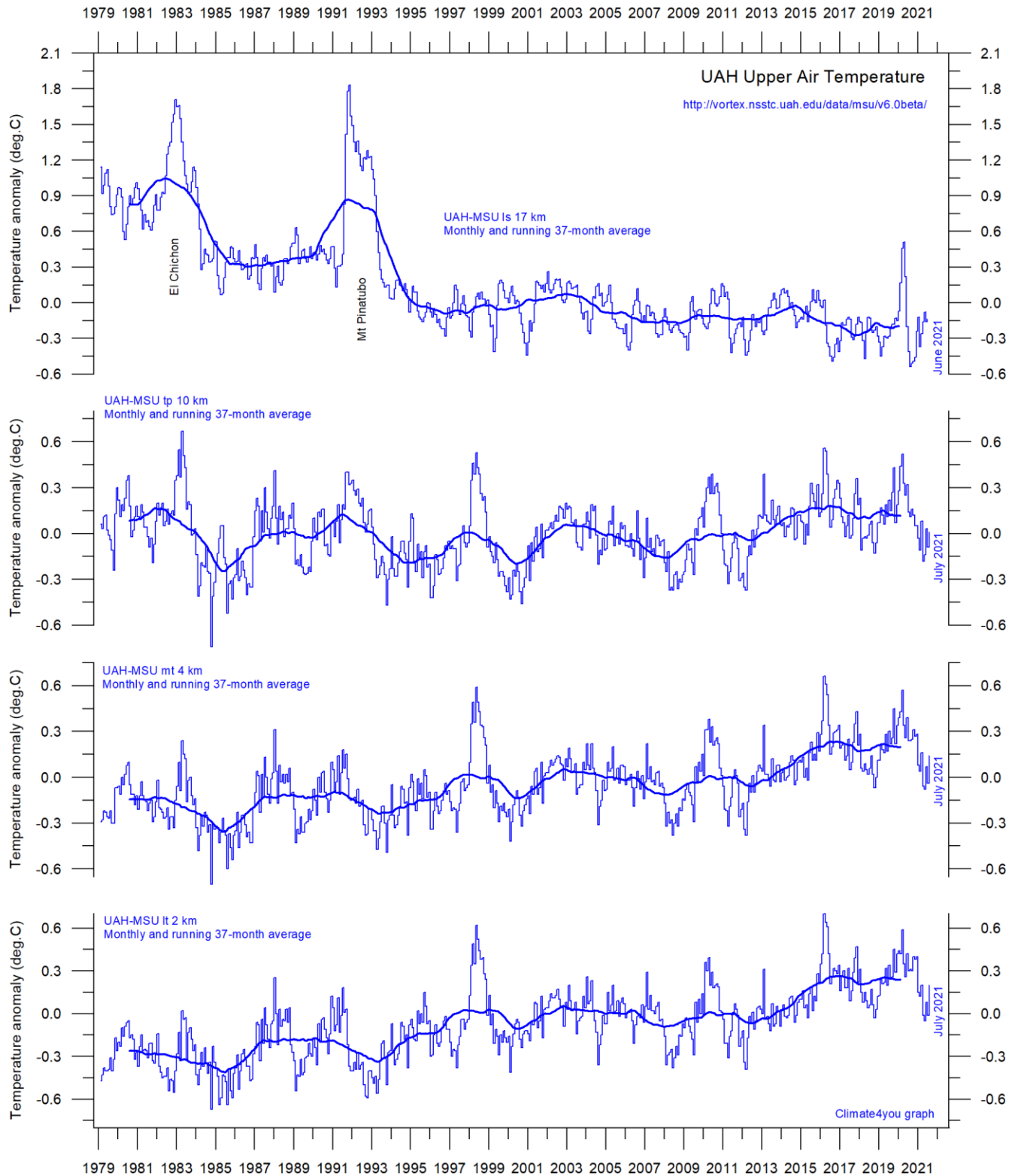


Global monthly average lower troposphere temperature since 1979 measured over land and oceans, respectively, according to [University of Alabama](#) at Huntsville, USA. Thick lines are the simple running 37-month average, nearly corresponding to a running 3-year average. Reference period 1991-2020.

Since 1979, the lower troposphere over land has warmed much more than over oceans, suggesting that the overall warming is derived mainly from incoming solar radiation.

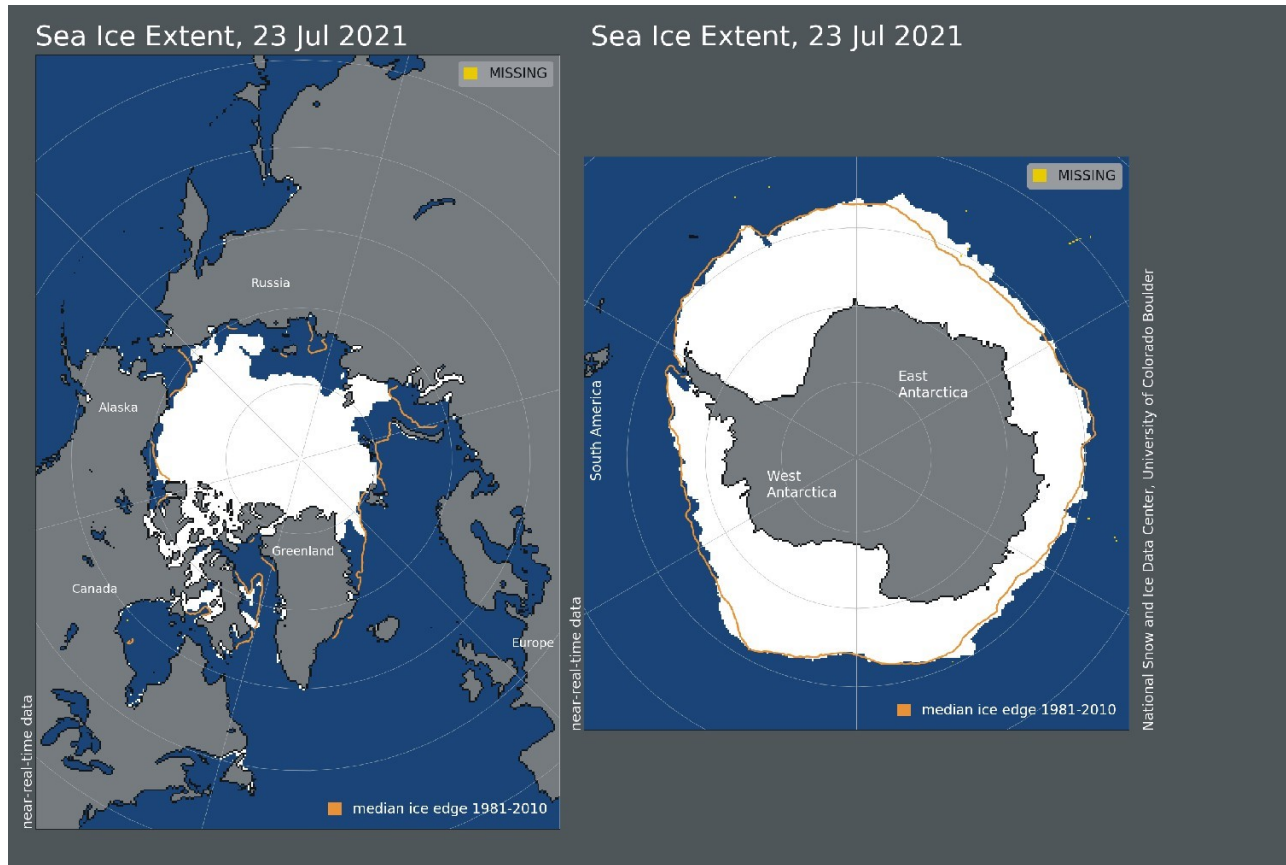
In addition, there may be supplementary reasons for this divergence, such as, e.g., variations in cloud cover and changes in land use.

Troposphere and stratosphere temperatures from satellites, updated to July 2021



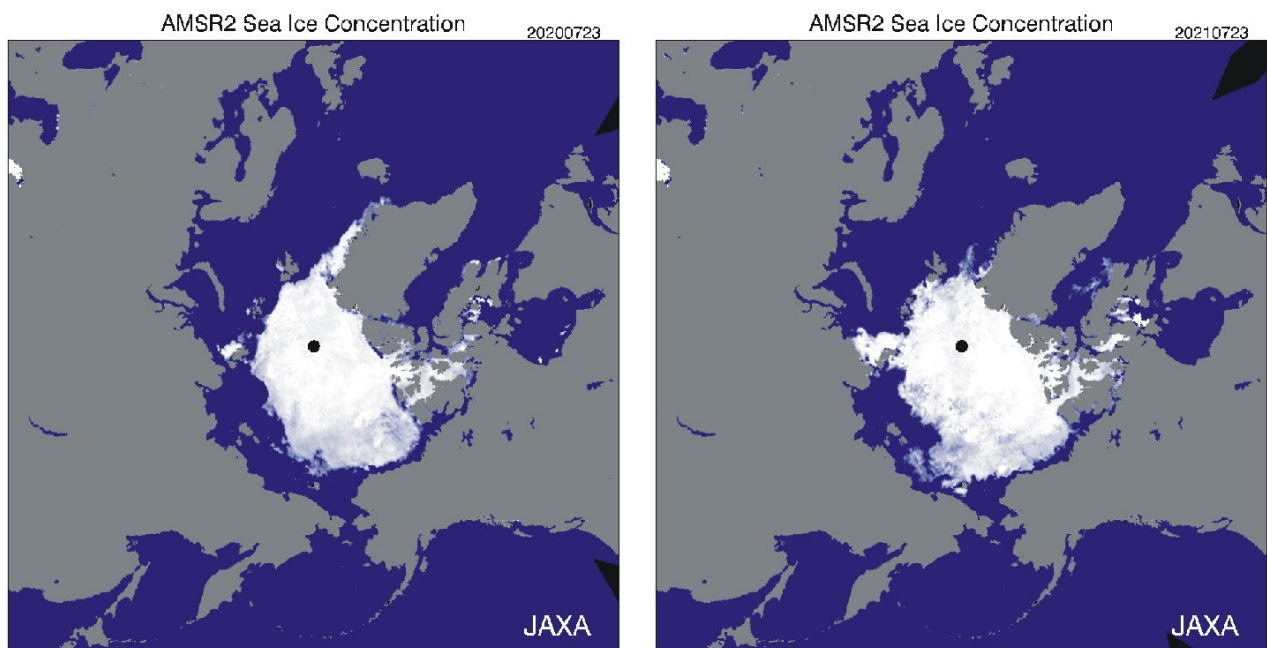
Global monthly average temperature in different according to University of Alabama at Huntsville, USA. The thin lines represent the monthly average, and the thick line the simple running 37-month average, nearly corresponding to a running 3-year average. Reference period 1991-2020.

Arctic and Antarctic sea ice, updated to July 2021

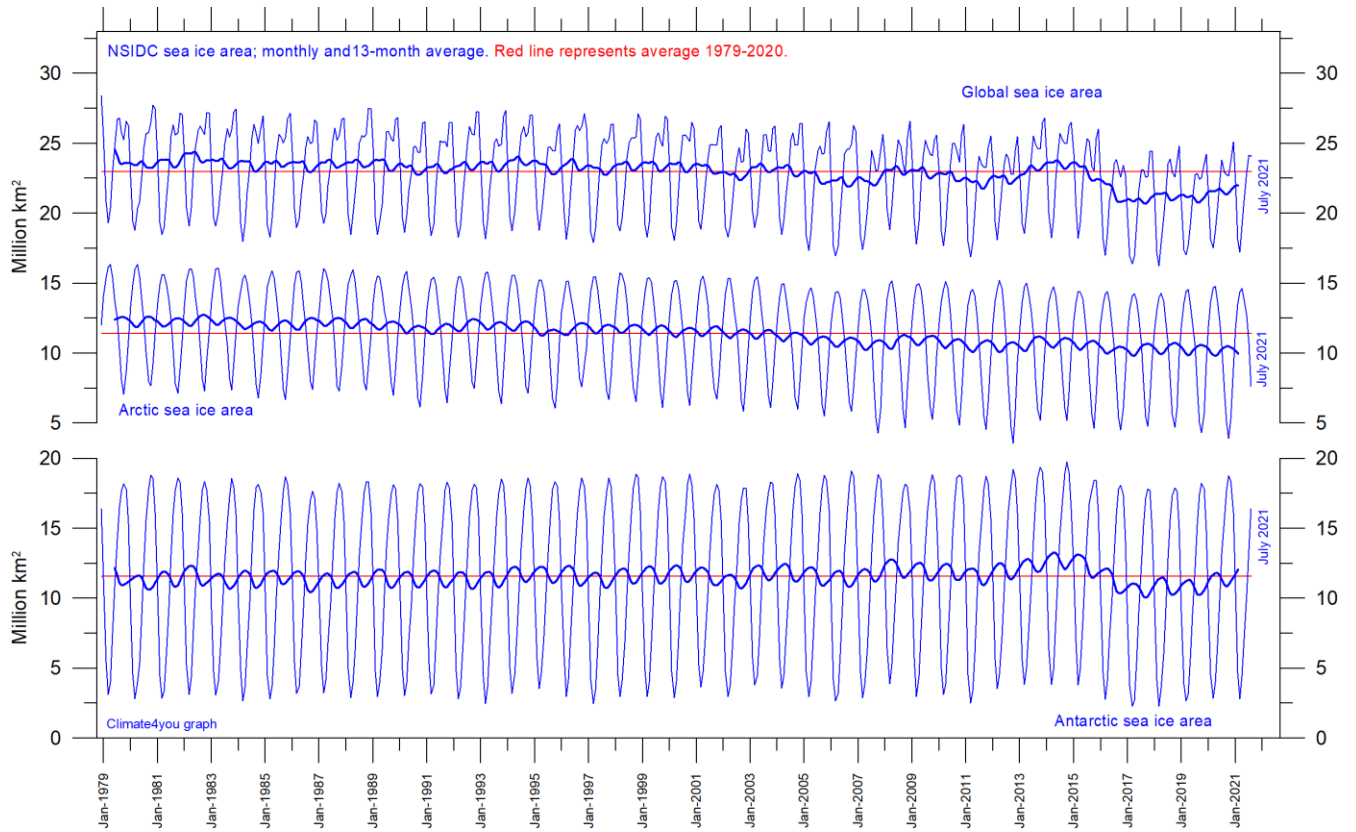


32

Sea ice extent 23 July 2021. The median limit of sea ice (orange line) is defined as 15% sea ice cover, according to the average of satellite observations 1981-2010 (both years included). Sea ice may therefore well be encountered outside and open water areas inside the limit shown in the diagrams above. Map source: National Snow and Ice Data Center (NSIDC).



Diagrams showing Arctic sea ice extent and concentration 23 July 2020 (left) and 2021 (right), according to the Japan Aerospace Exploration Agency (JAXA).



Graphs showing monthly Antarctic, Arctic, and global sea ice extent since November 1978, according to the [National Snow and Ice data Center \(NSIDC\)](#).

33

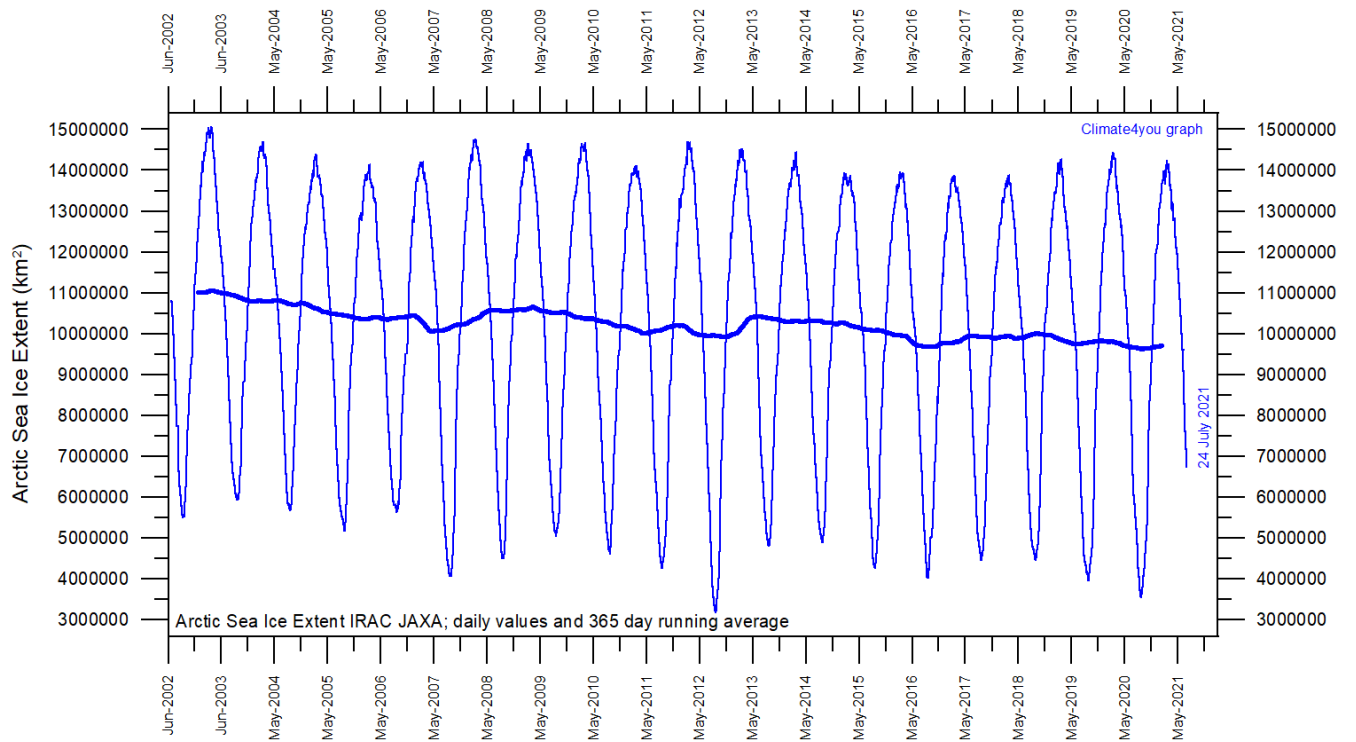
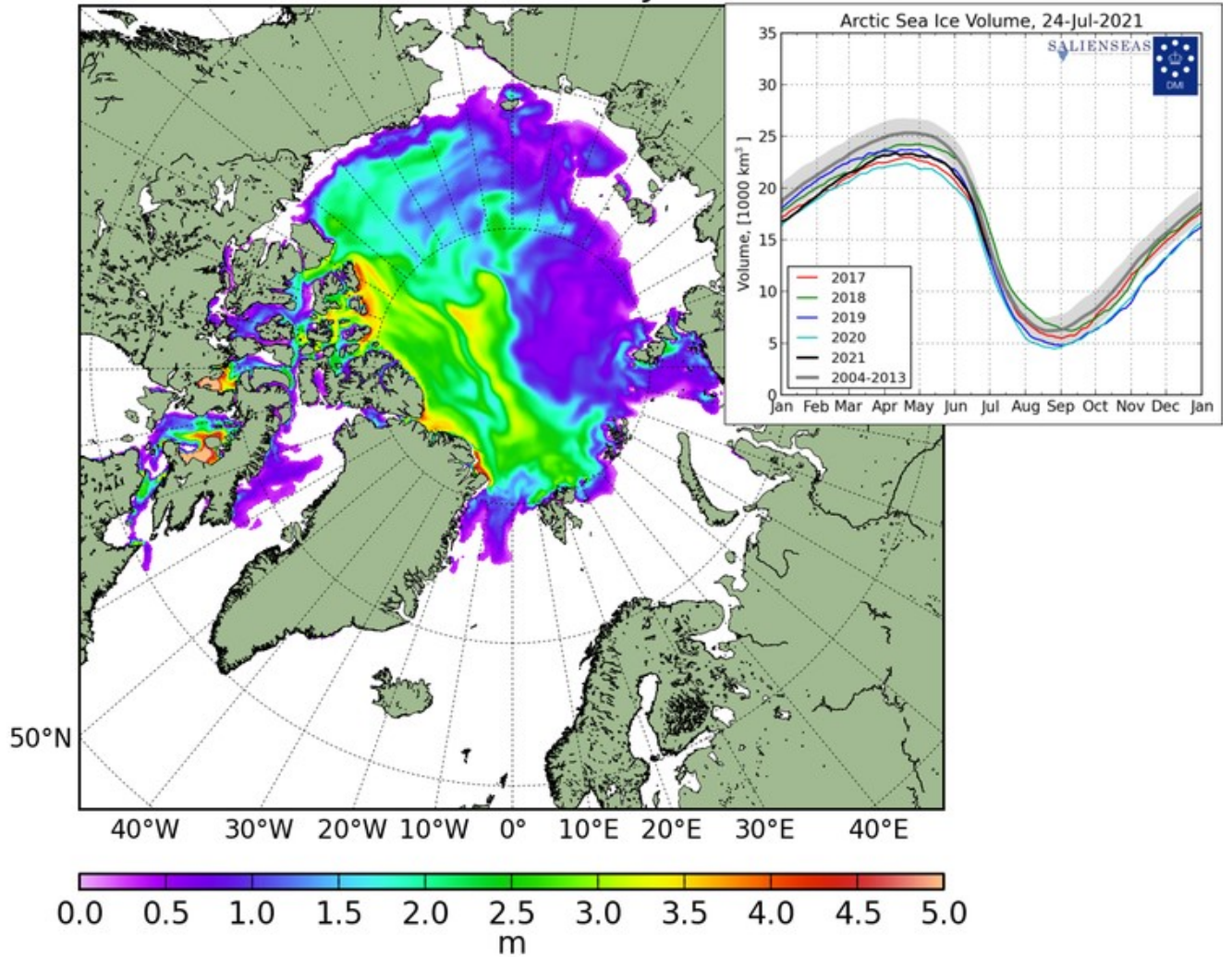
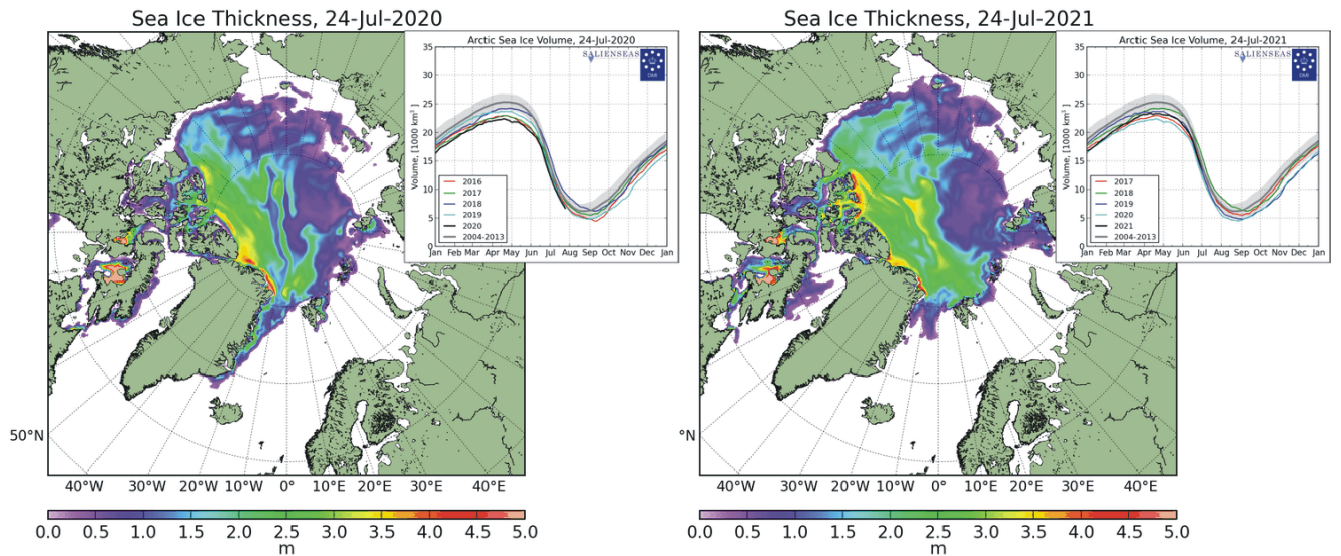


Diagram showing daily Arctic sea ice extent since June 2002, to 24 July 2021, by courtesy of [Japan Aerospace Exploration Agency \(JAXA\)](#).

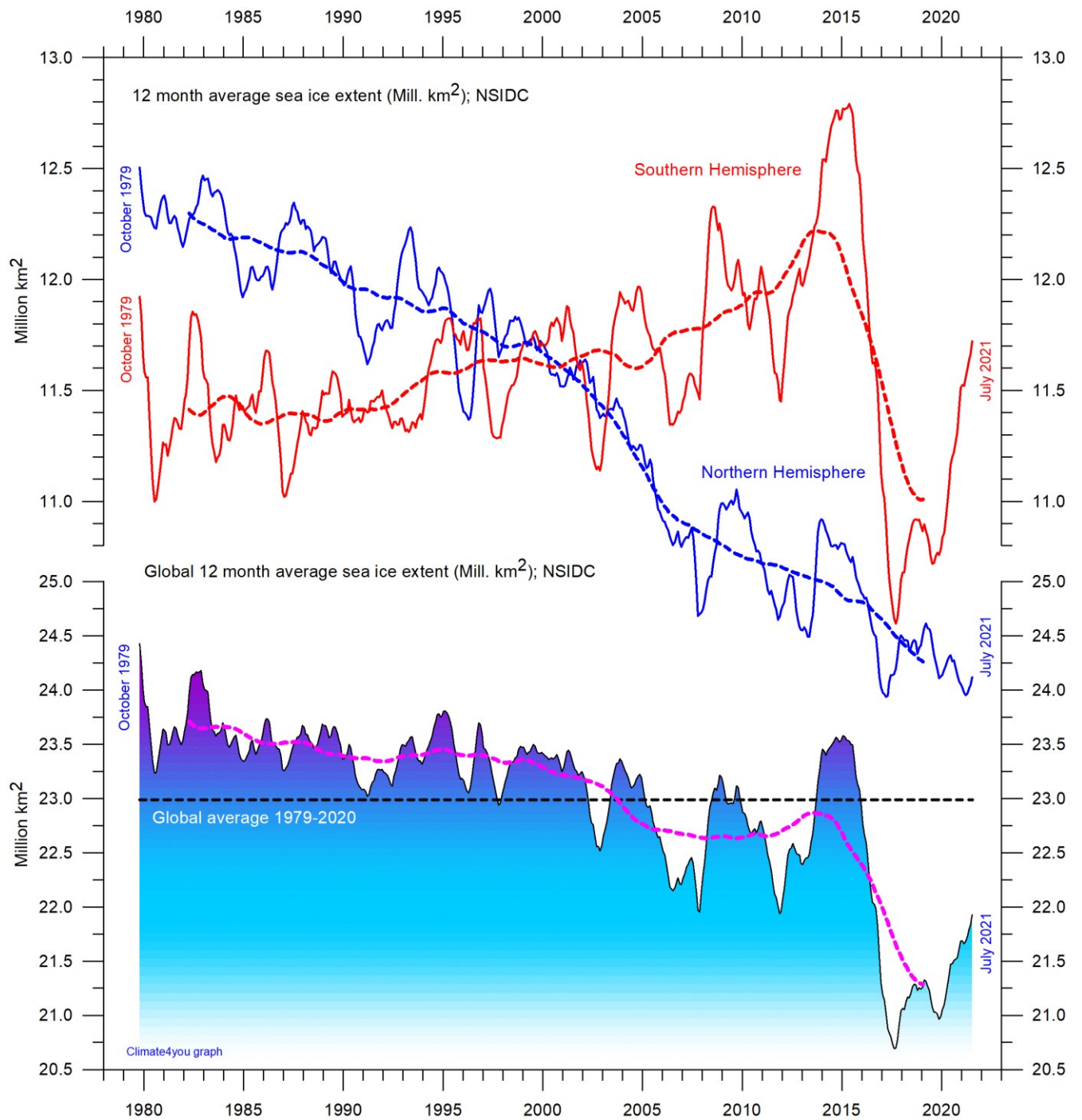
Sea Ice Thickness, 24-Jul-2021



34



Diagrams showing Arctic sea ice extent and thickness 24 July 2020 (left) and 2021 (right and above) and the seasonal cycles of the calculated total arctic sea ice volume, according to [The Danish Meteorological Institute \(DMI\)](#). The mean sea ice volume and standard deviation for the period 2004-2013 are shown by grey shading.



12 month running average sea ice extension, global and in both hemispheres since 1979, the satellite-era. The October 1979 value represents the monthly 12-month average of November 1978 - October 1979, the November 1979 value represents the average of December 1978 - November 1979, etc. The stippled lines represent a 61-month (ca. 5 years) average. Data source: National Snow and Ice Data Center (NSIDC).

Sea level in general

Global (or eustatic) sea-level change is measured relative to an idealised reference level, the geoid, which is a mathematical model of planet Earth's surface (Carter et al. 2014). Global sea-level is a function of the volume of the ocean basins and the volume of water they contain. Changes in global sea-level are caused by – but not limited to - four main mechanisms:

1. Changes in local and regional air pressure and wind, and tidal changes introduced by the Moon.
2. Changes in ocean basin volume by tectonic (geological) forces.
3. Changes in ocean water density caused by variations in currents, water temperature and salinity.
4. Changes in the volume of water caused by changes in the mass balance of terrestrial glaciers.

In addition to these there are other mechanisms influencing sea-level, such as storage of ground water, storage in lakes and rivers, evaporation, etc.

Mechanism 1 is controlling sea-level at many sites on a time scale from months to several years. As an example, many coastal stations show a pronounced annual variation reflecting seasonal changes in air pressures and wind speed. Longer-term climatic changes playing out over decades or centuries will also affect measurements of sea-level changes. Hansen et al. (2011, 2015) provide excellent analyses of sea-level changes caused by recurrent changes of the orbit of the Moon and other phenomena.

Mechanism 2 – with the important exception of earthquakes and tsunamis - typically operates over long (geological) time scales and is not significant on human time scales. It may relate to variations in the seafloor spreading rate, causing volume changes in mid-ocean mountain ridges, and to the slowly changing configuration of land and oceans. Another effect may be the slow rise of basins due to isostatic offloading by deglaciation after an ice age. The floor of the Baltic Sea and the Hudson Bay are presently rising, causing a slow net transfer of

water from these basins into the adjoining oceans. Slow changes of excessively big glaciers (ice sheets) and movements in the mantle will affect the gravity field and thereby the vertical position of the ocean surface. Any increase of the total water mass as well as sediment deposition into oceans increase the load on their bottom, generating sinking by viscoelastic flow in the mantle below. The mantle flow is directed towards the surrounding land areas, which will rise, thereby partly compensating for the initial sea level increase induced by the increased water mass in the ocean.

Mechanism 3 (temperature-driven expansion) only affects the uppermost part of the oceans on human time scales. Usually, temperature-driven changes in density are more important than salinity-driven changes. Seawater is characterised by a relatively small coefficient of expansion, but the effect should however not be overlooked, especially when interpreting satellite altimetry data. Temperature-driven expansion of a column of seawater will not affect the total mass of water within the column considered and will therefore not affect the potential at the top of the water column. Temperature-driven ocean water expansion will therefore not in itself lead to any lateral displacement of water, but only locally lift the ocean surface. Near the coast, where people are living, the depth of water approaches zero, so no measurable temperature-driven expansion will take place here (Mörner 2015). Mechanism 3 is for that reason not important for coastal regions.

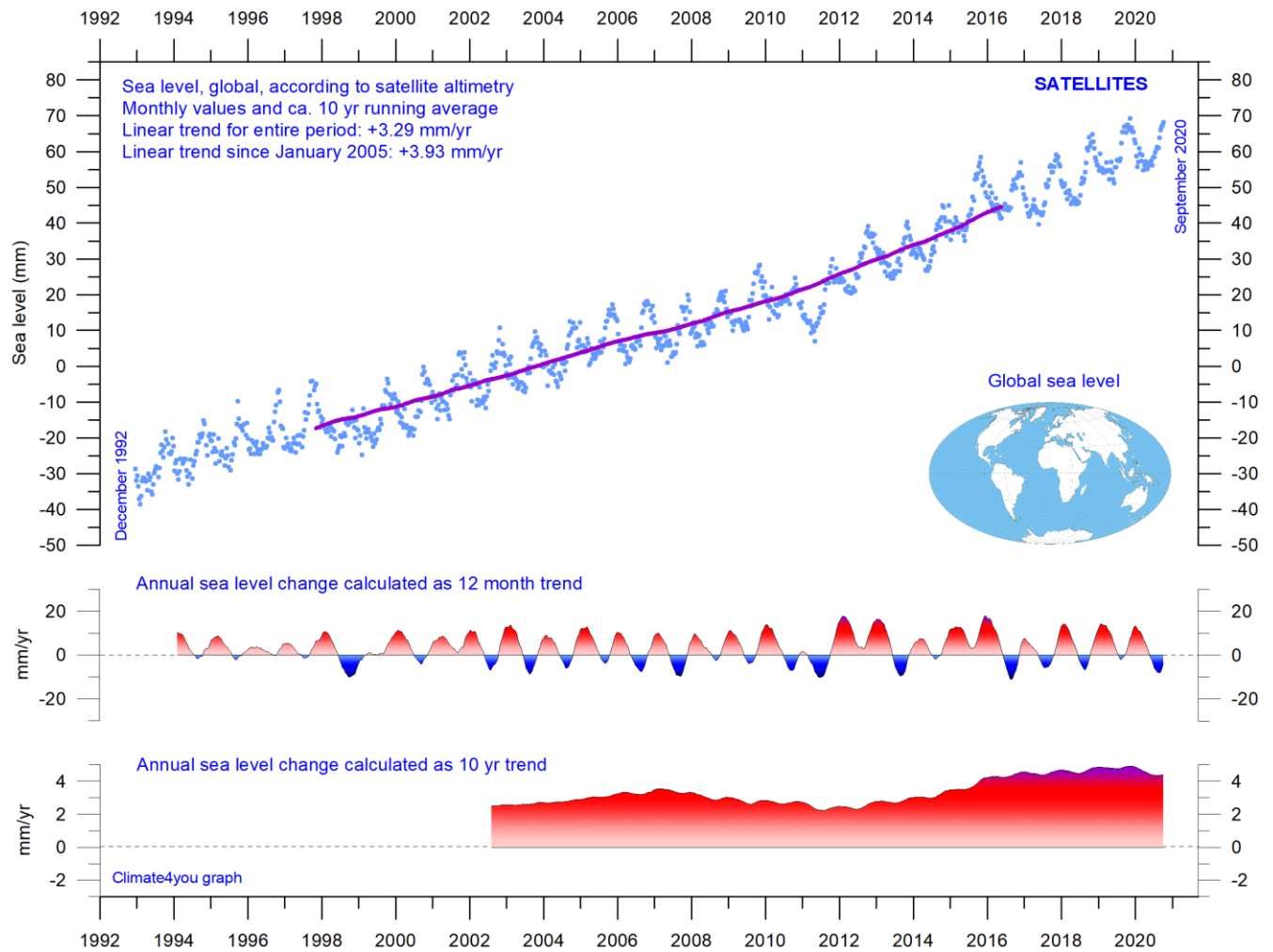
Mechanism 4 (changes in glacier mass balance) is an important driver for global sea-level changes along coasts, for human time scales. Volume changes of floating glaciers – ice shelves – has no influence on the global sea-level, just like volume changes of floating sea ice has no influence. Only the mass-balance of grounded or land-based glaciers is important for the global sea-level along coasts.

Summing up: Presumably, mechanism 1 and 4 are the most important for understanding sea-level changes along coasts.

References:

- Carter R.M., de Lange W., Hansen, J.M., Humlum O., Idso C., Kear, D., Legates, D., Mörner, N.A., Ollier C., Singer F. & Soon W. 2014. Commentary and Analysis on the Whitehead & Associates 2014 NSW Sea-Level Report. Policy Brief, NIPCC, 24. September 2014, 44 pp. <http://climatechangereconsidered.org/wp-content/uploads/2014/09/NIPCC-Report-on-NSW-Coastal-SL-9z-corrected.pdf>
- Hansen, J.-M., Aagaard, T. and Binderup, M. 2011. Absolute sea levels and isostatic changes of the eastern North Sea to central Baltic region during the last 900 years. *Boreas*, 10.1111/j.1502-3885.2011.00229.x. ISSN 0300-9483.
- Hansen, J.-M., Aagaard, T. and Huijpers, A. 2015. Sea-Level Forcing by Synchronization of 56- and 74-Year Oscillations with the Moon's Nodal Tide on the Northwest European Shelf (Eastern North Sea to Central Baltic Sea). *Journ. Coastal Research*, 16 pp.
- Mörner, Nils-Axel 2015. Sea Level Changes as recorded in nature itself. *Journal of Engineering Research and Applications*, Vol.5, 1, 124-129.

Global sea level from satellite altimetry, updated to September 2020



Global sea level since December 1992 according to the Colorado Center for Astrodynamics Research at University of Colorado at Boulder. The blue dots are the individual observations, and the purple line represents the running 121-month (ca. 10 year) average. The two lower panels show the annual sea level change, calculated for 1 and 10-year time windows, respectively. These values are plotted at the end of the interval considered.

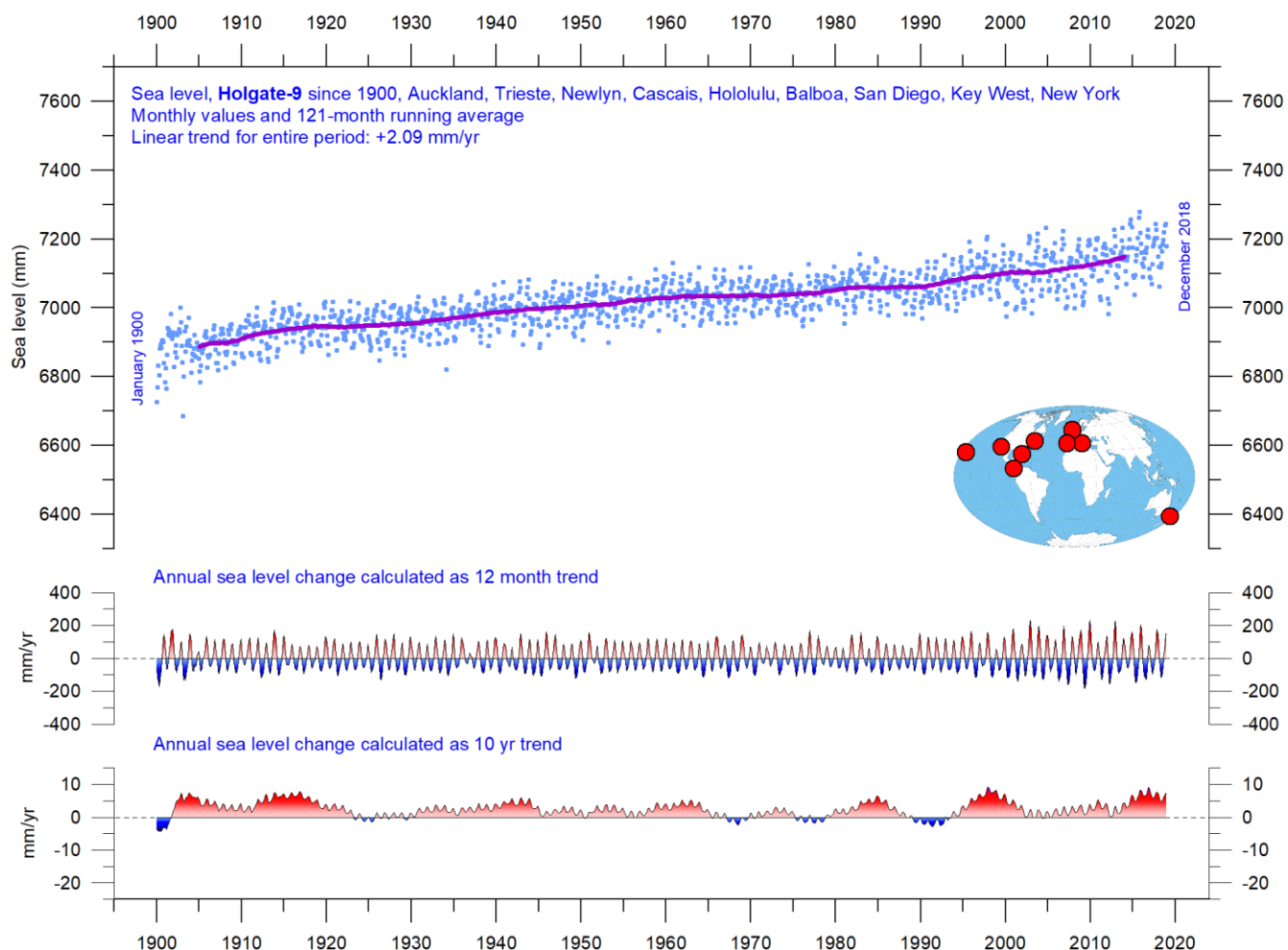
Ground truth is a term used in various fields to refer to information provided by direct observation as opposed to information provided by inference, such as, e.g., by satellite observations.

In remote sensing using satellite observations, ground truth data refers to information collected on location. Ground truth allows the satellite data to be related to real features observed on the planet surface. The collection of ground truth data enables calibration of remote-sensing

data, and aids in the interpretation and analysis of what is being sensed or recorded by satellites. Ground truth sites allow the remote sensor operator to correct and improve the interpretation of satellite data.

For satellite observations on sea level ground true data are provided by the classical tide gauges (example diagram on next page), that directly measures the local sea level many places distributed along the coastlines on the surface of the planet.

Global sea level from tide-gauges, updated to December 2018



Holgate-9 monthly tide gauge data from PSMSL Data Explorer. *Holgate (2007)* suggested the nine stations listed in the diagram to capture the variability found in a larger number of stations over the last half century studied previously. For that reason, average values of the *Holgate-9* group of tide gauge stations are interesting to follow, even though Auckland (New Zealand) has not reported data since 2000, and Cascais (Portugal) not since 1993. Unfortunately, by this data loss the *Holgate-9* series since 2000 is underrepresented with respect to the southern hemisphere and should therefore not be overinterpreted. The blue dots are the individual average monthly observations, and the purple line represents the running 121-month (ca. 10 year) average. The two lower panels show the annual sea level change, calculated for 1 and 10-year windows, respectively. These values are plotted at the end of the interval considered.

Data from tide-gauges all over the world suggest an average global sea-level rise of 1-2 mm/year, while the satellite-derived record (page 37) suggest a rise of about 3.3 mm/year, or more. The noticeable difference (about 1:2) between the two data sets is remarkable but has no

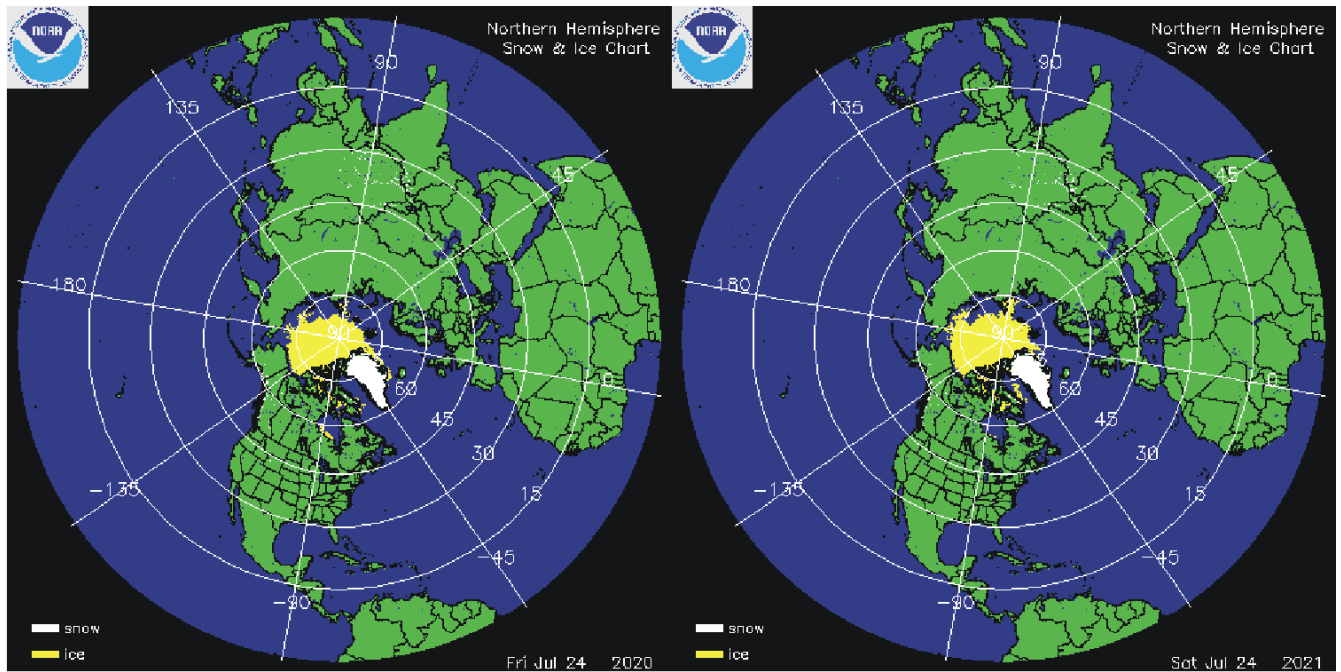
generally accepted explanation. It is however known that satellite observations are facing several complications in areas near the coast. Vignudelli et al. (2019) provide an updated overview of the current limitations of classical satellite altimetry in coastal regions.

References:

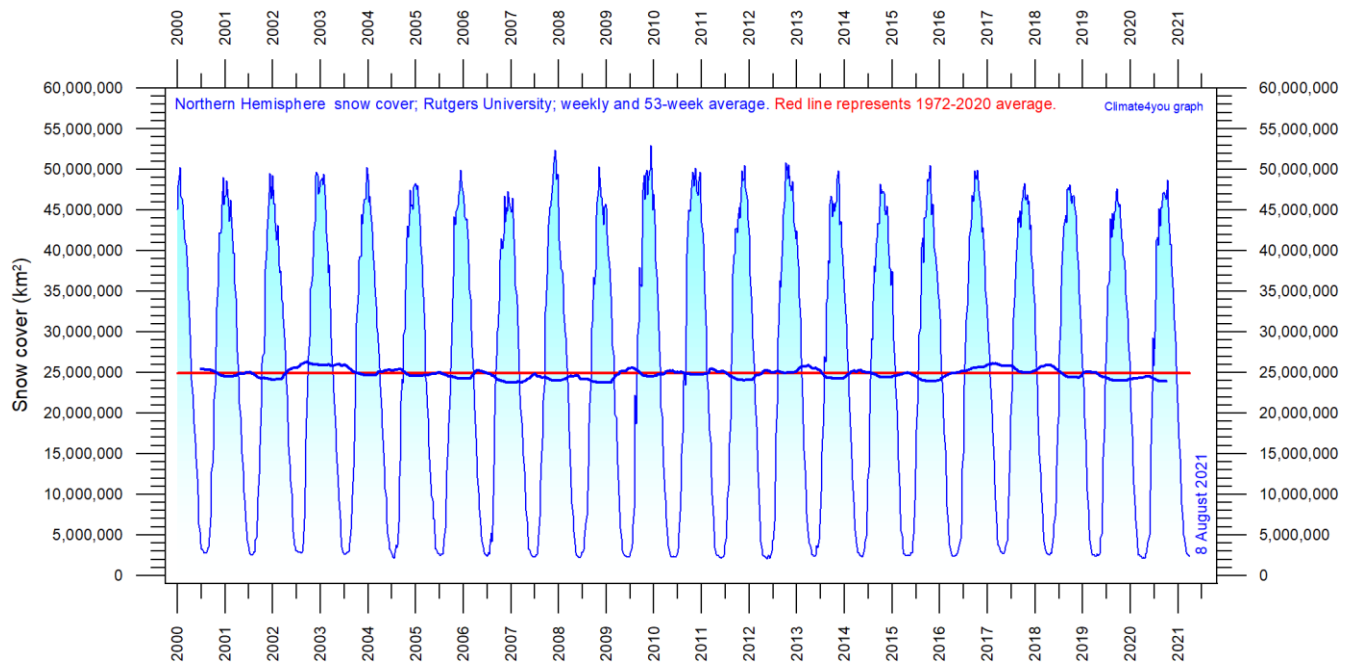
Holgate, S.J. 2007. On the decadal rates of sea level change during the twentieth century. *Geophys. Res. Letters*, 34, L01602, doi:10.1029/2006GL028492

Vignudelli et al. 2019. Satellite Altimetry Measurements of Sea Level in the Coastal Zone. *Surveys in Geophysics*, Vol. 40, p. 1319–1349. <https://link.springer.com/article/10.1007/s10712-019-09569-1>

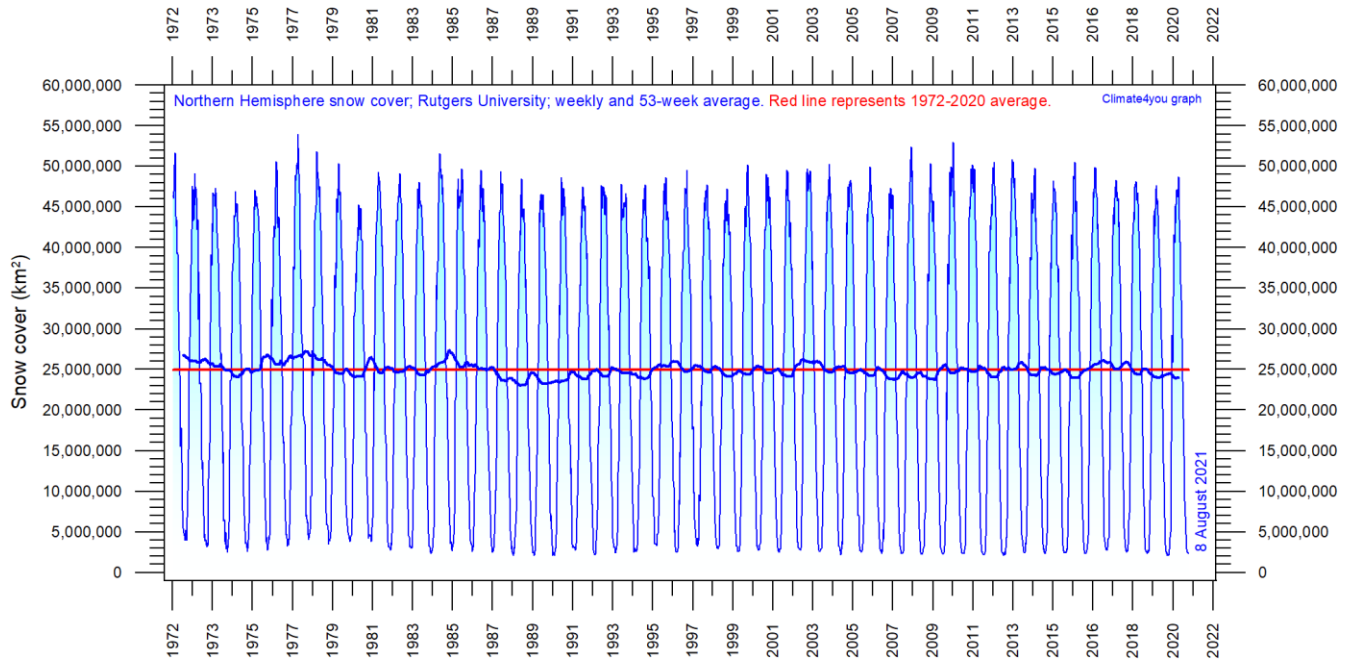
Northern Hemisphere weekly and seasonal snow cover, updated to July 2021



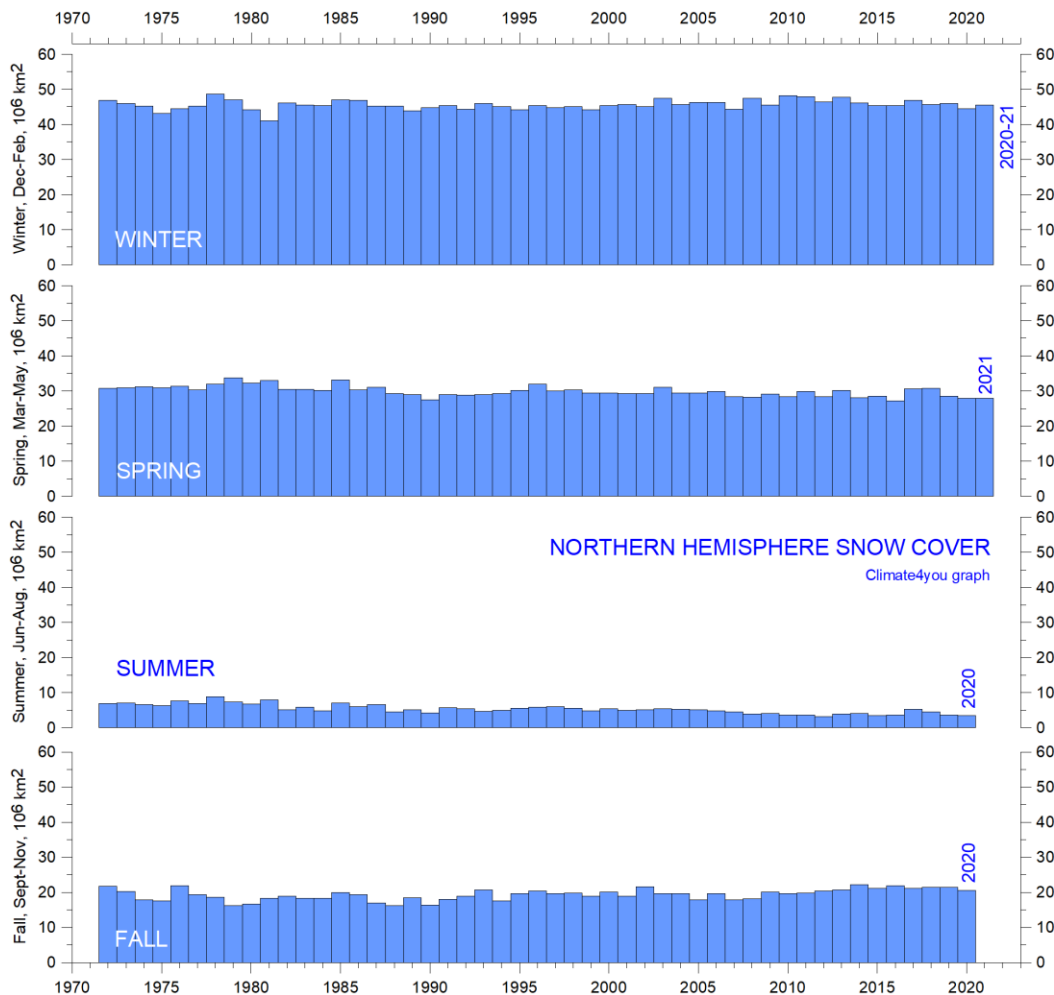
Northern hemisphere snow cover (white) and sea ice (yellow) 24 July 2020 (left) and 2021 (right). Map source: [National Ice Center \(NIC\)](#).



Northern hemisphere weekly snow cover since January 2000 according to Rutgers University Global Snow Laboratory. The thin blue line is the weekly data, and the thick blue line is the running 53-week average (approximately 1 year). The horizontal red line is the 1972-2020 average.

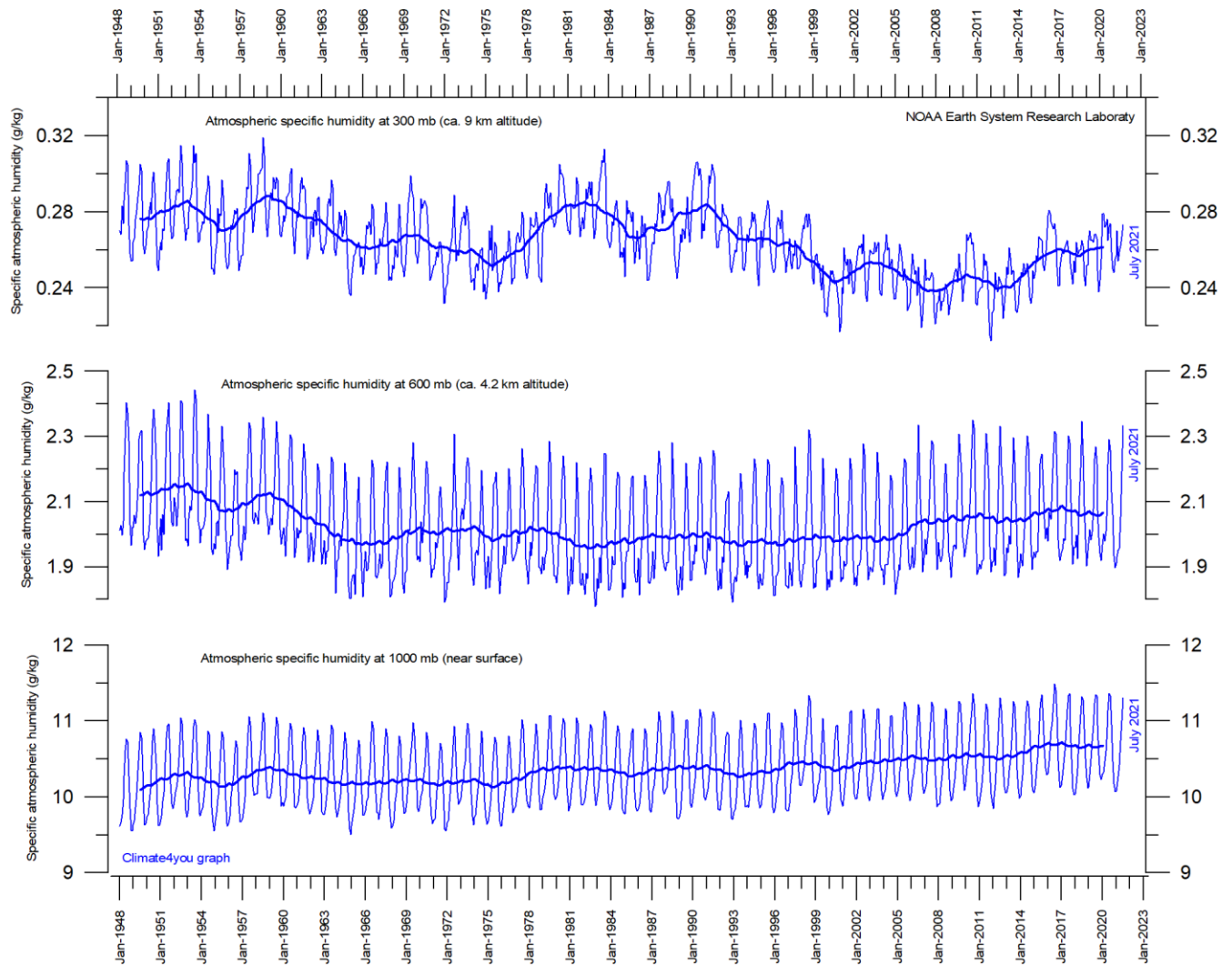


Northern hemisphere weekly snow cover since January 1972 according to Rutgers University Global Snow Laboratory. The thin blue line is the weekly data, and the thick blue line is the running 53-week average (approximately 1 year). The horizontal red line is the 1972-2020 average.



Northern hemisphere seasonal snow cover since January 1972 according to Rutgers University Global Snow Laboratory.

Atmospheric specific humidity, updated to July 2021



41

Specific atmospheric humidity (g/kg) at three different altitudes in the lower part of the atmosphere (the Troposphere) since January 1948 (Kalnay et al. 1996). The thin blue lines show monthly values, while the thick blue lines show the running 37-month average (about 3 years). Data source: [Earth System Research Laboratory \(NOAA\)](#).

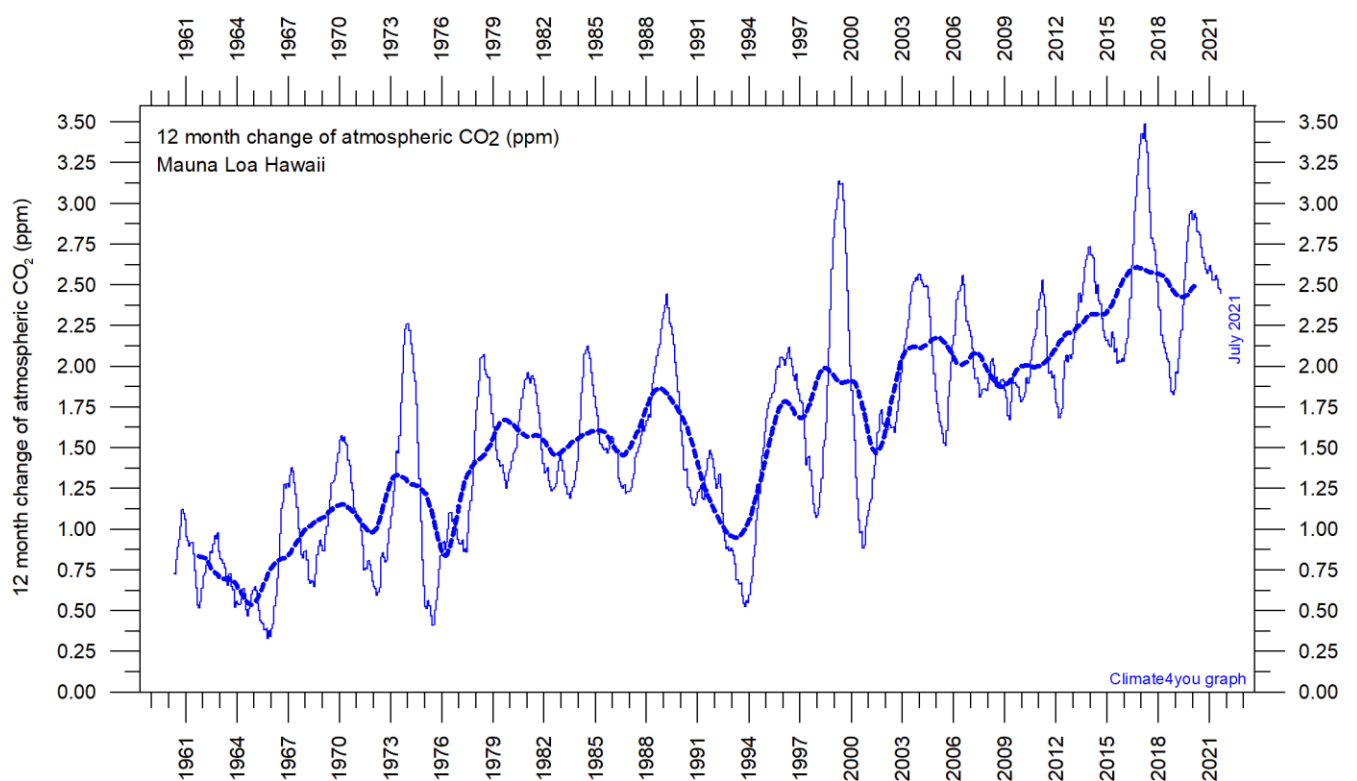
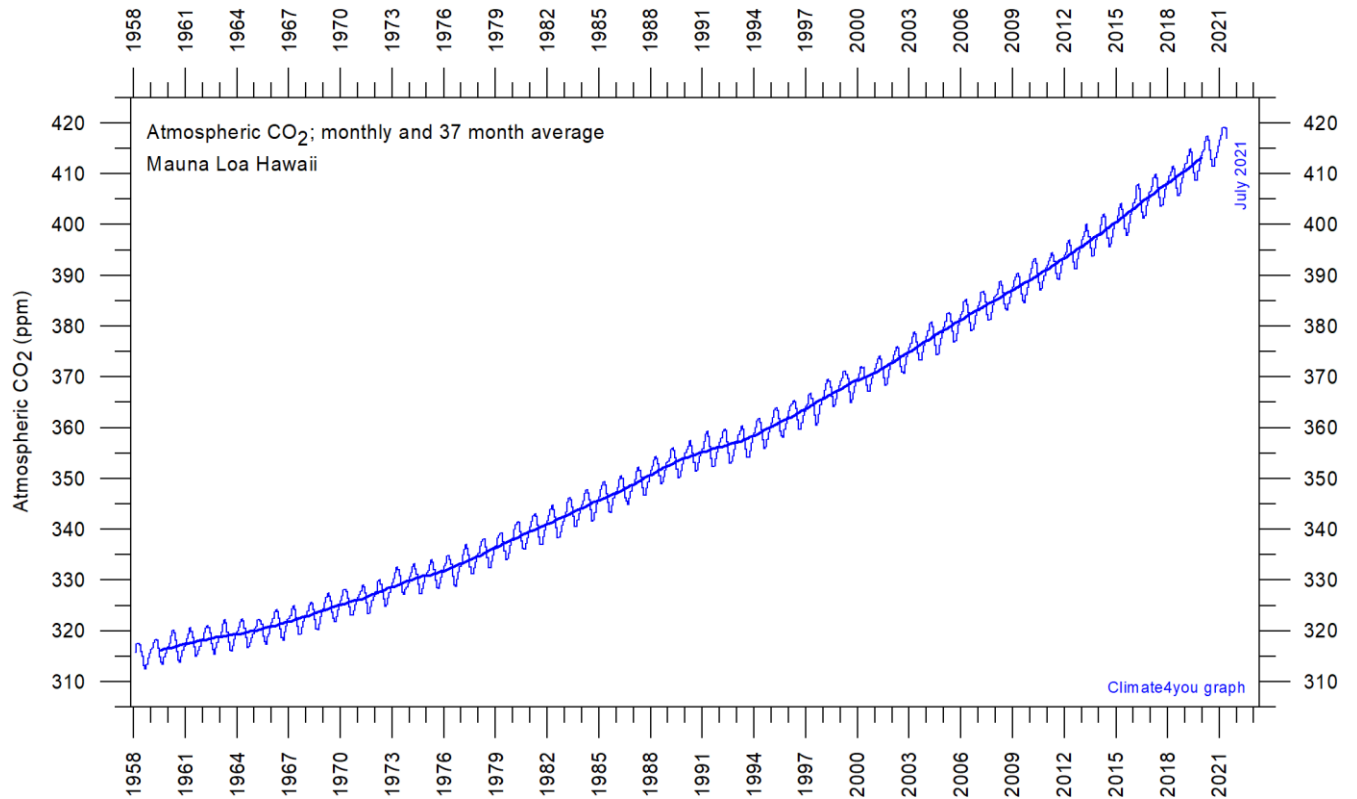
Water vapor is the most important greenhouse gas in the Troposphere. The highest concentration is found within a latitudinal range from 50°N to 60°S. The two polar regions of the Troposphere are comparatively dry.

The diagram above shows the specific atmospheric humidity to be stable or slightly increasing up to about 4-5 km altitude. At higher levels in the Troposphere (about 9 km), the specific humidity has been decreasing for the duration of the record (since 1948), but with shorter

variations superimposed on the falling trend. A Fourier frequency analysis (not shown here) shows these variations to be influenced especially by a periodic variation of about 3.7-year duration.

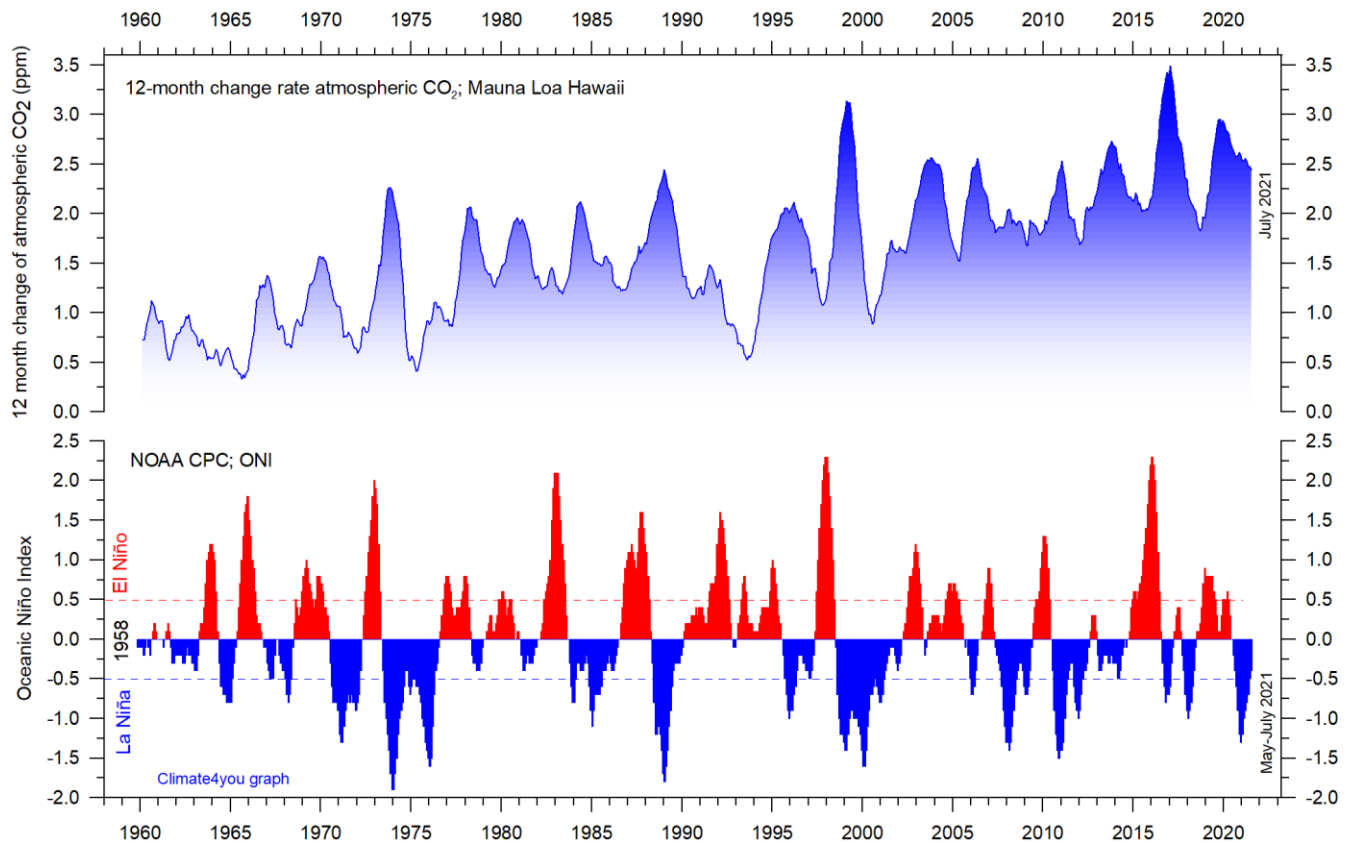
The persistent decrease in specific humidity at about 9 km altitude is particularly noteworthy, as this altitude roughly corresponds to the level where the theoretical temperature effect of increased atmospheric CO₂ is expected initially to play out.

Atmospheric CO₂, updated to July 2021



Monthly amount of atmospheric CO₂ (upper diagram) and annual growth rate (lower diagram); average last 12 months minus average preceding 12 months, thin line) of atmospheric CO₂ since 1959, according to data provided by the [Mauna Loa Observatory](#), Hawaii, USA. The thick, stippled line is the simple running 37-observation average, nearly corresponding to a running 3-year average. A Fourier frequency analysis (not shown here) shows the 12-month change of Tropospheric CO₂ to be influenced especially by periodic variations of 2.5- and 3.8-years' duration.

The relation between annual change of atmospheric CO₂ and La Niña and El Niño episodes, updated to July 2021



Visual association between annual growth rate of atmospheric CO₂ (upper panel) and Oceanic Niño Index (lower panel). See also diagrams on page 40 and 22, respectively.

Changes in the global atmospheric CO₂ is seen to vary roughly in concert with changes in the Oceanic Niño Index. The typical sequence of events is that changes in the global atmospheric CO₂ to a certain degree follows changes in the Oceanic Niño Index, but clearly not in all details. Many processes, natural as well as anthropogenic, controls the amount of atmospheric CO₂, but oceanographic processes are clearly particularly important (see also diagram on next page).

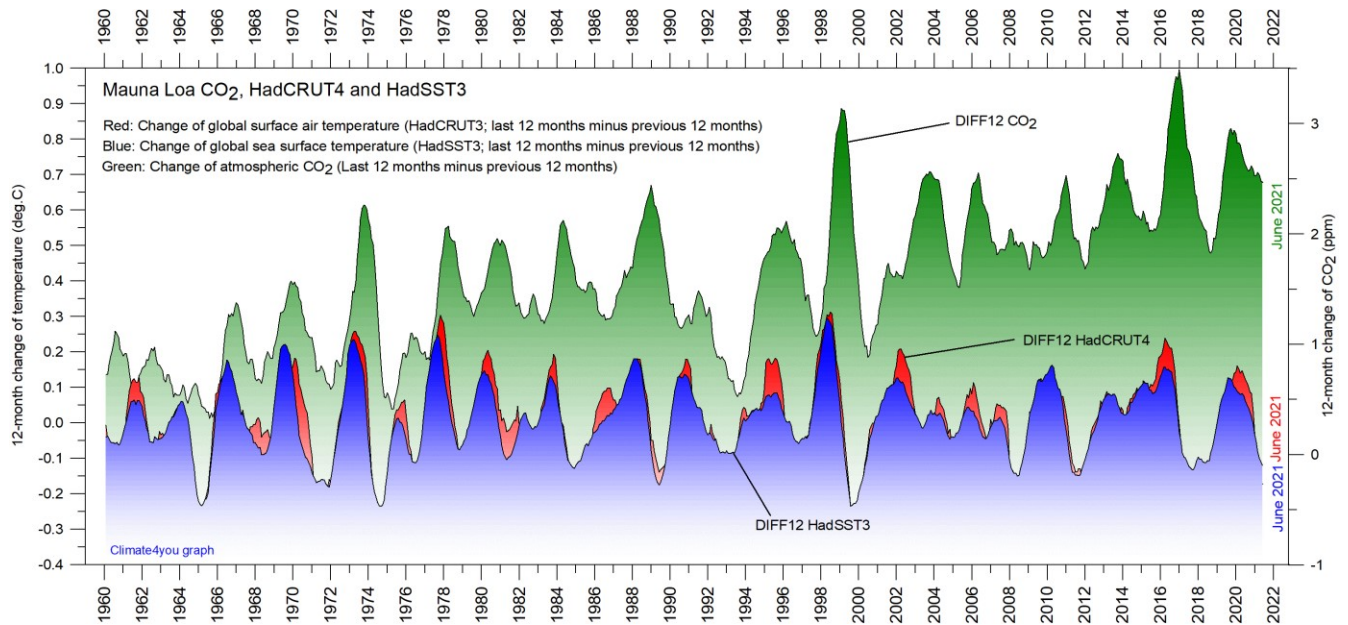
Atmospheric CO₂ and the present coronavirus pandemic

Modern political initiatives usually assume the human influence (mainly the burning of fossil fuels) to represent the core reason for the observed increase in atmospheric CO₂ since 1958 (diagrams on page 42).

The present (since January 2020) coronavirus pandemic has resulted in a marked reduction in the global consumption of fossil fuels. It is therefore interesting to follow the effect of this on the amount of atmospheric CO₂.

However, there is still no clear effect to be seen of the above reduction in release of CO₂ from fossil fuels. Presumably, the basic explanation for this is that the human contribution is too small compared to the numerous natural sources and sinks for atmospheric CO₂ to appear in diagrams showing the amount of atmospheric CO₂ (see, e.g., the diagrams on p. 42-44).

The phase relation between atmospheric CO₂ and global temperature, updated to June 2021



12-month change of global atmospheric CO₂ concentration ([Mauna Loa](#); green), global sea surface temperature ([HadSST3](#); blue) and global surface air temperature ([HadCRUT4](#); red dotted). All graphs are showing monthly values of DIFF12, the difference between the average of the last 12 months and the average for the previous 12 months for each data series.

44

The typical sequence of events is seen to be that changes in the global atmospheric CO₂ follow changes in global surface air temperature, which again follow changes in global ocean surface temperatures. Thus, changes in

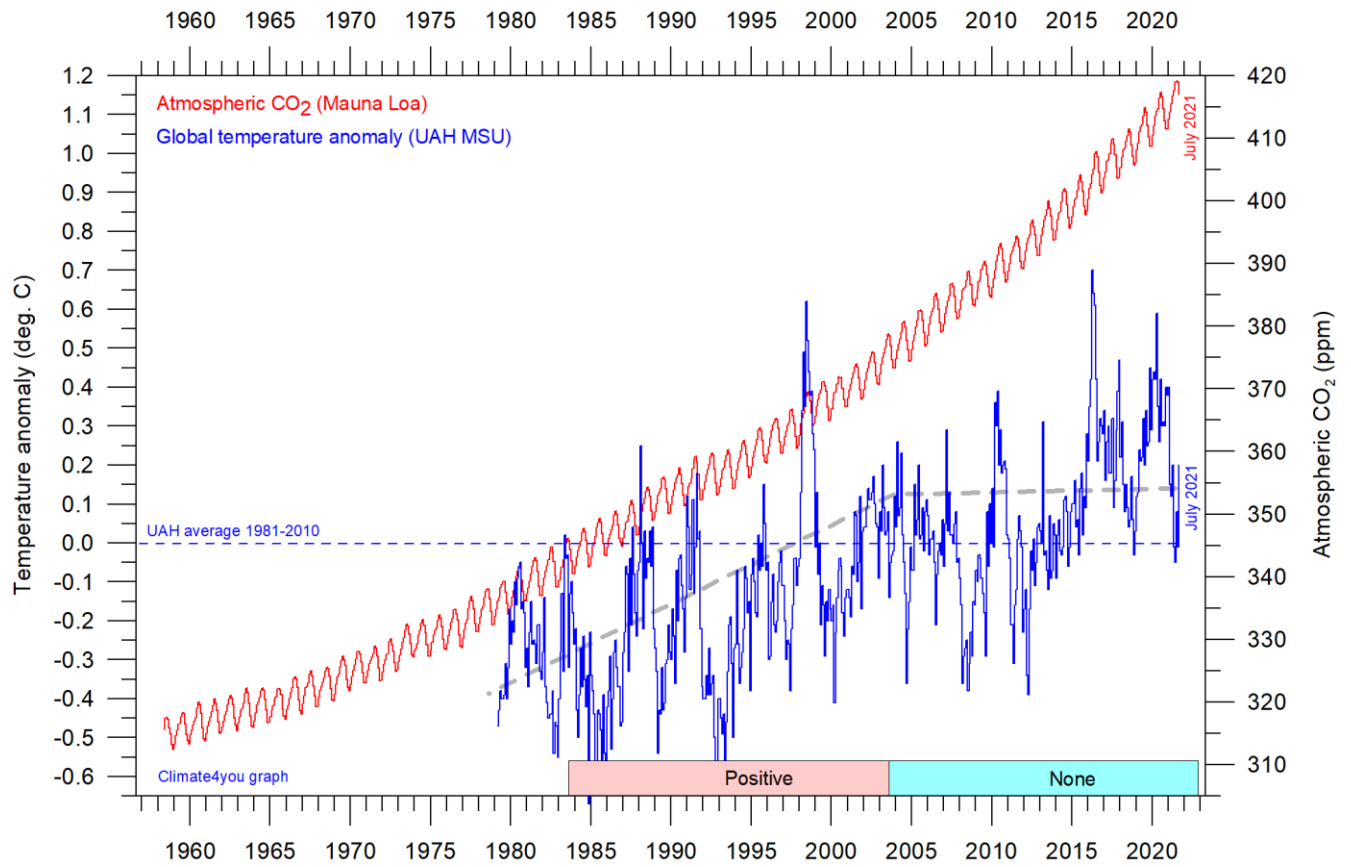
global atmospheric CO₂ are lagging 9.5–10 months behind changes in global air surface temperature, and 11–12 months behind changes in global sea surface temperature.

References:

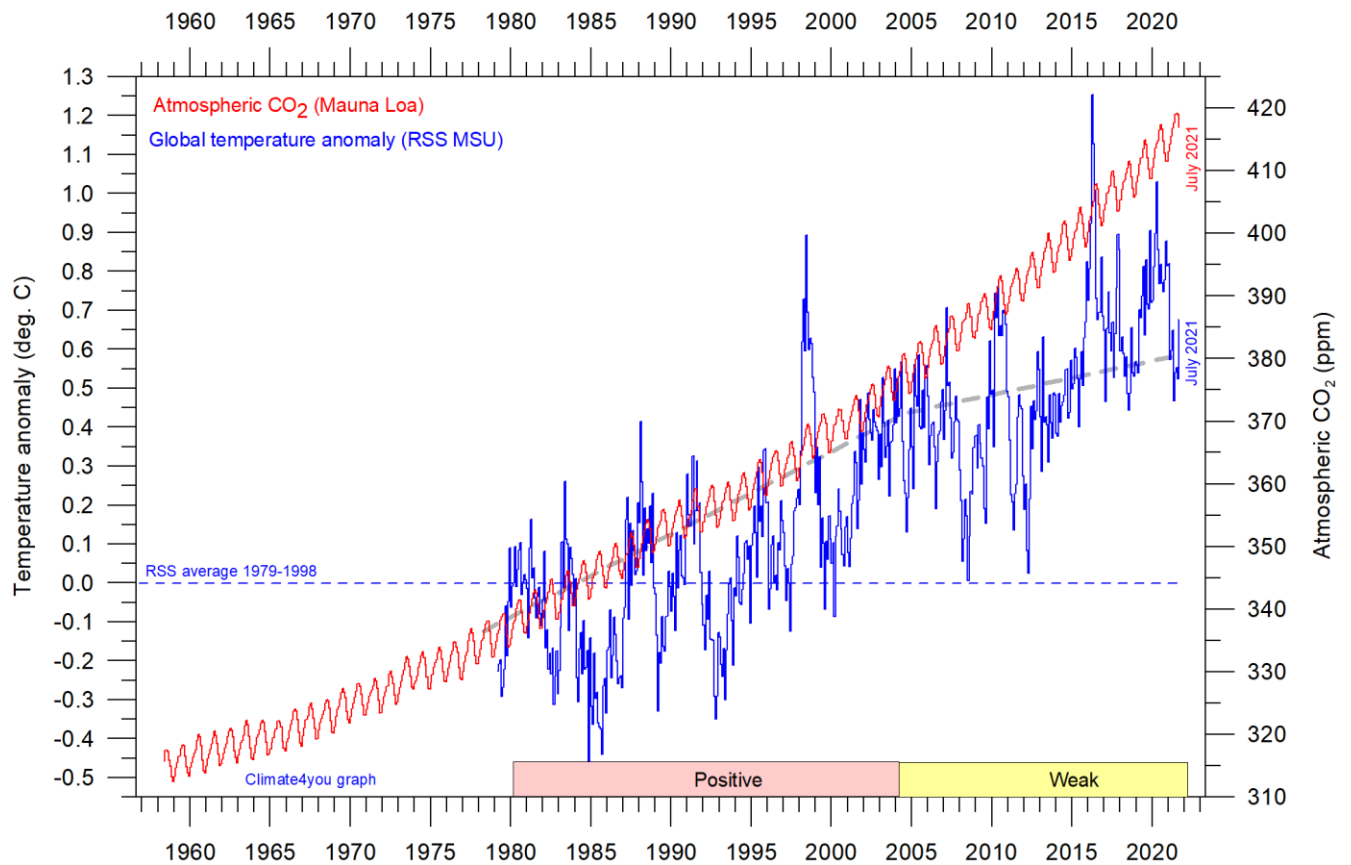
Humlum, O., Stordahl, K. and Solheim, J-E. 2012. The phase relation between atmospheric carbon dioxide and global temperature. *Global and Planetary Change*, August 30, 2012.

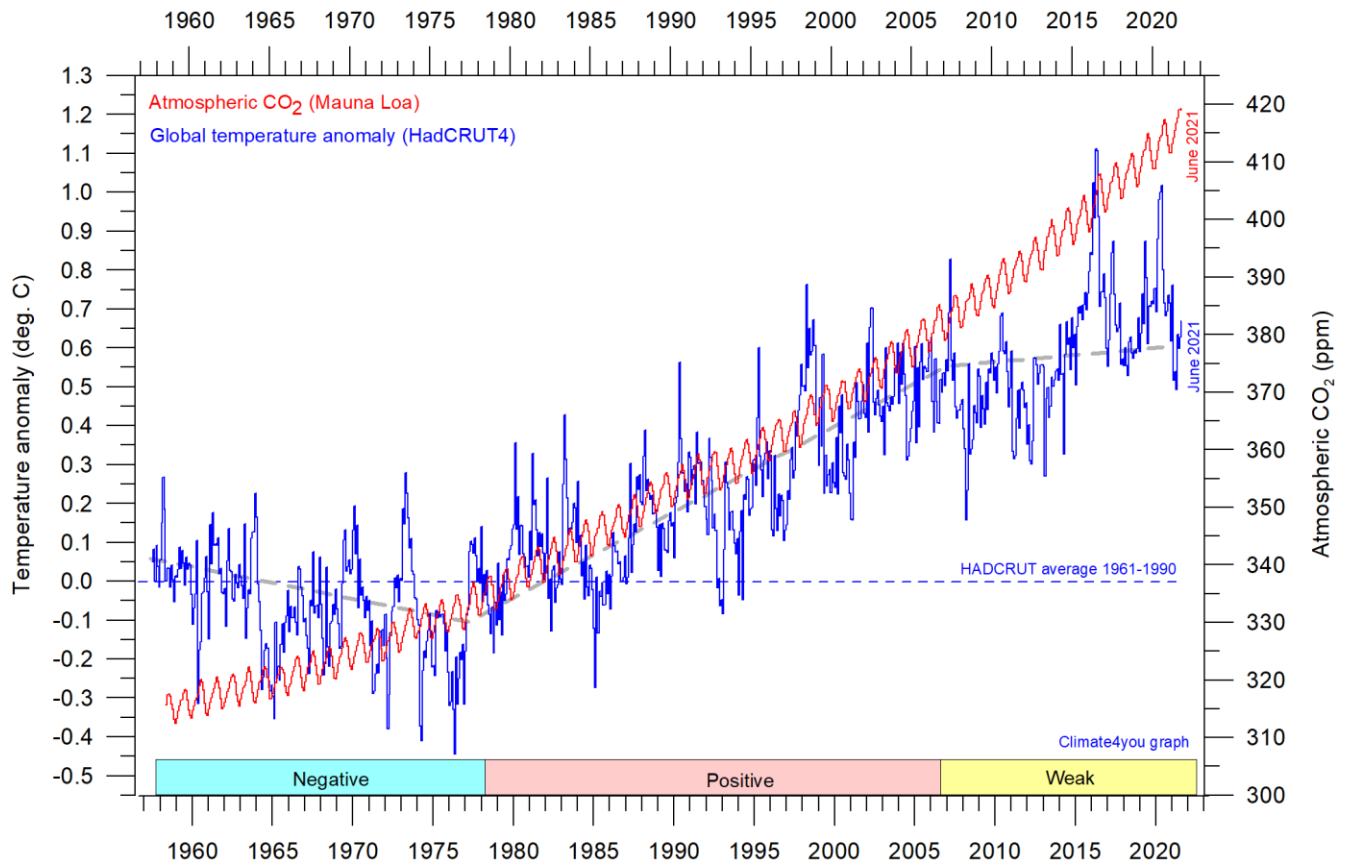
<http://www.sciencedirect.com/science/article/pii/S0921818112001658?v=s5>

Global air temperature and atmospheric CO₂, updated to July 2021

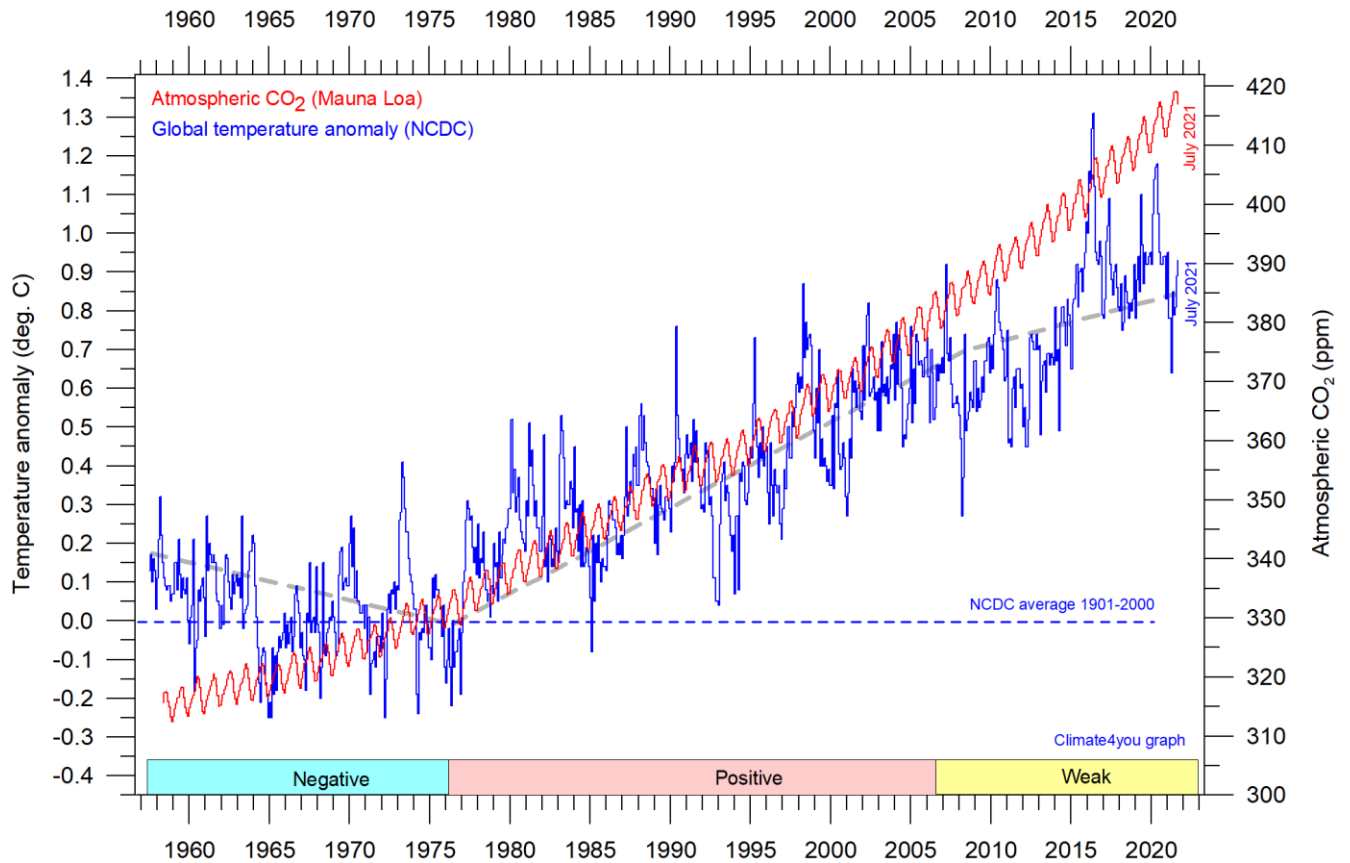


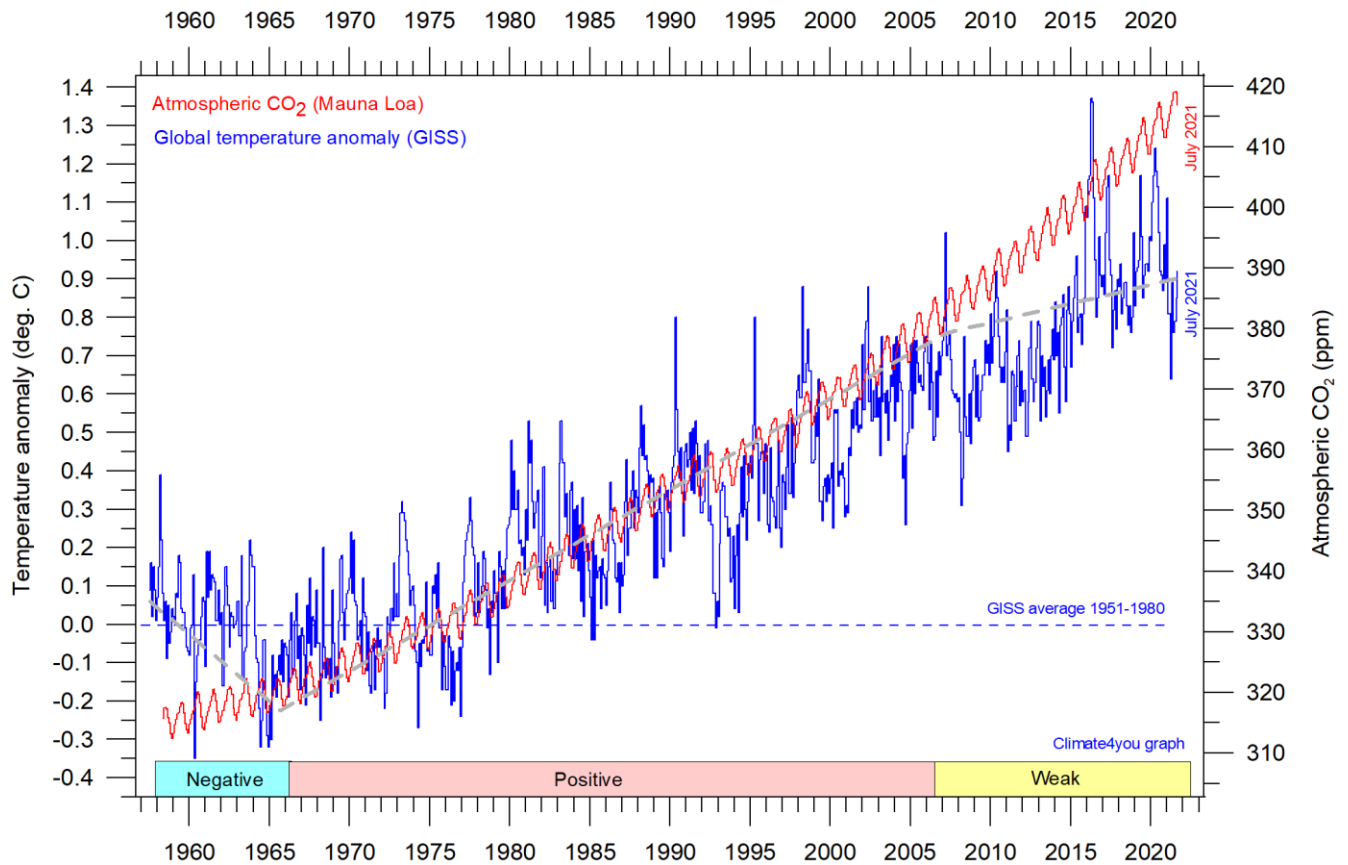
45





46





Diagrams showing UAH, RSS, HadCRUT4, NCDC and GISS monthly global air temperature estimates (blue) and the monthly atmospheric CO₂ content (red) according to the [Mauna Loa Observatory](#), Hawaii. The Mauna Loa data series begins in March 1958, and 1958 was therefore chosen as starting year for all diagrams above. Reconstructions of past atmospheric CO₂ concentrations (before 1958) are not incorporated in this diagram, as such past CO₂ values are derived by other means (ice cores, stomata, or older measurements using different methodology), and therefore are not directly comparable with direct atmospheric measurements. The dotted grey line indicates the approximate linear temperature trend, and the boxes in the lower part of the diagram indicate the relation between atmospheric CO₂ and global surface air temperature, negative or positive.

Most climate models are programmed to give the greenhouse gas carbon dioxide CO₂ significant influence on the calculated global air temperature. It is therefore relevant to compare different air temperature records with measurements of atmospheric CO₂, as shown in the diagrams above.

Any comparison, however, should not be made on a monthly or annual basis, but for a longer time, as other effects (oceanographic, cloud cover, etc.) may override the potential influence of CO₂ on short time scales such as just a few years.

It is of cause equally inappropriate to present new meteorological record values, whether daily, monthly, or

annual, as demonstrating the legitimacy of the hypothesis ascribing high importance of atmospheric CO₂ for global air temperatures. Any such meteorological record value may well be the result of other phenomena. Unfortunately, many media repeatedly fall into this trap.

What exactly defines the critical length of a relevant period length to consider for evaluating the alleged importance of CO₂ remains elusive and still represents a theme for discussions.

Nonetheless, the length of the critical period must be inversely proportional to the temperature sensitivity of CO₂, including feedback effects. Thus, if the net temperature effect of atmospheric CO₂ is strong, the critical period will be short, and vice versa.

However, past climate research history provides some clues as to what has traditionally been considered the relevant length of period over which to compare temperature and atmospheric CO₂.

After about 10 years of concurrent global temperature- and CO₂-increase, IPCC was established in 1988. For obtaining public and political support for the CO₂-hypothesis the 10-year warming period leading up to 1988 most likely was considered important. Had the global temperature instead been decreasing at that time, political support for the hypothesis probably would have been difficult to obtain in 1988.

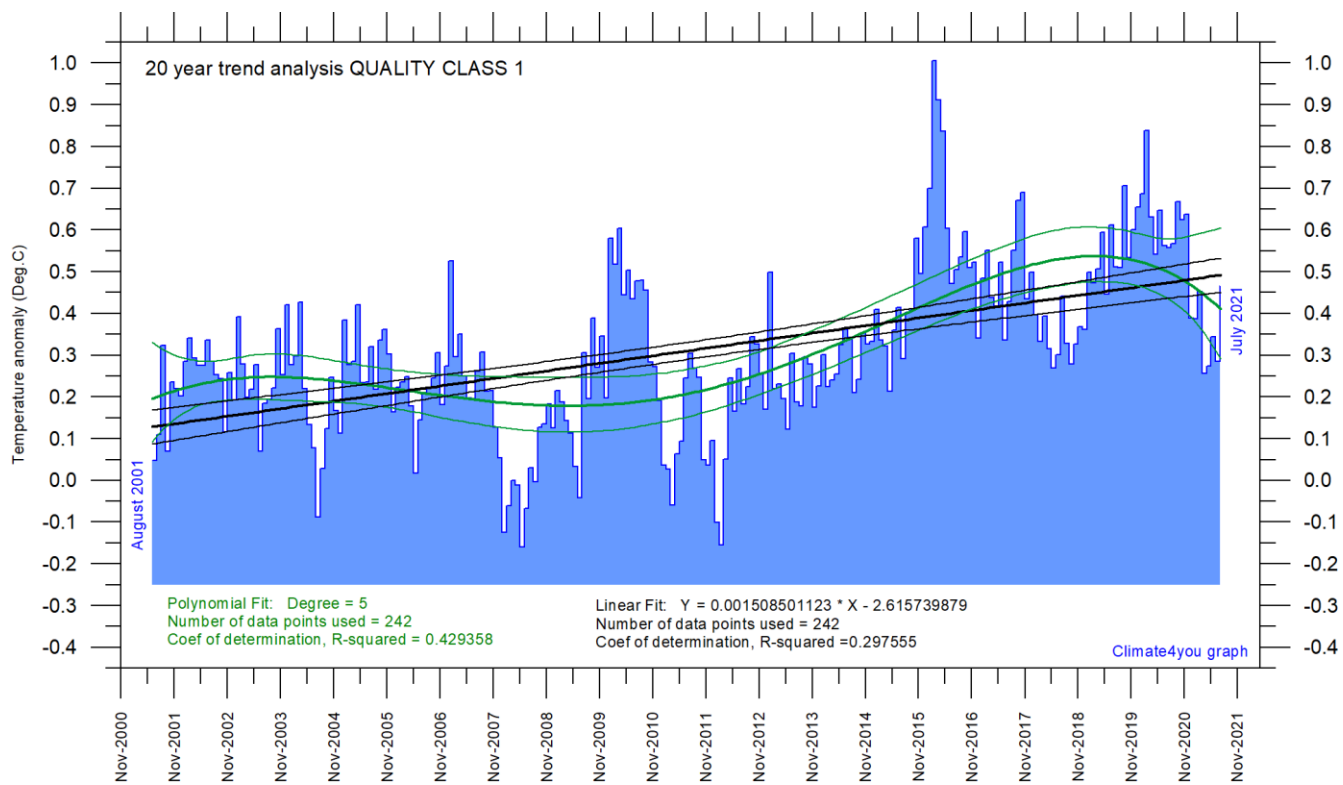
Based on the previous 10 years of concurrent temperature- and CO₂-increase, many climate

scientists in 1988 presumably felt that their understanding of climate dynamics was enough to conclude about the importance of CO₂ for affecting observed global temperatures.

Thus, it may with confidence be concluded that 10 years in 1988 was considered a period long enough to demonstrate the effect of increasing atmospheric CO₂ on global temperatures. The 10-year period is also basis for the anomaly diagrams shown on page 2.

Adopting this approach as to critical time length (at least 10 years), the varying relation (positive or negative) between global temperature and atmospheric CO₂ has been indicated in the lower panels of the diagrams above.

Latest 20-year QC1 global monthly air temperature changes, updated to July 2021



49

Last 20 years' global monthly average air temperature according to Quality Class 1 (UAH and RSS; see p.6 and 9) global monthly temperature estimates. The thin blue line represents the monthly values. The thick black line is the linear fit, with 95% confidence intervals indicated by the two thin black lines. The thick green line represents a 5-degree polynomial fit, with 95% confidence intervals indicated by the two thin green lines. A few key statistics are given in the lower part of the diagram (please note that the linear trend is the monthly trend).

In the enduring scientific climate debate, the following question is often put forward: Is the surface air temperature still increasing or has it basically remained without significant changes during the last 15-16 years?

The diagram above may be useful in this context and demonstrates the differences between two often used statistical approaches to determine recent temperature trends. Please also note that such fits only attempt to describe the past, and usually have small, if any, predictive power.

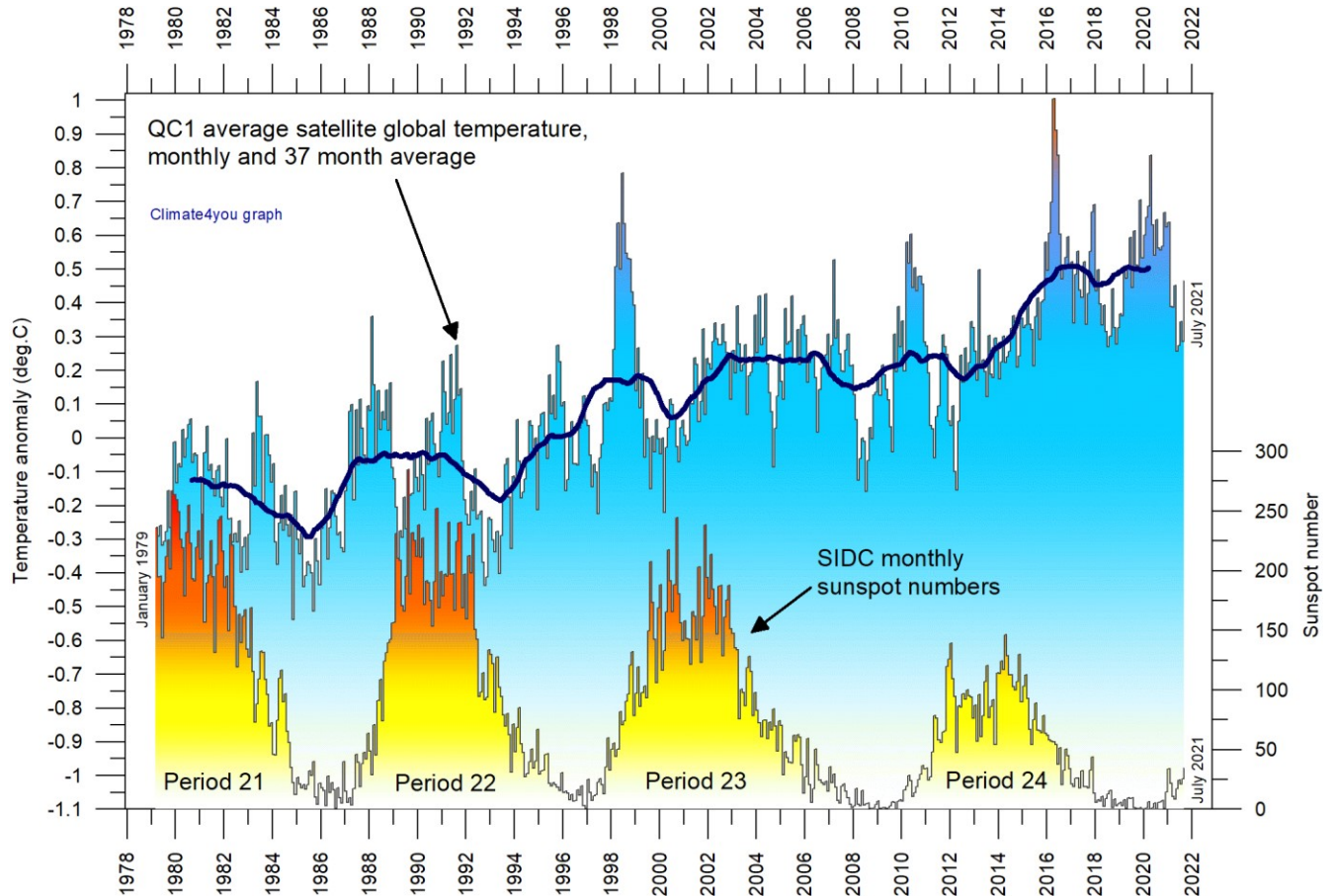
In addition, before using any linear trend (or other) analysis of time series a proper statistical model should be chosen, based on statistical justification.

For global temperature time series, there is no *a priori* physical reason why the long-term trend should be linear in time. In fact, climatic time series often have trends for which a straight line is not a good approximation, as is clearly demonstrated by several of the diagrams shown in the present report.

For an commendable description of problems often encountered by analyses of temperature time series analyses, please see [Keenan, D.J. 2014: Statistical Analyses of Surface Temperatures in the IPCC Fifth Assessment Report.](#)

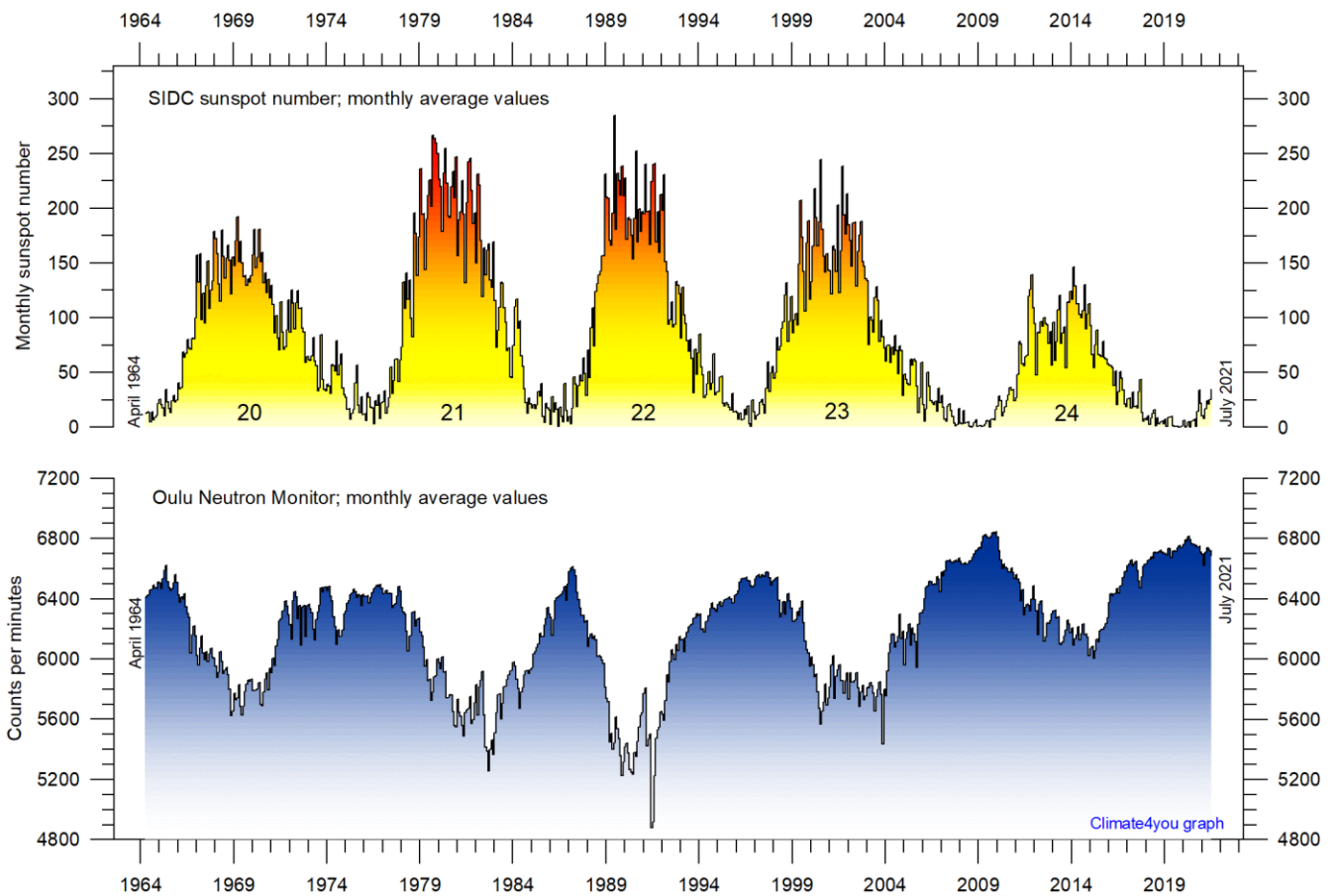
See also diagrams on page 12.

Sunspot activity (SIDC) and QC1 average satellite global air temperature, updated to July 2021



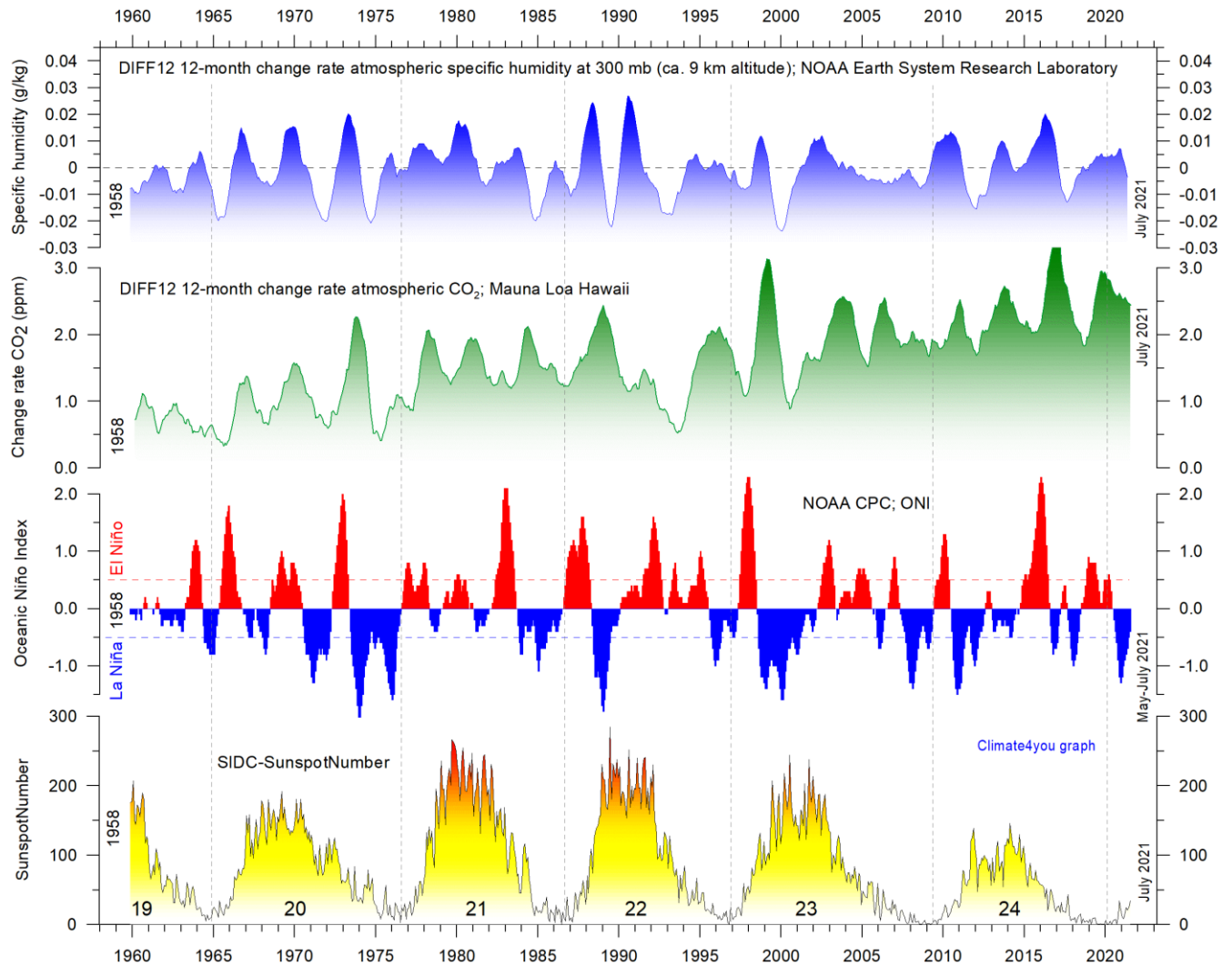
Variation of global monthly air temperature according to Quality Class 1 (UAH and RSS; see p.4) and observed sunspot number as provided by the Solar Influences Data Analysis Center (SIDC), since 1979. The thin lines represent the monthly values, while the thick line is the simple running 37-month average, nearly corresponding to a running 3-year average. The asymmetrical temperature 'bump' around 1998 is influenced by the oceanographic El Niño phenomenon in 1998, as is the case also for 2015-16. Temperatures in year 2019-20 was influenced by a moderate El Niño.

Monthly sunspot activity (SIDC) and average neutron counts (Oulu, Finland), updated to July 2021



Observed monthly sunspot number (Solar Influences Data Analysis Center (SIDC) since April 1964, and (lower panel) monthly average counts of the Oulu (Finland) neutron monitor, adjusted for barometric pressure and efficiency.

Monthly sunspot activity (SIDC), Oceanic Niño Index (ONI), and change rates of atmospheric CO₂ and specific humidity, updated to July 2021

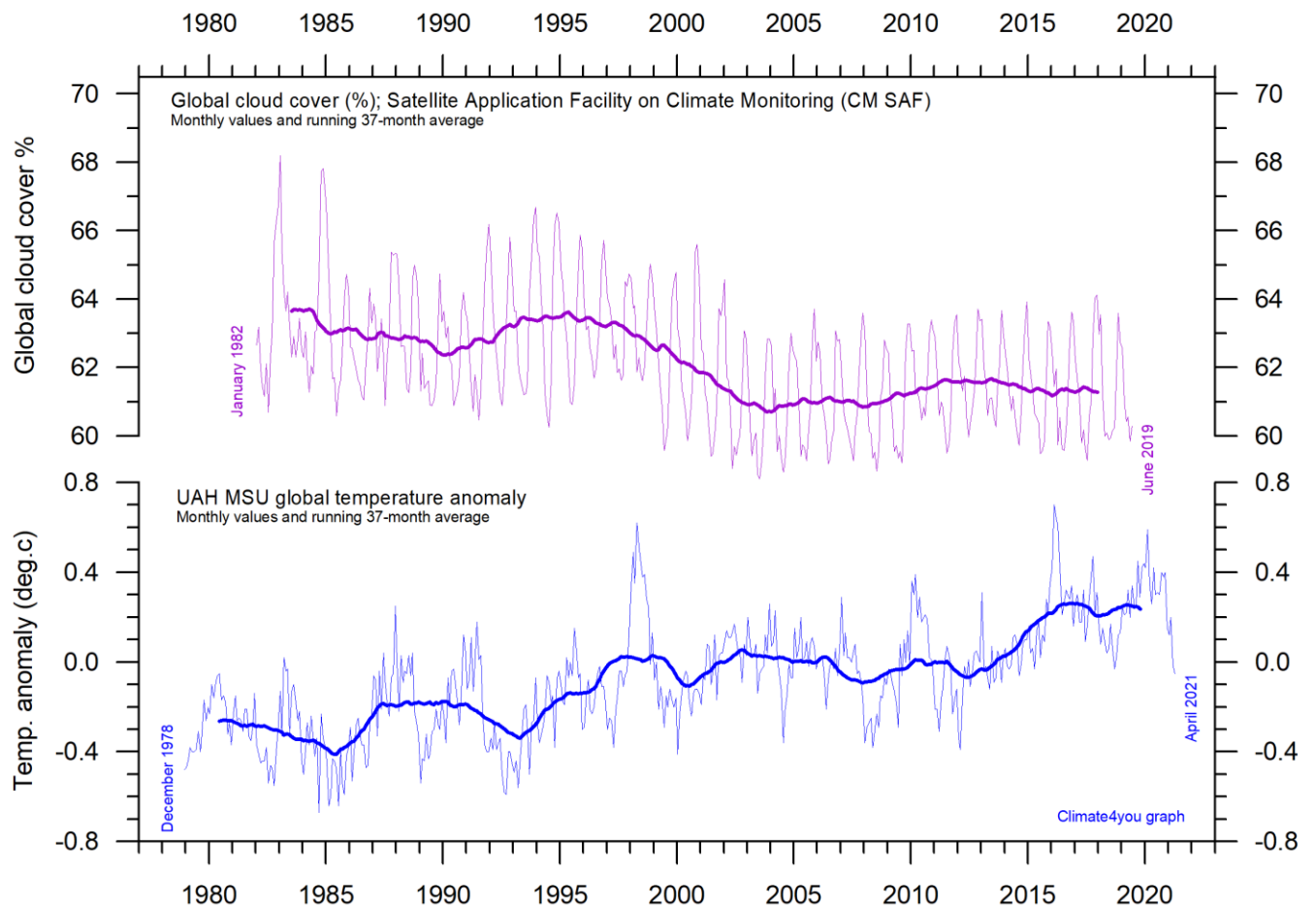


52

Visual association since 1958 between (from bottom to top) Sunspot Number, Oceanic Niño Index (ONI) and annual change rate of atmospheric CO₂ and specific humidity at 300 mb (ca. 9 km altitude). Upper two panels: Annual (12 month) change rate of atmospheric CO₂ and specific humidity at 300 mb since 1959, calculated as the average amount of atmospheric CO₂/humidity during the last 12 months, minus the average for the preceding 12 months (see also diagrams on page 43+44). Niño index panel: Warm (>+0.5°C) and cold (<0.5°C) episodes for the Oceanic Niño Index (ONI), defined as 3 month running mean of ERSSTv4 SST anomalies in the Niño 3.4 region (5°N-5°S, 120°-170°W)]. For historical purposes cold and warm episodes are defined when the threshold is met for a minimum of 5 consecutive over-lapping seasons. Anomalies are centred on 30-yr base periods updated every 5 years. Thin vertical stippled lines indicate the visually estimated timing of sunspot minima. The typically sequence following a sunspot minimum appears to be a warm El Niño episode followed by a cold La Niña episode. Effects on change rates of atmospheric CO₂ and atmospheric specific humidity are visually apparent, with ONI variations being followed by changes in first humidity, and then (last) by CO₂.

The above diagram is inspired by the Leamon et al. 2021 publication: Robert J. Leamon, Scott W. McIntosh, Daniel R. Marsh. Termination of Solar Cycles and Correlated Tropospheric Variability. Earth and Space Science, 2021; 8 (4) DOI: [10.1029/2020EA001223](https://doi.org/10.1029/2020EA001223)

Monthly lower troposphere temperature (UAH) and global cloud cover, updated to April 2021



53

Lower tropospheric air temperature and global cloud cover. Upper panel: Global cloud cover according to Satellite Application Facility on Climate Monitoring. Lower panel: Global monthly average lower troposphere temperature (thin line) since 1979 according to [University of Alabama](https://climate4you.com/) at Huntsville, USA. The thick lines represent the simple running 37-month average. Reference period for UAH is 1991-2020.

Cloud cover data citation: Karlsson, Karl-Göran; Anttila, Kati; Trentmann, Jörg; Stengel, Martin; Solodovnik, Irina; Meirink, Jan Fokke; Devasthale, Abhay; Kothe, Steffen; Jääskeläinen, Emmihenna; Sedlar, Joseph; Benas, Nikos; van Zadelhoff, Gerd-Jan; Stein, Diana; Finkensieper, Stephan; Håkansson, Nina; Hollmann, Rainer; Kaiser, Johannes; Werscheck, Martin (2020): CLARA-A2.1: CM SAF cCloud, Albedo and surface RAdiation dataset from AVHRR data - Edition 2.1, Satellite Application Facility on Climate Monitoring, DOI:10.5676/EUM_SAF_CM/CLARA_AVHRR/V002_01, https://doi.org/10.5676/EUM_SAF_CM/CLARA_AVHRR/V002_01.

Climate and history; one example among many

9 AD: Battle of the Teutoburg Forest



Topography of Germany (left) with insert showing location of map section to the right. Detailed map showing the location of the Battle at Teutoburg Forest (right).

54

The name of the [Teutoburg Forest](#) (Teutoburger Wald) in northwestern Germany is connected to one of the most famous battles from ancient history, the [clades Variana](#), the defeat of the Roman general Varus. In September 9 AD, a coalition of Germanic tribes, led by a nobleman named Arminius, defeated a large Roman army consisting of three legions and other units, forcing their commander [Publius Quintilius Varus](#) to commit suicide.

The result of the battle in Teutoburg Forest was that Germania remained independent and was never included in the Roman Empire. Presumably the Roman defeat was indeed one of the most decisive and influential battles in world history, and weather played no small role in the outcome of this battle.

In the last decade of the second century BC, the expanding Romans first encountered Germanic tribes. The [Cimbri](#) and [Teutones](#) were considered dangerous enemies, but ultimately defeated by the Roman commander Marius in two battles in BC 102 and 101. For two generations, all was then quiet on the northern front, but in BC 58, when [Julius Caesar](#) was waging war in eastern [Gaul](#), he got involved in a conflict with the Germanic leader [Ariovistus](#). At [Colmar](#), Caesar defeated his enemy, and Caesar subsequently bridged the [Rhine](#) and invaded the country east of the river, which he called [Germania](#).

Following his successful campaign, Caesar declared the river Rhine as a natural boundary between the Gallic barbarians ("Celts") and the Germanic tribes,

which in his official opinion were even more barbarous. Caesar needed a well-defined theatre of operations, and the Rhine was, from a military point of view, a good frontier. But from a cultural or ethnic point of view, it was not a natural frontier at all. The [Celtic](#) culture also existed on the east bank of the Rhine, and people speaking a Germanic language had already settled on the west bank.

In BC 39-38, [Marcus Vipsanius Agrippa](#) was governor of Gaul, and fought a war on the east bank of the Rhine on behalf of the [Ubians](#) against the [Suebians](#), a Germanic tribe that was notorious for its aggressiveness. After this campaign, Agrippa resettled the Ubians on the west bank of the Rhine and founded Cologne. The Rhine was now changing into being a frontier between an increasingly Roman Gaul and an increasingly Germanic Germania.

During this dynamic age, the tribes of the east bank sometimes raided the Roman empire west of the Rhine. This happened in the winter of BC 17-16, where the governor of [Gallia Belgica](#), [Marcus Lollius](#), was defeated by the [Sugambri](#). At this occasion the Fifth legion Alaudae lost its eagle standard: the ultimate disgrace to a Roman army unit. The emperor [Augustus](#) then understood that the Rhine frontier was still highly unstable and therefore sent his adoptive son [Drusus](#) to the north, to pacify the region and create a more stable frontier.

In the years BC 16-13, the Romans reorganized the strip of land along the Rhine. The region now became a military zone, where the army of [Germania Inferior](#) defended the Roman Empire against invaders from Germania. A second army group was called the army of [Germania Superior](#) was stationed further south along the Middle Rhine. In the summer of BC 11, Drusus managed to reach the river Elbe with his army. However, on his way back home, he fell badly from his horse and died. The Roman conqueror of Germania was only 29 years old.

Drusus was succeeded by his brother [Tiberius](#), a capable general who held the opinion that [Germania](#) was too cold and poor to ever represent a valuable part of the Roman Empire. On the other

hand, the armies could not be recalled immediately after the death of [Drusus](#), as this would look as if the Romans had been defeated. In the years BC 9 and 8, Tiberius therefore attacked the [Sugambri](#) and deported thousands of them to the west bank of the Rhine.

After this operation all now seemed quiet for a while along the upper reaches of the Rhine, and in AD 4, Augustus ordered Tiberius to advance northeast again, to finish the conquest of Germania. The whole of Germania was to become a normal, tax-paying province, cold unpleasant climate or not. The army of Germania Inferior therefore was ordered to march from the Rhine to the sources of the river [Lippe](#), where a camp was built at Anreppen. Next year, the legions had a rendez-vous with the Roman navy at the mouth of the Elbe, and Tiberius marched with his army along the [Elbe](#), which was to become the new northeastern frontier of the Roman Empire.

Meanwhile, the army of Germania Inferior was commanded by [Publius Quinctilius Varus](#), one of the most important senators of his age and a personal friend of Augustus. Varus was ordered to make a normal province of the country between the Lower Rhine and Lower Elbe, and indeed had some initial success in doing this. Then, everything suddenly went wrong, probably because Varus decided to impose [tribute](#) in the new Roman Province.

The taxes imposed by Varus provoked resistance among a population that had at first been willing to accept Roman rule but was not prepared to pay this amount of tribute. Presumably Varus did not take the gathering storm seriously, and as usual sent smaller groups of Roman troops to various places in Germania, which asked for them for the alleged purpose of guarding various positions, arresting robbers, or escorting provision trains. Thereby Varus did not keep his legions together, as would have been the proper procedure in a hostile country.

Next there came an uprising, first on the part of those who lived at large distances away from the Roman headquarter, deliberately so arranged, in order that Varus should march against them and so

be more easily overpowered while proceeding through what was supposed to be friendly country. Varus, on hearing the first news about the revolt of a far-away tribe, sensibly decided to regroup his army before taking any action.

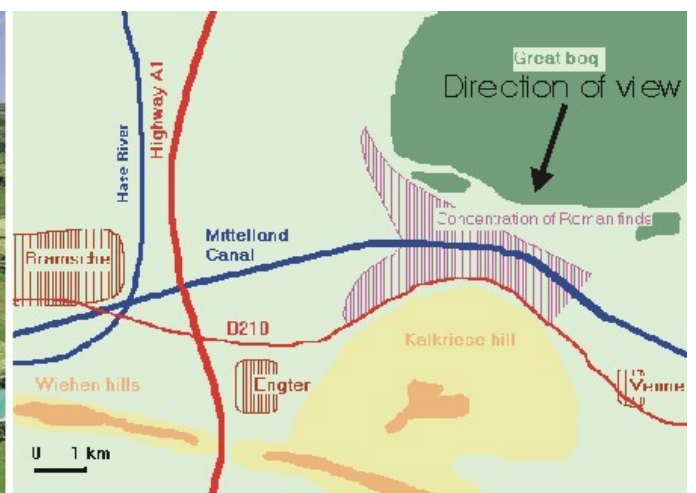
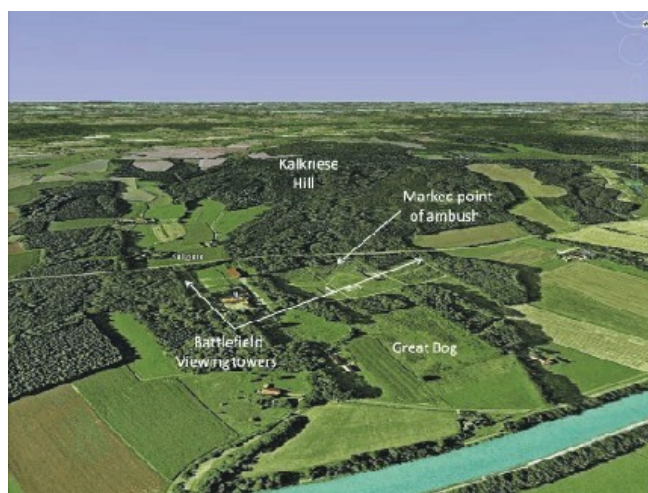
All sources agree that the Germanic leader of the uprising was [Arminius](#), a member of the [Cheruscan](#) tribe and until then a loyal supporter of Rome. The rebels (or freedom fighters) must have made their preparation during the late summer of 9 AD. However, not all Germanic leaders agreed with Arminius' policy, and his plan was apparently betrayed to Varus. What happened next is not entirely clear. Presumably Varus refused to listen, and instead rebuked the person(s) that could have saved him.

The battle in Teutoburg Forest took place in the year 9 AD, most likely in September. The battle's final stage took part at the northern foot of the [Kalkriese](#) hill, a site remarkably well-suited for an ambush. Although only 157 meters high, the Kalkriese is difficult to pass on its northern slope, because a traveller then must cross many deep brooks and rivulets, and in the level terrain north of the Kalkriese extends a difficult wetland for large

distances. However, in between this great bog and the hill exists a more accessible zone up to several hundred meters wide, consisting of stable, [Quaternary](#) sandy deposits. The most accessible part of this corridor has a width of only 220 meters. It therefore comes as no big surprise that much later, in the 19th century, German engineers choose this natural east-west corridor along the northern slope of Kalkriese for the construction of both the main road B218 and the [Mittelland Canal](#) further to the north.

In September 9 AD, Varus' forces included three [legions](#) (Legio XVII, Legio XVIII, and Legio XIX), six cohorts of auxiliary troops (non-citizens or allied troops) and three squadrons of cavalry. The Roman forces were not marching in combat formation and were interspersed with large numbers of camp-followers.

As they entered the forest shortly northeast of the modern town [Osnabrück](#), they found the forest track narrow and muddy, and at the same time a violent rainstorm began. Apparently, Varus neglected to send out advance reconnaissance parties, but instead advanced with all his forces along the narrow track in one long formation.



Overview illustration of the Kalkriese Battlefield from [Mike Anderson's Ancient History Blog](#) (left). The Mittelland Canal is seen in the foreground (direction of view towards SW). Overview map showing the main features of the battlefield (right).

On this narrow track the Roman line soldiers rapidly became stretched out perilously long; estimates are somewhere between 15 and 20 km in total. The Roman forces were then suddenly attacked by Arminius's Germanic warriors armed with light swords, large lances, and narrow-bladed short spears. The Germanic warriors quickly managed to surround the entire Roman army and rained down [javelins](#) on the intruders from the surrounding forest.

The German leader, Arminius, had grown up in Rome as a citizen and became a Roman soldier, understood Roman tactics very well and could thus direct his troops to counter them effectively, using locally superior numbers against the dispersed Roman legions. Indeed, the German warriors presumably used a very efficient tactic of isolating individual, manageable parts of the extended Roman column, to defeat them one by one. 1930 years later similar efficient '[motti](#)' tactics were successfully employed by the Finnish army against the much bigger Red Army during the Finnish-USSR winter war 1939-40, again assisted by the prevailing weather.

The Roman main force however managed to set up a fortified night camp near Engter, and the next morning the remaining Roman soldiers managed to break out into the open country north of the [Wiehen Hills](#), near the modern town of [Ostercappeln](#). The break-out cost heavy losses, as did a further attempt to escape by marching through another forested area, with the torrential rains continuing.

According to [Cassius Dio](#), Roman History (*Historia Romana*, in 80 books):

They were still advancing when the fourth day dawned, and again a heavy downpour and violent wind assailed them, preventing them from going forward and even from standing securely, and moreover depriving them of the use of their weapons. For they could not handle their bows or their javelins with any success, nor, for that matter, their shields, which were thoroughly soaked. Their opponents, on the other hand, being for the most

part lightly equipped, and able to approach and retire freely, suffered less from the storm.

The continuing rain prevented the Roman forces from using their otherwise efficient bows, because their [sinew](#) strings become slack when wet. This rendered the Roman soldiers virtually defenceless as their shields also became waterlogged and soft.

The Romans then undertook a night march to escape, but marched into another trap that Arminius had set, at the foot of Kalkriese Hill north of Osnabrück. There, the sandy, open strip on which the Romans could march easily was constricted by the hill to the south, so that there was a gap of only about 2-300 m between the woods and swampland with high vegetation at the edge of the Great Bog to the north. The Roman soldiers probably expected nothing at this stage but were suddenly attacked on their left flank by part of the Germanic forces hiding in the swamp. Moreover, the Roman forces found the road ahead blocked by a fortified trench, and, towards the forest, an earthen wall had been built along the roadside, permitting the Germanic tribesmen to attack the Romans from cover. The Roman forces was surrounded on three sides.

The Romans made a desperate attempt to storm the wall to break one part of the Germanic pincer but failed. The highest-ranking officer next to Varus, Legatus Numonius Vala, abandoned the troops by riding off with the cavalry; however, he too was overtaken by the Germanic cavalry and killed. The Germanic warriors then stormed the field and slaughtered the now disintegrating Roman forces.

Varus did what the Romans considered the honourable thing: he committed suicide. One commander, Praefectus Ceionius, shamefully surrendered and later took his own life, while his colleague Praefectus Eggius heroically died leading his doomed troops to the bitter end. The Roman defeat was a major one, and at that time it rarely happened that legionary soldiers lost a battle, and the loss of no less than three legions was one of the worst defeats in Roman history.

Archeological excavations in the area north of Kalkriese have shown that the staff of at least one legion was present, and the presence of cavalry and auxiliary infantry is also attested. There were also noncombatants and perhaps women at Kalkriese mountain battlefield. In total, around 15,000–20,000 Roman soldiers must have died; not only Varus, but also many of his officers are said to have taken their own lives by falling on their swords in the approved manner.

Other Roman soldiers from Germania had already reached the Rhine, and the news that something terrible had happened spread upstream along the river. Even in [Rome](#), the populace was afraid, and the emperor Augustus ordered that watch be kept by night throughout the city.

According to [Suetonius](#), Augustus, 23.4:

He (Augustus) was so greatly affected that for several months in succession he cut neither his beard

nor his hair, and sometimes he could dash his head against a door, crying "Quintilius Varus, give me back my legions!"

The battle in the Teutoburg Forest had a profound effect on 19th century German nationalism; the Germans, at that time still divided into many individual German states, identified with the Germanic tribes as shared ancestors of one "German people" and came to associate the imperialistic Napoleonic French and Austro-Hungarian forces with the invading Romans who were destined for defeat. This was part of the background on which [Bismarck](#), the German statesman, much later could unify numerous German states into a powerful [German Empire](#) under Prussian leadership, and thereby create a "balance of power" that preserved peace in Europe from 1871 until 1914. Today, the place where the final battle at Kalkriese took place has been transformed into a museum and an archaeological park, Varusschlacht (Varus Battle).

References

[Mike Anderson's Ancient History Blog](#)

All diagrams in this report, along with any supplementary information, including links to data sources and previous issues of this newsletter, are freely available for download on www.climate4you.com

Yours sincerely,

Ole Humlum (Ole.Humlum@gmail.com)

Arctic Historical Evaluation and Research Organisation, Longyearbyen, Svalbard

20 August 2021.